Biological oxygen production from oxygen-to-argon ratios and oxygen isotopologues in the Atlantic Ocean

Alba M. González-Posada

Thesis submitted for the degree of Doctor of Philosophy
University of East Anglia, UK

November 2012

Abstract

Marine primary producers play an important role in controlling the atmospheric carbon dioxide through photosynthesis and export of organic matter into the deep ocean. In this thesis I used two biogeochemical techniques based on O_2/Ar ratios and O_2 isotopologues to measure net community production (*N*) and gross oxygen production (*G*) in two different areas relevant for the marine C cycle: the South Atlantic subtropical gyre and the North Atlantic during a spring bloom. The former despite small rates of production it is relevant for the global marine C cycle due to the large area it covers; in addition the study of this gyre may contribute to clarify the ongoing debate on whether subtropical gyres are net autotrophic or heterotrophic. The North Atlantic is a main component of the global C production because of the large the amount of C that is fixed during the spring bloom. *N* was estimated from continuous measurements of O_2/Ar ratios with a Membrane Inlet Mass Spectrometer and *G* from discrete samples both in the USW of RSS James Cook (South Atlantic) and R/V Knorr (North Atlantic). Discrete samples were processed in a newly built gas extraction line and analyze in an Isotope Ratio Mass Spectrometer at UEA. The gas extraction line was built for the separation of O_2 and Ar from N_2 without isotopic fractionation. This thesis shows that the South Atlantic Gyre produced O_2 at a rate of 10±3 mmol m^{-2} d^{-1} in March/April 2009, thus was net autotrophic. Interestingly *G* (177±96 mmol m^{-2} d^{-1}) was much higher than previous estimates. This difference could be due to other processes that might fractionate the O_2 without fixing any carbon such as the Mehler reaction. Measurements of *N* made in the North Atlantic during a spring bloom in May 2008 showed the highly variable and heterogeneous nature of the area. Within the bloom *N* had an average value of 67 mmol m^{-2} d^{-1} with *N* increasing from 60 to 170 mmol m^{-2} d^{-1}, followed by a short period of net heterotrophy and finishing at 5 mmol m^{-2} d^{-1}. These changes were associated with changes in the species composition, with diatoms dominating first followed by the increase of nanophytoplankton. These techniques show O_2/Ar and O_2 isotopologues to be useful and accurate proxies for production with the potential for complete automation of O_2/Ar measurements.

Acknowledgements

I would like to express my sincere appreciation and gratitude to my supervisors Jan Kaiser and Dorothea Bakker. They both contributed with ideas that shaped this project. I was amazed by Jan's ability to find clever solutions in the office, lab and at sea, but I especially appreciate his sharp intellect, his attention to detail and the little pushes he gave me when I needed them. Dorothea Bakker dedicated many hours to discuss specific details of my work, and I thank her especially for always being available for advice and lending a hand when needed.

I also would like to give special thanks to Johanna Gloël, lab-partner and officemate, who became a great friend; she was of incredible help and support in all the aspects of my thesis. Her incredible common sense was always of great help! During the writing up of my thesis, Sue Palminteri became my editor. Her dedication and patience greatly improved my writing skills.

In the lab I am indebted to many people but especially to Alina Marca Bell, who introduced me to the insides of Isotope Ratio Mass Spectrometry. Also I highly appreciate the time and assistance that Osamu Abe dedicated to me while building the extraction line used in this study. I also want to thank all the technicians either from the Stable Isotope Lab or not, which were always available to lend a hand: Andy Macdonald, Stephen Woodward and Paul Disdle.

In the office to all the people that allowed me to distract them in 01.37K. Starting with the ones I distracted the most (just because they were sitting closer to me): Sophie Chollet, Johanna Gloel, Michal Bochenek, Rachel Gibson, Jan Strauss, Cansu Bayindirli, Phil Wilson, Michelle Fernandes, Paul Lancaster, Rafaella Nobili and in the old times Janina Woeltjen, Marie Racault, Amandine Caruana, Claire Powel, Nuno Nunes and Mat Jones. Also thanks to the friends from offices afar which would agree to have lunch in lgmac, especially to Maria Martínez de Alvaro which brought back the Spanish spirit that I was beginning to loose, Tiziana Luisetti, Mi Tian, Maria-José Marín Altaba, Christiana Faria, and Maribel Velasco. And also to all the friends that left UEA before me but without whom this PhD would not have been the same: Clara Moyano, Agnieszka Latawiec, Sue Palminteri and Karel Castro-Morales.

At sea I would like to thank the Principal Investigators that allowed me to take part on both cruises: Mary Jane Perry and Brian King. I am indebted to many people that helped me during the cruises, in particular Nicole Bale, Nathan Briggs, Giorgio Dall'Olmo, Toby Westberry, Sinhue Torres, Mark Moore, Niki Silvera and Steve Woodward.

An “¡OLÉ!”to my family. They always have been supportive and understanding throughout this whole process. Starting with my parents without whom I would never have started this PhD, but also thanks to my brother Miguel, as well as all my other sisters and brothers and to all my little sobrininos.

A very special thank you to Charlene and Alan Lobo who basically adopted me and took care of me especially in the final stages of the thesis. I cannot say a thank you big enough for everything they did for me showing me all the warmth from Spain with a Goan accent.

And a warm thanks to Lorenzo who encouraged me to always see the bigger picture and whatever the weather always was there for me.

Contents

Chapter 1. Introduction

1.1. Relevance of the ocean in the global carbon cycle

Carbon dioxide (CO_2) is one of the most important anthropogenic greenhouse gases in the atmosphere. Since the industrial revolution the concentration in the atmosphere has been steadily increasing due to the input by human activities such as fossil fuel use and cement production.

However, only 40 % of the CO_2 emitted by human activity has remained in the atmosphere. The rest has been absorbed by land and ocean reservoirs. The oceans store 50 times more CO_2 than the atmosphere and 17 times more than the land biosphere (Denman *et al.*, 2007).

Marine carbonate chemistry is believed to play an important role in controlling the concentration of CO_2 in the atmosphere (Takahashi *et al.*, 1993). The following processes control the distribution of CO_2 in the ocean: the solubility of CO_2 (solubility pump), the carbonate chemistry, ocean circulation and biological removal from the euphotic zone to deeper waters (biological pump).

Dissolved inorganic carbon (DIC) is composed of the inorganic carbon species dissolved CO_2, carbonic acid (H_2CO_3) bicarbonate (HCO_3^-) and carbonate (CO_3^{2-}). When CO_2 gas enters in the ocean, it reacts in a series of equilibrium reactions that form H_2CO_3, HCO_3^- and CO_3^{2-}:

$$CO_2(aq) + H_2O \leftrightarrows H_2CO_3$$

$$H_2CO_3 \leftrightarrows HCO_3^- + H^+$$

$$HCO_3^- \leftrightarrows CO_3^{2-} + H^+$$

The solubility pump (Volk and Hoffert, 1985) results in transport of inorganic carbon from the surface of the ocean to its interior. This pump acts in cold dense waters that sink to the deep ocean, carrying large amounts of dissolved inorganic carbon (DIC) and isolating them from the surface.

The biological pump (Volk and Hoffert, 1985) is fuelled by photosynthesis in the surface ocean. Photosynthesis is carried out by autotrophic organisms, transferring CO_2 into organic matter. A simplified reaction equation of photosynthesis is

$$n\,CO_2(aq) + n\,H_2O + h\nu \rightarrow nO_2 + (CH_2O)_n$$

The organic matter formed could either sink or be transported by the thermohaline circulation to deeper layers and therefore be removed from contact with the atmosphere (biological pump) or could be respired or remineralised.

$$n\,O_2 + (CH_2O)_n \rightarrow n\,CO_2 + n\,H_2O$$

CO_2 is produced during respiration and consumed during photosynthesis; O_2 behaves inversely so that their concentration changes are opposite to each other. When disregarding the physical effects of the solubility of O_2 in the water, O_2 can be used as a biogeochemical tracer for net community production (*N*) (Craig and Hayward, 1987; Emerson, 1987; Spitzer and Jenkins, 1989). The O_2 produced by photosynthesis is called gross oxygen production (*G*). *N* is equal to *G* minus community respiration (*R*).

1.2. Areas of study

This thesis presents data from two different regions of the Atlantic Ocean. The first region is the North Atlantic during the spring bloom. The second region is the oligotrophic South Atlantic gyre in the austral autumn season.

Despite covering only 15 % of the global ocean area, the North Atlantic accounts for 23 % of the total oceanic uptake of anthropogenic carbon (Sabine *et al.*, 2004). From a biological point of view the North Atlantic is relevant because of the large amount of CO_2 that is fixed during the spring bloom and then exported to the deep ocean. This bloom is special in a way that the magnitude of the export which occurs is not comparable to other areas in the world.

Oligotrophic subtropical gyres occupy about 40% of the earth surface. These oceanic "deserts" are characterized by low concentrations of nutrients and low rates of photosynthesis. Because of their sheer size they are nevertheless relevant for global carbon budgets. Currently there is an ongoing debate whether these big open ocean areas are net sources or sinks of CO_2 to the atmosphere (Ducklow and Doney, 2013). On the one hand, Duarte *et al.* (2013) consider oligotrophic areas as net heterotrophic ecosystems. In contrast

to Williams *et al.* (2013) that consider them to be net autotrophic. While Duarte *et al.* (2013) suggest that these areas are supported by organic carbon inputs from the continental shelf, nutrients from the atmosphere or by non-photosynthetic autotrophy and mixotrophic metabolic pathways. Williams *et al.* (2013) argues that these areas must be net autotrophic because *in situ* O_2 methods despite their uncertainties show autotrophy (they might be wrong in the quantity but not in the sign), because the observed ^{13}C enrichment in DIC could only be explained by positive *N* and because neither horizontal or vertical transport and mixing nor atmospheric inputs of organic matter would be sufficient to support these communities.

Specifically, it is not clear whether the South Atlantic is a net source or sink of CO_2. Studies determining the metabolic balance of this region with bottle incubations gave mixed results. Net heterotrophy was found by González *et al.* (2002) in spring and autumn and by Gist *et al.* (Gist *et al.*, 2009) in autumn only, whereas Serret *et al.* (2006) and Gist *et al.* (2009) found net autotrophy in spring.

1.3. Production measurements in the ocean

Different methodologies to measure the productivity in the ocean measure different properties and these will be explained first.

Gross production is the total organic matter produced by photosynthesis without any respiratory losses. It is related to the transfer of electrons from H_2O to the terminal electron acceptor, CO_2. It might be expressed in terms of amount of C fixed in amount of O_2 produced. However, there are some photobiological reactions such as photorespiration or the Mehler reaction that produce O2 without C fixation.

Respiration: This includes all processes which transfer electrons from organic matter to O_2 with the subsequent production of CO_2. Respiration can be carried out by autotrophs and heterotrophs. Thus, **net primary production** is the difference between gross production and autotrophic respiration; and **net community production** is gross production minus all respiratory processes by autotrophs and heterotrophs (Falkowski and Raven, 1997).

There are several techniques to measure organic matter production in the ocean and thus different terms to define production in the ocean. They can be separated into *in vitro* methods where bottle incubations are used to determine the different rates and *in situ* methods where production is determined from specific biogeochemical tracers in the region of

study. The main in vitro measurements are: ^{14}C incubation, $H_2{}^{18}O$ incubation, ^{15}N incubation and dark and light O_2 bottle incubations.

^{14}C incubations are widely used as a productivity measurement technique. Described by Steeman Nielsen (1952) the method consists of adding ^{14}C-labelled DIC to the sample and incubating for 12-24 h at ambient or simulated ambient light levels (to capture all production over a diurnal cycle) or <2 h at multiple light levels (to derive a production-irradiance flux curve, which is then used to work out integrated production rates). There are some caveats when using this methodology as photorespiration, remineralisation of particulate organic carbon ($PO^{14}C$) and dissolved organic carbon ($DO^{14}C$) excretion can lead to a low bias in measured production rates (Bender, 1999; Williams and Lefevre, 1996). Thus, the measurements performed by this method are considered to represent something in between gross and net production, and they are often referred to as "(^{14}C) primary productivity". Also, being an incubation method, it suffers from bottle effects such as the reduction of autotrophs during incubation time (Calvo-Díaz *et al.*, 2011; Fernández *et al.*, 2003), the increase of heterotrophs (Calvo-Díaz *et al.*, 2011) or the exclusion of grazers (Bender, 1999), which can introduce both low or high biases in the desired production rates.

$H_2{}^{18}O$ incubations consist of incubating samples with spiked water ($H_2{}^{18}O$) and measuring the proportion of ^{18}O present in the dissolved O_2 in the water at the end of the incubation period (Bender *et al.*, 1987). The advantage of this technique over the ^{14}C method is that the pool of O_2 is much larger than that of POC and thus ^{18}O labelled-O_2 is less likely to be recycled than $PO^{14}C$ (Bender *et al.*, 1999). The disadvantage is that like the ^{14}C measurements it is an in vitro method with the associated problems. Furthermore, there are processes that are not fixing any carbon but increase the amount of ^{18}O-labelled O_2 such as the Mehler reaction (Bender *et al.*, 1999).

^{15}N assimilation studies consists of the incubation of a sample injected with a compound (usually nitrate or ammonium) with a known ^{15}N signature. The incorporation of this compound into the particulate organic nitrogen pool is used to measure **new production** (this means NO_3^- based production) or recycled production (this means NH_4^+ based production) (Neess *et al.*, 1962). Like the other methods mentioned above, this in vitro method might suffer from bottle effects.

O_2 bottle incubations are based on differences of *in vitro* dissolved O2 changes between light and dark incubated bottles (Gaarder and Gran, 1927). This method aims to measure net community production, gross production and community respiration.

In situ methods on the other hand, provide measurements that are not biased by incubation techniques. Examples are remote measurement of chlorophyll *a* concentrations from satellites; mixed layer budgets of different compounds (O_2, NO_3^-, DIC, thorium ^{234}Th) and fast rate repetition fluorescence (FRRF).

Satellites chlorophyll production estimates using remotely sensed chlorophyll fluorescence are calibrated with ^{14}C primary production measurements (Behrenfeld and Falkowski, 1997) This is a useful tool as it can give estimates on a world-wide scale unachievable by other techniques that often only provide snapshots of production rates at the exact sampling time and place. However, the ^{14}C method has drawbacks associated with it. For example, depending on incubation conditions and sampling location, the derived production estimates may lie somewhere between net and gross primary production. Also, the satellite only measures chlorophyll concentrations in the top-most surface layer and these measurements are not very accurate in areas where coloured dissolved organic matter (CDOM) concentrations are high (Arrigo *et al.*, 2011). Additionally, chlorophyll concentrations are not a direct measure of carbon fixation rates since carbon-to-chlorophyll ratios may vary according to species and other factors.

Fast rate repetition fluorometer analysis aims to determine photosynthesis rates (gross primary production) by measuring the physiological state of photosystem II (Kolber *et al.*, 1998) (PS II). It looks at the electron flow through PS II (Suggett *et al.*, 2001). The disadvantage of this method is that the electron flow through PS II is not only dependant on photosynthesis rates, but it also depends on phytoplankton community composition as well as nutrient limitation (Suggett *et al.*, 2009).

Net community production can be inferred from budgets of O_2, DIC, ^{234}Th deficiencies and nutrient inventories (Bender *et al.*, 1992; Buesseler *et al.*, 1992; Chipman *et al.*, 1993; Emerson, 1987). Their advantage is that they measure actual *in situ* properties and are inherently unbiased by incubation artefacts. However, their use requires the budgets of these compounds to be well characterized in terms of physical transport and time trends, as well as, in the case of O_2, wind-speed gas exchange parameterisations, which may have significant uncertainties.

Recently, two new techniques to measure net (*N*) and gross (*G*) oxygen production in the mixed layer from measurements of O_2/Ar and O_2 isotopes have been developed. They have the advantage that they are *in situ* methods and therefore do not suffer from bottle effects. They also require less sampling and processing time compared to *in vitro* methods. Another advantage of these methods is that they integrate over the residence time of the gases in the

mixed layer and are therefore representative of longer time periods compared to other techniques, which might miss short-lived production spikes. However, vertical mixing with waters below the mixed layer or horizontally sometimes have to be taken into account where there are significant O_2 gradients.

1.4. Use of O_2/Ar and O_2 isotopes for the measurement of net and gross production

1.4.1. Net community production measured by O_2/Ar ratios

Craig and Hayward (1987) described the use of oxygen and argon as an indicator of net community production based on the similar solubilities and diffusivities of these gases. This means that both are similarly affected by physical processes like bubble injection and changes in barometric pressure and temperature. However O_2 takes part in biological processes (photosynthesis and respiration) while Ar is an inert gas, which means that it has no biological sources or sinks.

Therefore the O_2/Ar ratio can be used to separate O_2 supersaturation into a biological and a physical component (Craig and Hayward, 1987; Spitzer and Jenkins, 1989). Biological supersaturation, $\Delta(O_2/Ar)$, expresses O_2 supersaturation in excess of Ar supersaturation and can be written as:

$$\Delta(\mathrm{O_2/Ar}) = \frac{c(\mathrm{O_2})/c(\mathrm{Ar})}{c_{\mathrm{sat}}(\mathrm{O_2})/c_{sat}(\mathrm{Ar})} - 1 \qquad (1.1)$$

where c(O2)/c(Ar) represents the ratio of concentration of O_2 and Ar; c_{sat}(O2)/c_{sat}(Ar) is the ratio of the saturation concentration of O_2 (Garcia and Gordon, 1992) and Ar (Hamme and Emerson, 2004).

Based on this, the biological O_2 air-sea flux (F_{bio}) is defined as (Kaiser, 2005):

$$F_{\mathrm{bio}}(\mathrm{O_2/Ar}) = \Delta(\mathrm{O_2/Ar})\, k_{\mathrm{w}}\, c_{\mathrm{sat}}(\mathrm{O_2}) \qquad (1.2)$$

where k_w is the weighted gas transfer coefficient which is calculated taking into account the wind speed history of the water following Reuer *et al.* (2007). Positive F_{bio} values correspond to loss from the oceanic mixed layer.

F_{bio} can be considered to be equal to N, assuming steady state and neglecting vertical and horizontal exchange of O_2 and Ar.

$$N = F_{\mathrm{bio}} \tag{1.3}$$

A breakthrough in the measurements of N based on O_2/Ar was achieved by the continuous measurements of O_2/Ar using membrane inlet mass spectrometry (MIMS). MIMS was developed by Kana *et al.* (1994) and it has been used widely in several oceanographic studies, e.g. Kaiser *et al.* (2005), Tortell *et al.* (2005b), Gueguen *et al.* (2008) and Nemcek *et al.* (2008). The short term reproducibility of the O_2/Ar ratio measurement is 0.05% Kaiser (2005).

MIMS consist of a semipermeable membrane that allows the extraction of the gases dissolved in the water, which are then led to a quadrupole mass spectrometer for analysis. The semipermeable membrane separates a liquid phase and a vacuum gas transfer line connected to a quadrupole mass spectrometer. The sample (liquid phase) is constantly brought to the membrane by a water pump. When the sample reaches the membrane, a portion of the gas in the water enters the vacuum due the difference of pressure between the liquid phase and the vacuum gas phase. A schematic view of this system is depicted in Figure 1. Gas molecules are brought to an ionization chamber where they are ionized and sent to the flight tube where they are selected according to their mass/charge ratio (m/z) by a specific radio-frequency. This radio-frequency is tailored to a specific m/z, so that ions of this m/z going through the flight tube are directed to the detector. The changes in radiofrequency through the rods of the mass spectrometer allow collecting different m/z ratios. The fast shifts of this radiofrequency allow measurement of 20 different ions every 10 s.

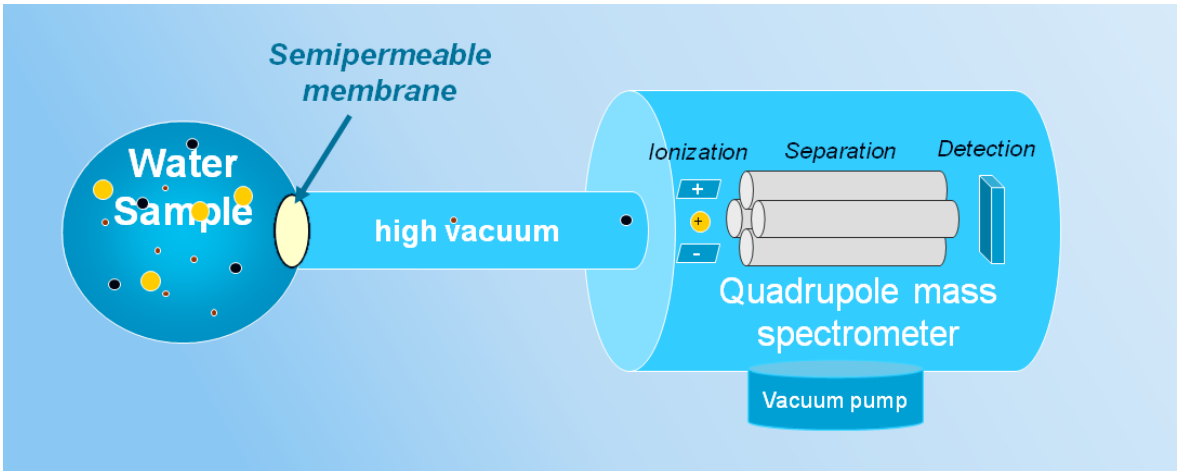

Figure 1: Schematic view of membrane inlet mass spectrometer taken from Kana (2007) from (http://www.hpl.umces.edu/~kana/index_files/Onlinetraining.htm, accessed 23/10/12)

1.4.2. Gross Production

O_2 has three stable isotopes: ^{16}O, ^{17}O and ^{18}O, which differ in their number of neutrons with 8, 9 and 10 neutrons, respectively. The most abundant isotope is ^{16}O with an abundance of 99.758%, followed by ^{18}O with 0.204% and ^{17}O with 0.038%. Isotope abundance is normally reported as delta (δ) quantities with the abundance ratio of the heavier isotope over the lighter isotope versus a known reference. This is expressed as:

$$^{*}\delta_{\mathrm{sample/ref}} = {}^{*}R_{\mathrm{sample}}/{}^{*}R_{\mathrm{ref}} - 1 \quad (1.4)$$

$$^{*}R = {}^{*}c(^{*}\mathrm{O})/{}^{*}c(^{16}\mathrm{O}) \quad (1.5)$$

The superscript * on $^{*}\delta$, $^{*}R$ and *O represents the isotopes ^{17}O or ^{18}O. R_{sample} and R_{ref} are the ratio of abundance of isotopes ^{18}O or ^{17}O over the ^{16}O in the sample and reference respectively. For these studies the preferred reference is tropospheric air.

The change in isotopic composition through a process from B to A like photosynthesis, respiration, gas evasion or gas invasion can be expressed with the fractionation ($^{*}\varepsilon$):

$$ {}^{*}\varepsilon_{\mathrm{A-B}} = \frac{{}^{*}\delta_{\mathrm{A}} - {}^{*}\delta_{\mathrm{B}}}{1 + {}^{*}\delta_{\mathrm{B}}} \quad (1.6) $$

Where * stands again for the isotope of study, in this case ^{18}O or ^{17}O; δ expresses the $^{18}O/^{16}O$ or $^{17}O/^{16}O$ anomaly in the state A or B as indicated by the subscripts.

Luz and Barkan (2000) found that the isotopic composition of oxygen can be used to trace the gross production in the ocean. The method is based on the different isotopic composition of the oxygen gas in the air, O_2 and the oxygen in the water molecule H_2O. This isotopic anomaly of O_2 in the air comes from the non mass dependent fractionation in the reactions of O_2 and CO_2 in the troposphere and stratosphere (Lämmerzahl, 2002; Thiemens *et al.*, 1995; Yung *et al.*, 1991) which results in a depletion of ^{17}O in atmospheric O_2, which is different from the isotopic composition of oxygen in the water molecule H_2O. Marine photosynthesis produces dissolved O_2, which carries the isotopic signature (with a small fractionation) of water. This contrasts with the isotopic signature of dissolved O_2 coming from air-sea exchange. Therefore the analysis of O_2 isotopes dissolved in water can be an indicator of marine oxygen production

Following Luz and Barkan (2000) and Kaiser (2011b), excess ^{17}O in dissolved O_2 in sea water with respect to atmospheric O_2 is calculated as:

$$ {}^{17}\Delta = {}^{17}\delta - \gamma_{\mathrm{R}}\, {}^{18}\delta \quad (1.7) $$

$$ \gamma_{\mathrm{R}} = {}^{17}\varepsilon_{\mathrm{R}} / {}^{18}\varepsilon_{\mathrm{R}} \quad (1.8) $$

$^{17}\Delta$ represents the dissolved O_2 measured excess of ^{17}O versus atmospheric air; $^{17}\delta$ and $^{18}\delta$ represent the anomaly of ^{17}O and ^{18}O versus air respectively; γ_R is the expected mass dependant fractionation for the respiration fractionation ratio of $^{17}\varepsilon_R$ /$^{18}\varepsilon_R$.

Generally $^{17}\delta$ and $^{18}\delta$ are expressed in per mill (‰) and $^{17}\Delta_{dis}$ in parts per million, that is ppm (note that some authors use per meg, which is the same as ppm). Luz and Barkan (2000) propose the calculation of the dimensionless gross oxygen production rate (g) as the ratio of the gross oxygen production (G) over the gas gross O_2 influx from the atmosphere:

$$g = \frac{G}{k_{\mathrm{w}}\, c(\mathrm{O_2})} \tag{1.9}$$

$$G = k_{\mathrm{w}}\, c(\mathrm{O_2})\, g \tag{1.10}$$

Where k_w is the weighted gas transfer coefficient or piston velocity.

Luz and Barkan proposed *g* to be approximated by the ratio of the difference between the dissolved ^{17}O excess and saturated ^{17}O excess value over the difference between the ^{17}O excess only due to photosynthesis and the dissolved ^{17}O excess:

$$g_{\mathrm{LB}} = \frac{(^{17}\Delta_{\mathrm{dis}} - {}^{17}\Delta_{\mathrm{sat}})}{(^{17}\Delta_{\mathrm{p}} - {}^{17}\Delta_{\mathrm{dis}})} \tag{1.11}$$

where $^{17}\Delta_{dis}$ is the $^{17}\Delta$ measured in the samples, $^{17}\Delta_{sat}$ is the $^{17}\Delta$ when the O_2 present in the water is only due to exchange with the atmosphere and biological processes are negligible and $^{17}\Delta_p$ is the value in a system, where there is no exchange with the atmosphere and the O_2 is only formed by biological activity.

In 2011, Kaiser (2011b) and Prokopenko *et al.* (2011) independently within 8 days of publication proposed the calculation of *g* without any mathematical approximation. Both calculations are very similar and their only difference is that Prokopenko *et al.* (2011) do not take the small fractionation during invasion and evasion of O_2 from air-sea gas exchange ($^*\varepsilon_I$ and $^*\varepsilon_E$) into account. For this work is adopted the calculation of *g* as defined by Kaiser (2011b, equation 48), g_K as it is considered to be more accurate from a theoretical point of view.

$$g_{\mathrm{K}} = \frac{(1+\Delta(\mathrm{O_2}))(^{17}\varepsilon_{\mathrm{E}} - \gamma_{\mathrm{R}}\,{}^{18}\varepsilon_{\mathrm{E}}) - \frac{^{17}\varepsilon_{\mathrm{I}} - {}^{17}\delta}{1+{}^{17}\delta} + \gamma_{\mathrm{R}}\frac{^{18}\varepsilon_{\mathrm{I}} - {}^{18}\delta}{1+{}^{18}\delta}}{\frac{^{17}\delta_{\mathrm{P}} - {}^{17}\delta}{1+{}^{17}\delta} - \gamma_R\frac{^{18}\delta_{\mathrm{P}} - {}^{18}\delta}{1+{}^{18}\delta}} \tag{1.12}$$

$$\Delta(\mathrm{O_2}) = \frac{c(\mathrm{O_2})}{c_{\mathrm{sat}}(\mathrm{O_2})} - 1 \tag{1.13}$$

where $\Delta(O_2)$ is the saturation anomaly of O_2, calculated as in equation 1.12 with the in situ concentration of O_2, $c(O_2)$, and the saturation concentration of O_2, $c_{sat}(O_2)$, at in situ conditions (Garcia and Gordon, 1992). $^{17}\varepsilon_I$, $^{17}\varepsilon_{E,}$ $^{18}\varepsilon_I$, $^{18}\varepsilon_E$ are the invasion and evasion isotopic fractionation of O_2 at invasion and evasion of ^{17}O and ^{18}O respectively with the temperature at in situ conditions. $^{17}\delta$ and $^{18}\delta$ are the measured anomalies in the sample of ^{17}O and ^{18}O; $^{17}\delta_p$ and $^{18}\delta_p$ are the isotope delta ^{17}O and ^{18}O of photosynthetic O_2; and γ_R is the expected mass dependant fractionation for respiration fractionation ratio of $^{17}\varepsilon_R$ /$^{18}\varepsilon_R$.

Description of parameters use for the calculation of *g*:

As explained, $\boldsymbol{\gamma_R}$ is the expected fractionation for respiration; this was measured by Luz and Barkan (2005) to be 0.5179. It can also be defined as the kinetic respiratory slope for the dominant O_2 consumers in aquatic systems and thus represents the ratio between the $^{17}O/^{16}O$ and ^{18}O /^{16}O isotope effects in ordinary respiration (Luz and Barkan, 2005).

$\boldsymbol{\gamma_R}$ is obtained from the slope of the linear relationship of $\ln(1+^{17}\delta)$ versus $\ln(1+^{18}\delta)$ for respiration in a closed system. This value substitutes the value of 0.516 of Angert *et al.* (Angert *et al.*, 2003) which was only applicable for dark respiration through the cytochrome pathway, even though some authors still use it, e.g. Reuer *et al.* (2007).

$\boldsymbol{^{17}\Delta_{sat}}$ is the ^{17}O excess when a parcel of water is in equilibrium with the atmosphere. This is calculated as defined by Luz and Barkan (2009):

$$^{17}\Delta_{sat} = \ln(1 + {}^{17}\delta_{sat}) - \lambda \ln(1 + {}^{18}\delta_{sat}) \qquad (1.14)$$

$^{17}\delta_{sat}$ and $^{18}\delta_{sat}$ are the saturation delta of $^{17}O/^{16}O$ and $^{18}O/^{16}O$ respectively and are explained in detail later; and λ = 0.518 which is the (rounded) ratio between the $^{17}O/^{16}O$ and $^{18}O/^{16}O$ isotope effects which represents global respiration (Luz and Barkan, 2005).

$^{17}\Delta_{sat}$ has been measured by several studies and has been reported with values from 4 ppm to 18 ppm (Kaiser, 2011b, table 1). The reason for the disagreement between these measurements is not clear (Stanley *et al.*, 2010) It is possible that temperature might play a role in these differences but it would not explain all. Following Kaiser (2011b in the current research the temperature-dependent value reported by Luz and Barkan {, 2009 #105) was chosen.

The saturation delta value, ${}^{18}\delta_{sat}$, and its dependence on temperature was measured by Benson *et al.* (1979, table VIII row 2) and is described in equation 1.15.

$$ {}^{18}\delta_{sat} = e^{-0.00072951 + 0.42696 / (T/\mathrm{K})} - 1 \quad (1.15)$$

Where *T* is the temperature in Kelvin.

Following Kaiser (2011b), ${}^{17}\delta_{sat}$ is back-calculated with equation 1.14 and 1.15 and ${}^{17}\Delta_{sat}$ reported by Luz and Barkan (2009)

Fractionation of the ${}^{18}O/{}^{16}O$ during evasion (${}^{18}\varepsilon_E$) was measured by Knox *et al.*(1992) to be (-2.8±0.2) ‰. As in Kaiser (2011b) the rest of the parameters of the kinetic fractionation during evasion and invasion are calculated with the ${}^{*}\delta_{sat}$ and the ${}^{18}\varepsilon_I$ (Kaiser, 2011a; Kaiser, 2011b).

$$ {}^{18}\varepsilon_I = (1 + {}^{18}\varepsilon_E)(1 + {}^{18}\delta_{sat}) - 1 \quad (1.16)$$

$$ {}^{17}\varepsilon_I = (1 + {}^{18}\varepsilon_I)^{\kappa} \quad (1.17)$$

$$ {}^{17}\varepsilon_E = \frac{{}^{17}\varepsilon_I - {}^{17}\delta_{sat}}{1 + {}^{17}\delta_{sat}} \quad (1.18)$$

κ = is the triple isotopic fractionation of invasion and was assumed to be (0.516±0.015) covering the theoretical predicted mass dependent range of isotope effects (Kaiser, 2008)

Calculation of the photosynthetic delta ${}^{*}\delta_p$ depends on the photosynthetic fractionation (${}^{*}\varepsilon_p$) and the isotopic composition of the oxygen in the water (${}^{*}\delta_w$) (Kaiser and Abe, 2012).

$$ {}^{*}\delta_p = (1 + {}^{*}\delta_w)(1 + {}^{*}\varepsilon_p) - 1 \quad (1.19)$$

For the isotopic composition of sea water relative to atmospheric O_2, there are three studies with uncertainties in ${}^{17}\delta_{VSMOW}$ smaller than 0.05 ‰, Barkan and Luz (2005), Barkan and Luz (2011) and Kaiser and Abe (2012). They report the delta values of the international

standard Vienna Standard Mean Ocean Water ($^*\delta_{VSMOW}$) relative to Air-O_2. $^{18}\delta_{VSMOW}$ is assumed to equal the isotope delta of mean sea water ($^{18}\delta_{sw}$). $^{17}\delta_{sw}$ is 5 ppm depleted relative to $^{17}\delta_{VSMOW}$.

The three studies cited above do not agree in their $^*\delta_{VSMOW}$ values. The values reported by Barkan and Luz in 2005 and 2011 are $^{17}\delta_{VSMOW}$(B&L05) = (-11.931±0.010) ‰ and $^{18}\delta_{VSMOW}$(B&L05) = (-23.320±0.020) ‰; $^{17}\delta_{VSMOW}$(B&L11) = (-11.883±0.012) ‰ and $^{18}\delta_{VSMOW}$(B&L11) = (-23.324±0.017) ‰ and for Kaiser and Abe (2012), $^{17}\delta_{VSMOW}$(K&A) = (-12.102±0.040) ‰ and $^{18}\delta_{VSMOW}$(K&A) = (-23.647±0.030) ‰. It is not clear yet what the reason is for the difference, but Kaiser and Abe (2012) point out that the B&L05 comparison between two international reference standards SLAP (Standard Light Antarctic Precipitation) vs. VSMOW is different from previous widely accepted measurements (Gonfiantini, 1977, 1978). Thus in this thesis, the values of $^*\delta_p$ using the values from Barkan and Luz (2011) and Kaiser and Abe (2012) (Table 1) are reported.

Fractionation during photosynthesis, $^*\varepsilon_p$ has been reported to differ for different species (Eisenstadt *et al.*, 2010; Helman *et al.*, 2005). In total they describe five species which are listed in Table 1 which are *Synechocystis* (Helman *et al.*, 2005, cyanobacteria), *Nannocloropsis oculata* (Eisenstadt *et al.*, 2010, Eustigmatophyte), *Phaeodactylum tricornutum* (Eisenstadt *et al.*, 2010, diatom), *Emiliania huxleyi* (Eisenstadt *et al.*, 2010, coccolithophore) and *Chlamydomonas reinhardtii* (Eisenstadt *et al.*, 2010, green alga). Kaiser and Abe (2012) mention that previous measurements of the fractionation during photosynthesis of $^{18}O/^{16}O$, $^{18}\varepsilon_p$ have shown little fractionation for *Phaeodactylum tricornutum* (Guy *et al.*, 1993) in contrast with the values reported by Eisenstadt (2010); as well as contradicting theoretical values of Tcherkez and Farquhar (2007). The values of Eisenstadt *et al.* (2010) and Helman *et al.* (2005) are currently the only available data for both $^{17}\varepsilon_p$ and $^{18}\varepsilon_p$ at the moment. Here is used the biological end-member delta value as suggested by Kaiser and Abe (2012) and Barkan and Luz (2011) from the specific species $^*\delta_p$ values (Table 1).

Table 1: Photosynthesis fractionation $^*\varepsilon_p$ reported in the literature for different species and associated $^*\delta_p$ for these species. $^*\delta_p$ are reported according to $^*\delta_{VSMOW}$ as measured by Barkan and Luz (2011) and Kaiser and Abe (2012). Averages of all the species $^*\delta_p$ for each of the $^*\delta_{VSMOW}$ are also reported.

			Kaiser and Abe (2012)		Barkan and Luz (2011)	
	$^{17}\varepsilon_p$	$^{18}\varepsilon_p$	$^{17}\delta_p$	$^{18}\delta_p$	$^{17}\delta_p$	$^{18}\delta_p$
Synechocystis	0.250	0.467	-11.860	-23.191	-11.641	-22.868
Nannochloropsis oculata	1.496	2.850	-10.629	-20.864	-10.410	-20.540
Phaeodactylum tricornutum	2.314	4.426	-9.821	-19.326	-9.601	-19.001
Emiliania huxleyi	3.050	5.814	-9.094	-17.970	-8.874	-17.646
Chlamydomonas reinhardtii	3.653	7.040	-8.498	-16.773	-8.278	-16.448
Average			-9.980	-19.625	-9.761	-19.301

1.5. Overview of research

The aim of this thesis is to understand marine biological production in two distinct areas of the Atlantic Ocean: one in the North Atlantic during a spring bloom and other in the subtropical gyre in the South Atlantic. The objective is to use two relatively new techniques to estimate *N* and *G* in surface waters by continuous measurements of O_2/Ar ratios and discrete of O_2 isotopologues.

In Chapter 2 is presented an automated custom-made O_2 and Ar extraction line built jointly by my fellow PhD student Johanna Gloël and me. This was used for the analysis of discrete samples for their analysis of O_2 isotopologues and O_2/Ar ratios. The work is based on the work of Barkan and Luz (2003) with some modifications. The line is capable of measuring one standard and six samples in a single run, with all the processes controlled remotely by a computer.

In Chapter 3 are described the methods used for the collection, analysis, and calibration of the data used for this PhD research.

In Chapter 4 are presented continuous measurements of O_2/Ar ratios and discrete oxygen triple isotope measurements in the South Atlantic gyre in the austral autumn of 2009. From these measurements is estimated net and gross production and discussed the metabolic balance of the gyre as well as comparing them with previous *in vitro* estimates of net and gross

production. Also are related the results of this study to ancillary data like surface chlorophyll concentrations, nutrient concentration, and fast repetition rate fluorometer data.

In Chapter 5 are presented continuous oxygen concentration data as well as discrete triple oxygen isotope data and O_2/Ar for the North Atlantic Bloom Experiment in May 2008. High spatial heterogeneity is found in the bloom. The data is used to discuss estimates of net production based on different techniques. Results from this study are compared with results from Quay *et al.* (2012) and Alkire *et al.* (Alkire *et al.*, 2012) that were obtained during the same experiment. With the help of a Lagrangian float to indicate a specific patch of the bloom, is evaluated the data for different stages of the bloom and the evolution of its species composition.

In Chapter 6 are described the general conclusions of this thesis and are discussed future research priorities.

Chapter 2. Custom built gas extraction line

2.1. Introduction

The aim of the gas extraction line is to obtain O_2 (oxygen) and Ar (argon) from sea water samples for later analysis. This is done by extracting the gas phase from the seawater samples and by removing H_2O (water vapour), CO_2 (carbon dioxide) and N_2 (nitrogen).

At the end of the extraction process, the O_2 and Ar gases are cryogenically collected on molecular sieve pellets for later analysis with an isotope ratio mass spectrometer (IRMS). H_2O, CO_2 and N_2 gases need to be removed because they can interfere with the O_2 analysis in the IRMS. The presence of N_2 increases the measured $^{17}\delta$ value. The CO_2 might fake the presence of N_2, when there is none because the CO^+ fragment generated from CO_2 in the ion source is isobaric with N_2. H_2O adheres to the interior surfaces of the mass spectrometer and reacts with the gases present in the mass spectrometer, thus reducing the signal.

This extraction line was built jointly with another PhD student, Johanna Gloël, under the supervision of Jan Kaiser. The line that we built is presented in this chapter and was based on the design of Barkan and Luz (2003), with some modifications. These modifications were: 1) The gas chromatographic (GC) column for the separation of the N_2 was put at 0 °C in our case versus -80 °C in the original design; 2) We added an extra initial preparation step of the samples on which the sample was extracted from the sampling bottles and collected into glass tubes with molecular sieve; 3) We used a different setup, which included a 10 port-2 position valve instead of four 3-port 2-position valves. 4) The amount of samples per run was 7 instead of 10. 5) Processed samples are not frozen in liquid helium but in molecular sieves on liquid nitrogen. Most of the building, programming and tests in the line were done jointly by Johanna Gloël and myself (unless otherwise stated), but the following method description and all analyses are entirely my own.

2.2. Preparation line for the extraction of gas phase and removal of H_2O

The first preparation step was to extract most of the water from the bottles. The majority of the gas sample is at this point in the headspace of the bottle. This was done by connecting the bottle upside down to a container under vacuum with a maximum pressure of 10 mbar. This way, as much water as possible was extracted without affecting the headspace.

After this preparation step the samples were passed manually through a preparation line. The H_2O vapour left was removed by two traps: one surrounding the sample bottle (T0)

and the other trap (T1) on the way to the collection vial. Each collection vial had 5 molecular sieve pellets (≈0.04 g/pellet of 5 Å pore size, grain size 80-100 mesh) at liquid N_2 temperature (-196 °C) where the gas sample was trapped. The procedure was as follows: the sample bottle was put into an isopropanol bath with dry ice at –78 °C (T0) and was connected to the preparation line. The reason that the temperature for traps T0 and T1 was -78 °C and not at liquid nitrogen temperature is that otherwise O_2, Ar and N_2 might be adsorbed on ice at liquid N_2 temperatures (Barkan and Luz, 2003). The neck of the sample bottle was evacuated until the pressure in the line was below 5×10^{-4} mbar as measured by gauge G0 in the line. The valve to the pump was closed and the valve of the bottle was opened. The initial pressure was recorded by G0. Once the vial was opened the sample started to freeze onto the molecular sieve in the vial at liquid N_2 temperature. This setup was kept for approximately 15 min, until at least 99.5 % of the sample was frozen on the molecular sieve. Then the vial was closed and disconnected for later use on the O_2-Ar extraction line on the same day.

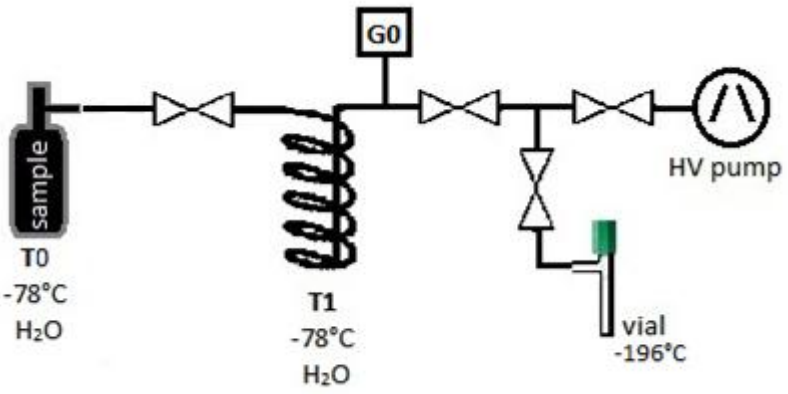

Figure 2.1: Diagram of the preparation line

2.3. The O_2-Ar extraction line

2.3.1. Description of the O_2-Ar line

The O_2-Ar line consists of several parts which can be grouped according to their function as the four different stages of sample treatment: I) sample inlet, II) removal of CO_2, III) removal of N_2 and IV) collection of samples.

I) Inlet:

Up to 7 vials can be connected to the inlet (Figure 2.2). Each vial connects via a Cajon Ultra Torr fitting to a springless diaphragm valve (6LVV-DPS5-C, Swagelok) with a pneumatic actuator. Each valve is connected to the system with 1/4" stainless steel tubing (SS) and Swagelok fittings. Only one vial at a time is open to the extraction system

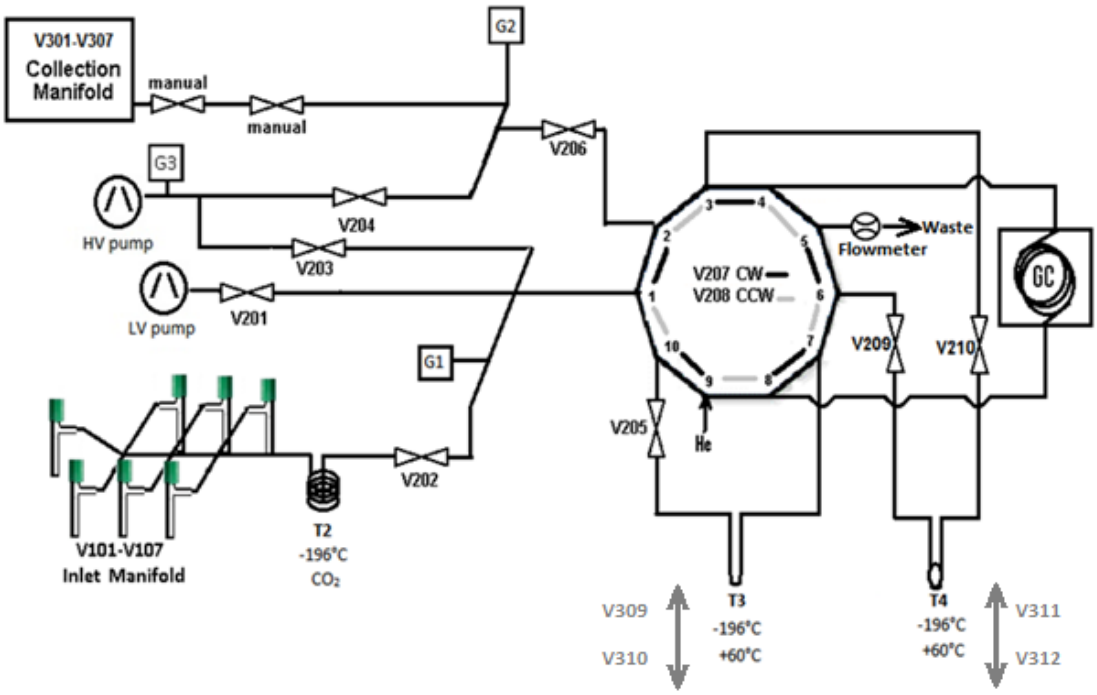

Figure 2.2: Schematic view of the extraction line with positions of valves (V), traps (T), pressure gauges (G1, G2 and G3), gas chromatographic column (GC), and pumps (LV, low vacuum diaphragm pump and HV, high vacuum turbo pump). Cold traps, V309-312 for moving dewars up and down.

II) Removal of CO_2:

Cryogenic trap, T2 (Figure 2.2) is used for the removal of CO_2 from the samples. The T2 glass trap is kept at -196 °C (liquid N_2) for freezing out the CO_2 in the sample. The trap is connected to the rest of the line with Cajon fittings. A pressure Pirani gauge (G1) located after T2 is used to record the movement of the gas.

III) Removal of N_2:

Two traps (T3 and T4) and a gas chromatographic column (GC) are used for the removal of N_2. The traps are kept at either -196 °C or 60 °C as desired. A gas chromatographic column between the traps separates the O_2 and Ar from the N_2. All these items are connected via a 2-position 10-port valve (Valco, A4L10UWM).

The traps T3 and T4 are built of 1/4"stainless steel tubing and filled with 5Å 80-100 mesh molecular sieve pellets with glass wool at both ends. When V205 is opened, the sample goes through the VALCO valve, is transferred to T3 which at this stage is -196 °C, while G1 records the movement of the sample. After most of the sample is frozen over on T3 (when the pressure in G1 is <0.5% of initial pressure), the Valco valve is changed to the second position and a flow of purified helium (He) at 8 ml min^{-1} is passed through T3, which is then heated to 60 °C by a heating tape. The He is grade CP (99.999 %) and is further purified on a 1.8 m-long column at -196 °C containing 45/60 mesh size molecular sieve 13X (Supelco). The sample is subsequently released from the molecular sieve in T3 to the chromatographic column held at 0 °C (Supelco, 13130-U).

The column allows the He to pass freely, while retaining O_2, Ar and N_2. Retention times for O_2 and Ar are similar while the retention time for N_2 is longer. This difference in the retention time allows to separate the O_2 and Ar from the N_2. Both O_2 and Ar go to T4 where they are adsorbed on the molecular sieve at -196 °C while the He flows out of the extraction system via a waste line. This waste line has sufficient volume (120 ml) to avoid any back flush from the room air to the line. After the O_2 and Ar have been released from the column and trapped on T4, the 10-port 2-position valve is switched again so that the N_2 can go to waste while the high vacuum pump removes the excess He while retaining the O_2 and Ar from T4 at -196 °C.

IV) Collection of the samples:

In the final stage T4 is isolated from the high vacuum pump and heated to 60 °C. One of the collection valves is opened and the sample starts to freeze in a collection tube, which has 0.05 g of molecular sieve (5Å 80-100 mesh size) and is kept at liquid N_2 temperature. The change in pressure due to the movement of the sample is recorded with the Pirani pressure gauge G2. After 5 min, most of the sample (>99.5 %) has frozen on the collection tube and the valve to the collection tube in the manifold is closed. After the sample has been collected, the

line is prepared for the next run by pumping down the excess of He for 30 minutes while T3 and T4 are heated at 180 °C for 5 minutes.

2.3.2. Automation of the O_2-Ar extraction line

The processes in the O_2-Ar extraction line were controlled from a computer running LabView (National Instruments, Texas, USA). This software is a graphical programming environment that allows controlling hardware as well as giving orders and taking measurements in the O_2-Ar line. The hardware consists of a chassis that connects a computer to the line through four modules. Two of these modules are the NI digital output modules which are used to send electrical signals that have two functions, first to control the temperature control box (in charge of heating the traps T3 and T4 when commanded by the program, see (Table 2.1) and secondly to control the 3 Clippard boards (EMC-12), which supply compressed air when commanded for opening/closing valves as well as for lowering/lifting the dewar vessels for T3 and T4 (Figure 2.3). The two other modules have an analogue input, one for reading voltages from thermocouples (for temperature) and the second one for reading voltages from the pressure gauges and the flow meter. The 10 port-2 position valve is switched by first opening valve V207 (or V208) and closing it 3 s later.

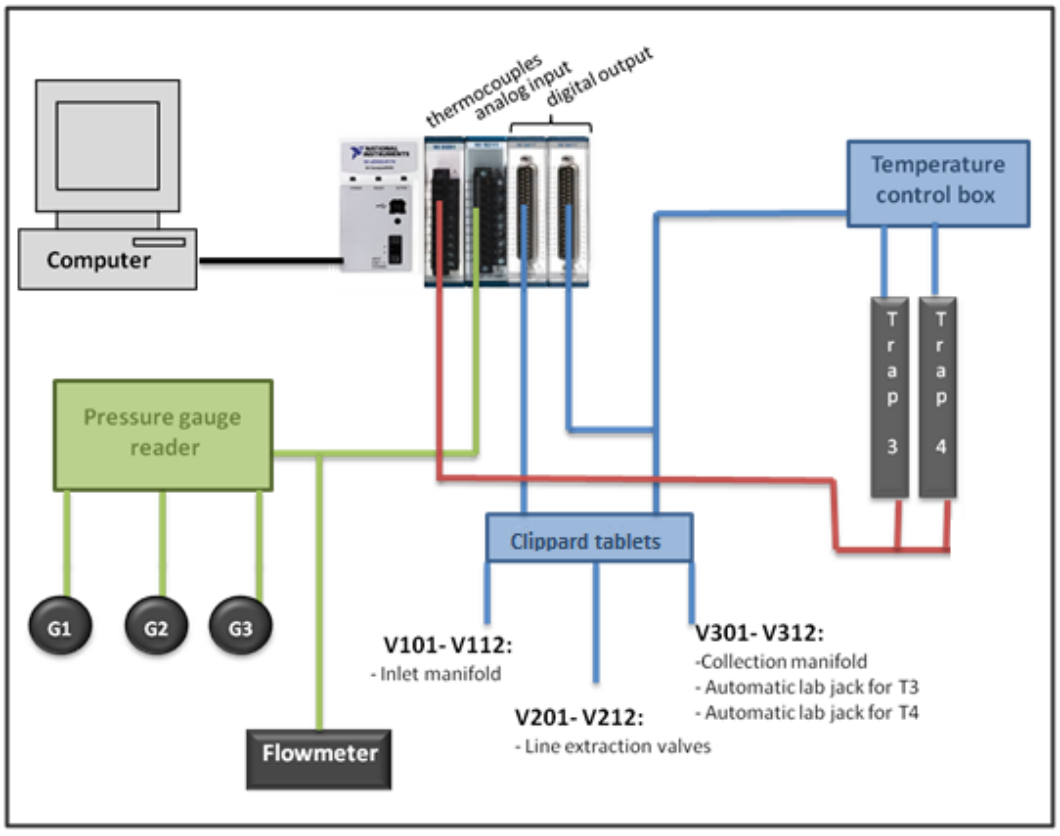

Figure 2.3: Schematic of the electronics wiring in the line with the data acquisition chassis

The fully automated extraction procedure consisted of a step-by-step command sequence case structure, which had the following steps:

1. Open valves V202, V203, V204, V205, V206, V209 and V210, while the position of the Valco valve is on 208 (counter clockwise position, CCW). The traps T3 and T4 are exposed to the high vacuum pump.
2. The software reads the pressure in G1, G2 and G3. If the readings are below 5×10^{-4} mbar for G1 and G2 and below 1.2×10^{-7} mbar for G3 the extraction can start. At this stage valves V203, V205 and V209 are closed. At the same time V309 and V311 are opened, which elevates the jacks with the dewars with LN_2 to immerse T3 and T4.
3. Open one of valve V10X of the sample (this can be any value from V101-V107).
4. Open V205 and the sample starts to freeze on T3. Maintain settings for 15 min.
5. Close V210 and open V209 and V207. V207 actuates the VALCO 10-port 2-way to the CW position, V207 is closed after 3 s but the CW position in the Valco remains such that the He flows through T3 until V210 (which has been kept closed) with He gas building up for 4 minutes in the line.
6. After this, open V210, so He flows to waste while the sample is kept in T3 adsorbed on the molecular sieve at -196 °C (liquid N_2 temperature).
7. After 2 minutes the He flow has become stable again. The dewar on T3 is lowered and T3 starts to be heated to 60 °C such that the sample on it is released and goes via the GC column (kept at 0 °C) to T4 (kept at -196 °C LN_2 temperature).
8. After 14 min V210 is closed and the VALCO valve is changed to the CCW position (by opening V208 and closing it after 3 s). T4, which is kept at -196 °C with LN_2 retains O_2 and Ar while the excess He is pumped away.
9. After 5 minutes of pumping, V204 is closed and V312 is opened such that the dewar surrounding T4 is lowered.
10. Start heating T4 to 60 °C. The corresponding valve on the collection manifold V30X (any of V301-V307 but analogous to the inlet valve V10X) opens and starts the freezing of the sample on the collection manifold which is at -196 °C. This lasts 5 min (when >99.5% of the sample has been frozen) into the collection finger.
11. Once the sample is frozen, valve V30_ is closed and V202-V206 and V209-V210 are opened. The line is evacuated for 30 minutes and T3 and T4 are heated at 180 °C before a new run can start.

Table 2.1: Key parts and equipment in the O_2-Ar line.

Item	Quantity	Model	Description	Use
Tubing			1/4" Stainless steel tubing	
			1/8" Stainless steel tubing	
Connections			1/4" and 1/8" Swagelok fittings	
			6 mm Cajun fittings	
			Filters for glass wool in T3 and T4	
Cold traps		T1, T2	Cryogenic glass trap	
		T3, T4	Cryogenic stainless steel trap	Filled with mol sieve and glass wool stoppers
VALCO valve	1	A4L10UWM	10 port 2 position valve, air actuated	Separation of O_2, Ar and N_2
Valves	22	6LVV-DPS5-C	Springless Diaphragm Valves	
Flow meter	1	AWM 3150V	Reads the flow	Shows the flow of O_2, Ar and N_2
Chromatographic column	1	13074-U	45/60 molecular sieve 5A (Supelco),9 ft	Separation of O_2, Ar and N_2
	1	13069-U	45/60 Molecular Sieve 13X (Supelco)	Purify the He carrier gas
Clippard	3	EMC-12	Control of valves and lab jacks	
Rope heaters	3	M2174/0295	Heating T3 and T4	
Pressure reader	1	TPG 256 A	Display and management of pressure readings	Connects pressure gauges and module
Pressure gauges	2	IKR 251	Compact cold cathode gauge	G1 and G2 pressure readings
	1	TPR 280	Compact Pirani gauge	GHV pressure readings
National Instruments	2	NI 9477	Digital output	Control of EMC-12 and temperature control box
	1	NI 9211	Analogue input for thermocouple readings	Temperature readings
	1	NI 9201	Analogue input	Flow meter and pressure readings
	1	NI cDAQ-9174	Chassis	Transmission of the modules to computer

2.3.3. Experiments to identify the optimal settings for the O_2-Ar extraction

The optimal timing for transferring the sample from vial to T3 and for transferring the sample from T4 to the collection manifold was found to be five minutes. In that time at least 99.5% of the initial sample pressure measured by G1 and G2 was frozen on T3 and the collection manifold.

The appropriate time for opening V210 after switching over (step 6 in the automation) was determined by me as follows: Figure 2.4 shows flow speed for an aliquot of O_2–Ar mixture which was frozen on T3 and then transferred to T4. The major differences between the chromatograms relate to the time when valve V210 was opened and He was allowed to flow to T4. As shown in Figure 2.4b there is no major difference in the chromatograms of the He flow independently of the time when V210 is opened.

Reverse flow through the flow meter can occur after opening valve V210 when the evacuated trap T4 fills up with He. The rate and duration of reverse flow decrease when the delay between switching over the 10-port valve and opening V210 is increased. This means that while V210 is closed, the accumulation of He gas avoids the creation of this negative flow. In the case of 4 minutes (see Figure 2.4a), the flow is positive directly after opening V210.

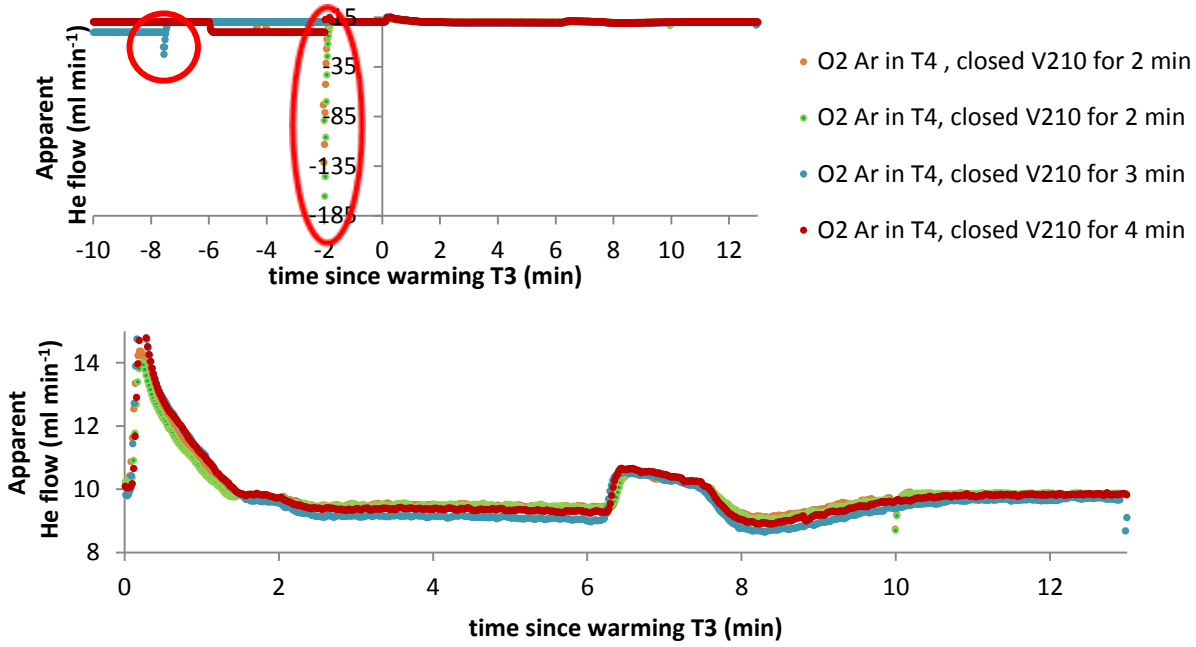

Figure 2.4: Chromatograms of aliquots of O_2-Ar when frozen on T4. Red circled areas show the time at which V210 was opened.

Johanna Gloël and Chris Brown determined the optimal temperature of the GC column. They found after several tests at different temperatures that at 0 °C the peaks of O_2 and Ar were separated sufficiently from N_2 for a reasonably rapid separation.

The exact retention times of O_2, Ar and N_2 on the GC column were determined as follows: T4 was left at room temperature, such that all the gases leaving from the column would directly go to waste and be recorded by the flow meter. In Figure 2.5, it can be seen that O_2 and Ar elute at the same time for both air and the O_2-Ar mixture. They are released between minutes 6.5 and 12.5 after heating T3. N_2 is released between 18 and 31 minutes, leaving a safe window for collecting the O_2 and Ar between 12.5 min and 18 min. We used 14 minutes in order to minimize contamination from N_2 as well as the duration of a run.

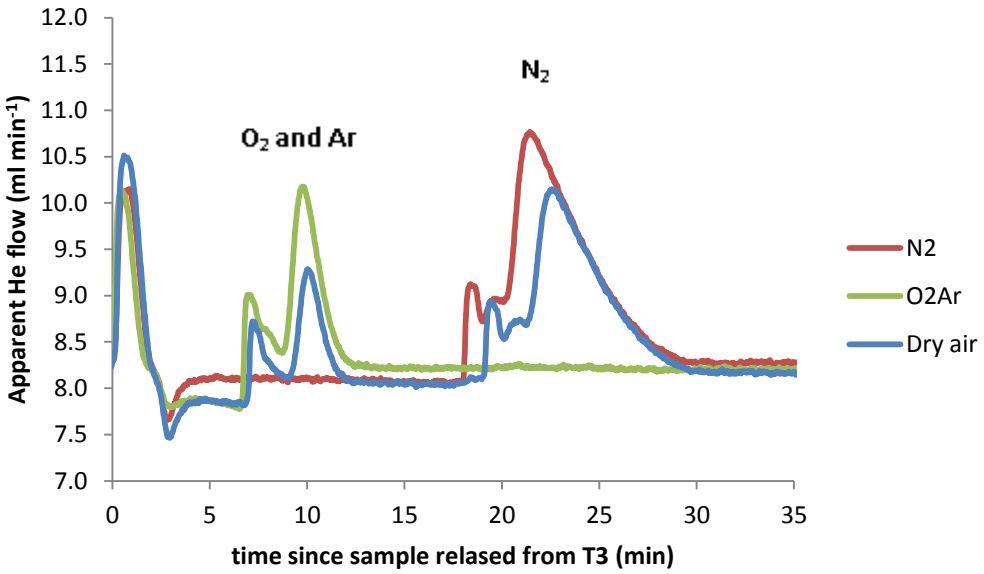

Figure 2.5: Chromatogram of N_2, O_2-Ar mixture and dry air after going through the gas chromatographic column indicating the retention times for O_2-Ar and N_2.

2.3.4. Performance tests of the line

Several tests were done in order to evaluate the performance in the line. These tests look at how different processes could cause isotopic fractionation, that is, change the isotopic composition of a sample going through the line. In order to do this, first it was evaluated how much the isotope ratio mass spectrometer (IRMS) could fractionate the samples. Secondly it was tested how samples would be affected by using the collection manifold and freezing them

in molecular sieve in the stainless steel tube. Thirdly it was evaluated the line itself by passing an aliquot of O_2–Ar gas mixture through the line in the same way as a sample, and then measured it in the IRMS versus the same unprocessed O_2-Ar mixture. Finally, the reproducibility was tested by passing several aliquots of the same dry air gas.

All these tests were evaluated by looking at the relative difference between a working reference (O_2-Ar mixture) and the sample. For the ^{17}O and ^{18}O isotopes this is be defined as:

$$^{*}\delta = {}^{*}R_{\text{sample}}/{}^{*}R_{\text{ref}} - 1 \quad (2.1)$$

$$\text{with } {}^{*}R = c({}^{*}\text{O})/c({}^{16}\text{O}) \quad (2.2)$$

where * stands for 17 and 18 for the $^{17}O^{16}O$ and $^{18}O^{16}O$ isotopologues of O_2. ^{16}O in the formula stands for O_2 formed by the two light isotopes ^{16}O, and ref refers to the working reference.

The relative difference in O_2/Ar ratios (*m*/*z* 32 for $^{16}O_2$ and *m*/*z* 40 for Ar) is:

$$\delta_{\text{sample/work\_ref}}(\text{O}_2/\text{Ar}) = \frac{R_{\text{sample}}(32/40)}{R_{\text{ref}}(32/40)} - 1 \quad (2.3)$$

The first test looked at the fractionation of the O_2-Ar mixture in the IRMS. It was done by comparing the same gas on standard and reference side (zero enrichment). This showed us that the IRMS was fractionating the sample, but to a very small degree (Table 2.2, row 1), which was within the precision of the instrument as seen from the standard deviations. In zero enrichments, the expected value is 0 for all parameters ($^{17}\delta$, $^{18}\delta$, $^{17}\Delta$ and $\delta(O_2/Ar)$). For 50 measurements, $^{17}\delta$ and $^{18}\delta$ were found to be -0.006±0.018 ‰ and -0.023±0.020 ‰ respectively, which resulted in a $^{17}\Delta$ excess of 6±20 ppm. The difference for $\delta(O_2/Ar)$ was 0.01±0.12 %.

For the second test it was prepared the collection manifold in the line in such a way that the Valco valve was in CW position (so that ports 1 and 2 in the VALCO were connected, see Figure 2.2), hence the gas would go straight from the inlet to the collection manifold. The

results of 13 samples are shown in Table 2.2, row 2. The difference between these results and the O_2-Ar zero enrichment were 0.002 ‰ for $^{17}\delta$, 0.010 for $^{18}\delta$ and -0.31 %for $\delta(O_2/Ar)$. All these results show enrichment in the heavier isotopes and molecules, which is positive for $^{17}\delta$ and $^{18}\delta$ and negative for $\delta(O_2/Ar)$. The direction of the fractionation points to a mass dependant fractionation. This means that the collection of the samples does fractionate but all samples and the dry air standard are affected in the same way. This reflects in $^{17}\Delta$ which does not change much, only 4 ppm which is within the standard deviation of the measurements of ±20 ppm for zero enrichment and ±9 ppm for this experiment. Also the standard deviation of each of the measurements (0.010 for $^{17}\delta$ and 0.021 for $^{18}\delta$) is within the standard deviation of the zero enrichment tests (0.018 for $^{17}\delta$ and 0.020 for $^{18}\delta$).

In the third experiment to test for possible fractionation a gas mixture of O_2-Ar was passed through the line and compared by IRMS against an unprocessed O_2-Ar mixture. The results are presented in Table 2.2, row 3. The results show that $^{17}\delta$ and $^{18}\delta$ are increased after passing through the line with an increase of 0.014 ‰ for $^{17}\delta$ and 0.040 ‰ for $^{18}\delta$ calculated as the difference of the O_2-Ar through the line minus the zero enrichment. On the other hand Barkan and Luz (2005) obtained less than 0.003 ‰ for both isotopes, in a similar experiment. Even though the difference here is larger than that of Barkan and Luz (2005), this small isotopic fractionation affects standards and samples in the same way and the effect cancels out for relative difference. The difference between the $^{17}\Delta$ of the processed and unprocessed sample indicates that the gas going through the line has a 6 ppm lower value. Such a small difference is irrelevant when compared with the standard deviation of the measurement of 13 ppm.

For $\delta(O_2/Ar)$ it was observed a decrease of the O_2/Ar ratio of 2 ‰ which agree well with the reported elemental changes of Barkan and Luz of 3 ‰ (2005). The changes in the elemental ratios are so small that their effect can be neglected.

Finally it was tested for drift in the O_2–Ar extraction line. This was done on consecutive measurements of dry air between 6th and 21st of May 2011. The results for this test are shown in Table 2.2 row 4. Variability of $^{17}\delta$, $^{18}\delta$ and $\delta(O_2/Ar)$ was within the variability of the O_2-Ar mixture going through the line.

Table 2.2: Results of the analysis by IRMS presented in rows in the following order: O_2-Ar zero enrichment; O_2-Ar frozen into the stainless steel tubes of the collection manifold; O_2-Ar through the line; and dry air through the line. Results are presented as the $^{17}O/^{16}O$ anomaly ($^{17}\delta$); $^{18}O/^{16}O$ anomaly ($^{18}\delta$); the relative difference in between the sample and standard in the O_2/Ar ratios as -$\delta(O_2/Ar)$-; and the ^{17}O excess ($^{17}\Delta$) as defined in chapter 1 and n is the number of measurements

	$^{17}\delta$ (‰)			$^{18}\delta$ (‰)			$\delta(O_2/Ar)$ (%)			$^{17}\Delta$ (ppm)			N
O_2-Ar zero enrichment	-0.006	±	0.018	-0.023	±	0.020	0.01	±	0.12	6	±	20	50
O_2-Ar frozen into SS	-0.004	±	0.010	-0.013	±	0.021	-0.30	±	0.16	2	±	9	13
O_2-Ar through the line	0.008	±	0.024	0.017	±	0.047	-0.21	±	0.23	0	±	13	19
dry air through line	-0.471	±	0.022	-0.864	±	0.043	13.31	±	0.13	-23	±	15	21

2.3.5. Comparison with other laboratories

A common practice for comparisons between laboratories is to measure the isotopic composition of O_2 in air saturated samples. The procedure for preparation of this water was similar to that of Barkan and Luz (2003) and it was prepared as follows. Artificial sea water was prepared by adding NaCl salt to a glass jar of 4 l in a water bath at 15.5 °C. The water was poisoned with $HgCl_2$ and was allowed to equilibrate for at least 24 h with the atmospheric air in the lab by stirring and bubbling it constantly. Equilibrated water was siphoned into sampling bottles and processed following the normal procedure described in this chapter after a period of equilibration of at least 24 h. The average ± standard deviation results for 12 samples were 0.354±0.063 ‰ for $^{17}\delta$, 0.653±0.122 ‰ for $^{18}\delta$, giving $^{17}\Delta$ = 15±5 ppm and with $\delta(O_2/Ar)$ = 0.20±0.18 %. The values here are referenced versus air which is the reference used in these studies. The $\delta(O_2/Ar)$ agrees well with what it was expected to fractionate if we compare the tests of O_2-Ar through the line with the zero enrichment which gives a difference of 0.22%. Moreover the standard deviation obtained for the equilibrated water 0.18% is comparable to those of the other tests (Table 2.2).

Despite the standard deviation of the measurements for $^{17}\delta$ (0.063 ‰) and $^{18}\delta$ (0.122 ‰) being greater than for the rest of the tests, the values for $^{17}\delta$ (0.354 ‰) and $^{18}\delta$ (0.653 ‰) were within the limits of the reported values in the literature (Table 2.3) for which the lowest reported values were of Reuer *et al*. (2007) of 0.340 ‰ and 0.642 ‰ and the highest by Luz and Barkan of 0.424 ‰ and 0.811 ‰ for $^{17}\delta$ and $^{18}\delta$ respectively.

Following from Luz and Barkan (2009) who reported a positive temperature dependence of $^{17}\Delta$ here is presented this relationship for all the reported data. Their

relationship was of $^{17}\Delta$=0.606 +1.7763 ϑ, which is very similar to the one reported here of $^{17}\Delta$=0.539 +2.5724 ϑ. The distance of our measurements (15±5) ppm to that of this relationship is of 4 ppm, which is within the standard deviation of our measurements. If we include only the relationship given by Luz and Barkan (2009) our measurements would be separated by only 3 ppm. This shows that despite the bigger uncertainties, our data agree well with other studies.

Table 2.3: Measurements of equilibrated waters for several studies. This table is modified version of table 1 compiled by Kaiser (2011b) adding the equilibrated measurements from this study. Reported are the source of the data, how the equilibrated waters were prepared, ϑ as the temperature of preparation, n the number of measurements , $^{17}O/^{16}O$ anomaly ($^{17}\delta$), $^{18}O/^{16}O$ anomaly ($^{18}\delta$) and the derived $^{17}\Delta$. A dash – means a value that has not been reported.

Reference	Preparation	ϑ (°C)	n	$^{17}\delta$ (‰)	$^{18}\delta$ (‰)	$^{17}\Delta$ (ppm)
Luz and Barkan (2000)	seawater	25	–	0.382	0.703	18 ± 2
Juranek and Quay (2005)	deionised	21	4	0.391	0.722	17 ± 3
Sarma *et al.* (2003)	distilled	22	10	0.371	0.691	13 ± 5
Sarma *et al*. (2006)	distilled	24	10	0.390	0.717	18 ± 2
Reuer *et al.* (2007)	35 g l^{-1} NaCl	11.2	14	0.416	0.792	6 ± 2
Reuer *et al.* (2007)	35 g l^{-1} NaCl	24.8	14	0.340	0.642	8 ± 3
Luz and Barkan (2009)	seawater	3.5	5	0.424	0.811	4 ± 1
Luz and Barkan (2009)	seawater	12.2	5	0.421	0.796	9 ± 1
Luz and Barkan (2009)	seawater	25	5	0.391	0.722	17 ± 2
Stanley *et al.* (2010)	–	–	–	0.382	0.722	8 ± 3
Stanley *et al.* (2010)	distilled	–	16	0.383	0.722	9 ± 2
This study	**35 g l^{-1} NaCl**	**15.5**	**13**	**0.354**	**0.653**	**15 ± 5**

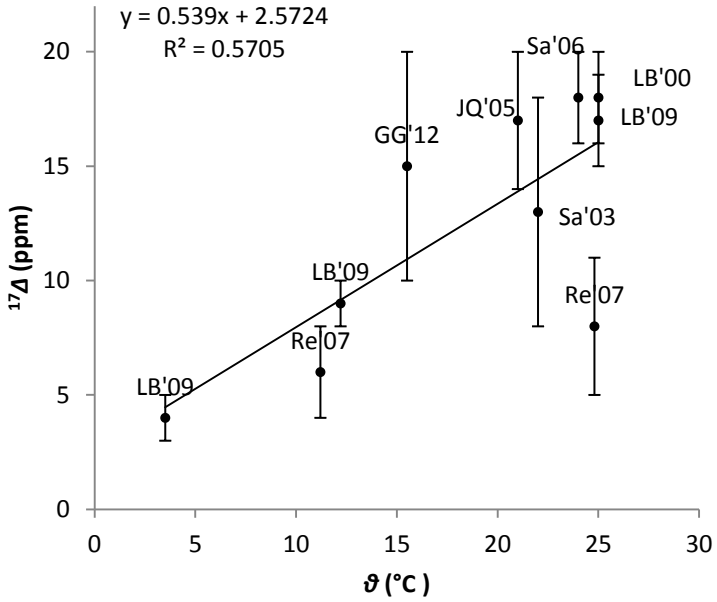

Figure 2.6: Relationship of temperature (ϑ) and $^{17}\Delta$ of values reported in the literature shown in Table 3. The labels on the points represent the authors of the data with Luz and Barkan (2000) (LB'00); Juranek and Quay (2005) (JQ'05); Sarma et al. (2003) (Sa'03); Sarma et al. (2006b) (Sa'06); Reuer et al. (2007) (Re'07); Luz and Barkan (2009) (LB'09); and this study (GG'12).

Chapter 3. Methods

3.1. Introduction

In this chapter is presented how core and ancillary data was collected, analysed and calibrated for the calculation of mixed-layer net community production (*N*) and gross production (*G*) from dissolved O_2 species in two different locations in Atlantic surface waters. *N* is estimated from continuous measurements of O_2/Ar in the underway seawater supply (USW) with a membrane inlet mass spectrometer (MIMS) and *G* from discrete samples collected in bottles and analysed later by isotope ratio mass spectrometry (IRMS).

First, are described the sampling campaigns, then the USW and the conductivity–temperature–depth (CTD) sensor on a rosette frame with Niskin bottles attached for sample collection. Next, is explained the sample collection and analysis of O_2 by the Winkler method and by an optode, followed by the sampling of O_2/Ar ratios by the MIMS as well as discrete sampling of seawater in evacuated bottles for analysis of O_2 isotopologues and O_2/Ar dissolved in the water. Finally, is described how it was evaluated the gas transfer coefficient *k* for use in the budget calculations of *N* and *G*.

3.2. Sampling campaigns

The North Atlantic Bloom experiment 2008 (NAB'08) took place south of Iceland in spring 2008. The data for this thesis was collected on the main process cruise on board R/V *Knorr*, which had cruise number KN193-03 and departed from Reykjavik on 1 May 2008 and returned to Reykjavik on 21 May. The region of study was centred on 26° W 61° N (Figure 3.1). The aim of NAB'08 was to study the evolution of the North Atlantic Spring Bloom in four dimensions (time, latitude, longitude and depth) using gliders and floats for the duration of the spring bloom. The cruise objectives were to calibrate and compare the productivity data derived from the autonomous platforms with other productivity measurement approaches (^{14}C incubation, oxygen isotopes).

The second cruise was cruise JC032 on board RRS *James Cook* along 24° S. The ship departed from Montevideo (Uruguay) on 7 March and arrived in Walvis Bay (Namibia) on 21 April 2009. This cruise was part of the CLIVAR (Climate Variability and Predictability) repeat hydrography program, which aims to repeat sections done during and since the WOCE (World Ocean Circulation Experiment) programme. The specific aim of the cruise was to assess the present-day circulation by calculating heat, freshwater and carbon transport across 24° S in comparison with previous cruises in the area like CLIVAR transects A9 at 19° S (1991), A10 at

30° S (1993, 2003) and 24° S (R/V *Oceanus*, 1983). The JC032 cruise was divided into 4 transects, with three sections across the Brazil Current and a fourth section that crossed the South Atlantic at 24° S (Figure 3.2). Samples for this research project were collected mainly from the USW with complementary measurements at CTD stations.

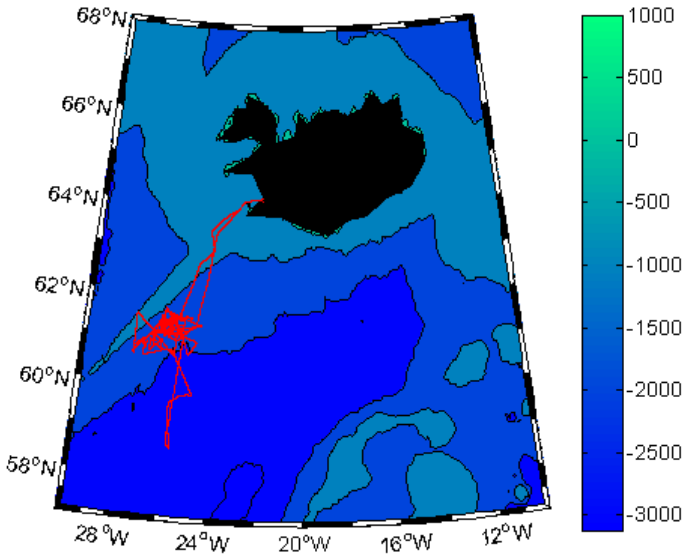

Figure 3.1: Map showing the location of the study. Blue colours represent depths in m as indicated by the colourbar. The black colouring represents depths above sea level, in this case Iceland. The red line represents the cruise track.

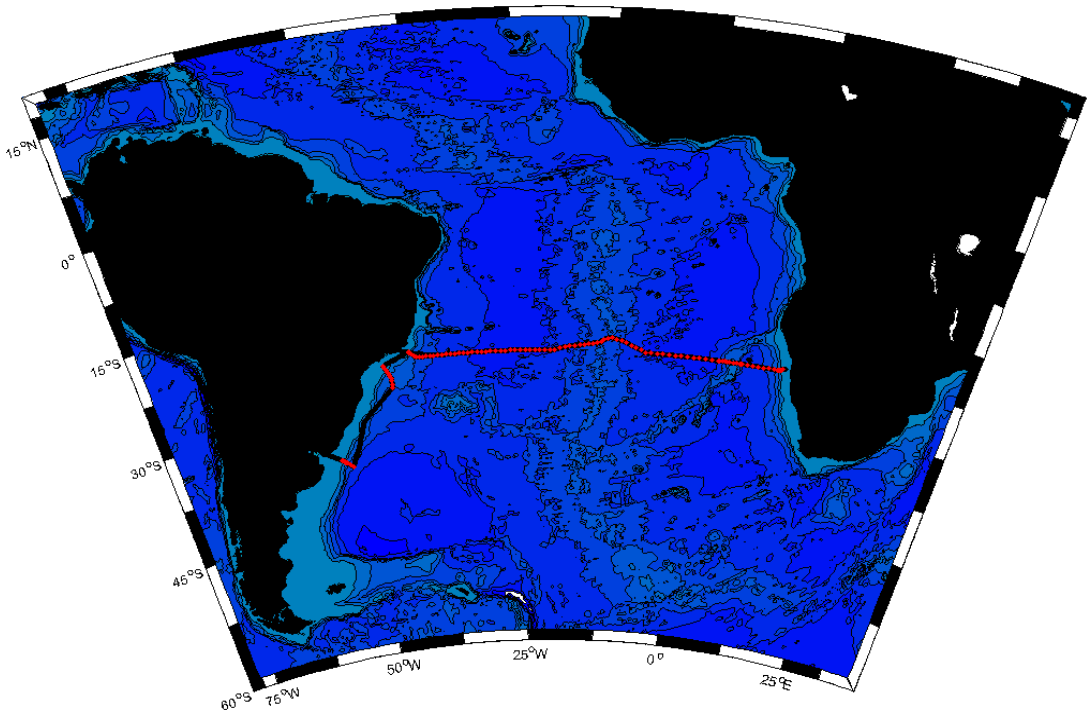

Figure 3.2: Map of the cruise track (black line) and the stations (red dots) occupied during cruise JC032, black lines indicate isobaths.

3.3. Underway sea water supply

The underway sea water supply (USW) provided seawater to the laboratories directly from the bow of the ship.

On R/V *Knorr* the intake was at 3.7 m below sea level. Sensors for measuring temperature and conductivity were located at the entrance of this intake (SBE). This temperature sensor was calibrated against the CTD sensor (Sea-Bird SBE 911plus) on the rosette frame. This was done with salinity as well.

For RRS *James Cook* the intake was located 5.5 m below the water level. A sensor in the intake of the USW continuously recorded sea surface temperature (SST, FSI OTM Remote Temperature 1370), and downstream from this, in the water sampling room, two conductivity sensors recorded salinity (FSI OCM conductivity 1333 and SBE45 Micro TSG 0231). SST was calibrated against 2 CTD temperature sensors. The salinity was calibrated against the CTD sensor and discrete samples taken every 4 h and analysed using a salinometer (Guildline Autosal 8400B, serial no. 68426).

Sampling the USW

The O_2 concentration, $c(O_2)$, in the surface waters was measured continuously by an optode, which was calibrated against discrete O_2 samples analysed by the Winkler method with the purpose of calculating the saturation state of the surface waters, expressed as saturation anomaly $\Delta(O_2)$. Also the oxygen-to-argon (O_2/Ar) ratio was determined continuously in the water from the USW with a MIMS. MIMS data were calibrated with equilibrated water standards.

Several meteorological sensors, including a barometer for atmospheric pressure and an anemometer to measure wind speed, were located on the foremast of both ships at 16 m (R/V Knorr) and 20 m (RRS James Cook) above sea level.

Table 3.1: Types and number of samples collected during KN193-03 and JC032. Also included is the purpose of their collection. *c*(O2) in the table stands for the concentration of O_2, *c*(Ar) the concentration of Ar, *Δ*(O_2/Ar) is the biological saturation anomaly of O_2 and $^{17}\delta$ and $^{18}\delta$ are the relative $^{17}O/^{16}O$ and $^{18}O/^{16}O$ isotope ratio differences between dissolved O_2 and atmospheric O_2.

		USW		CTD	
		no. samples	purpose	no. samples	purpose
Winkler	KN193-03	61 replicates	c(O2), calibrate optode	131	calibration CTD sensor
	JC032	149 replicates		others	
O_2 Optode	KN193-03	continuous	c(O_2), calculate c(Ar) MIMS	----	-------
	JC032			----	
MIMS	KN193-03	continuous	δ(O_2/Ar)	----	depth profile
	JC032			33	
Evacuated bottles	KN193-03	39	δ(O_2/Ar), $^{17}\delta$, $^{18}\delta$	51	O_2/Ar, $^{17}\delta$, $^{18}\delta$, comparison with USW
	JC032	57		17	

3.4. CTD

The CTD SBE 911 on R/V *Knorr* was mounted in a rosette with 24 Niskin bottles of 10 l. It had 2 temperature (SBE3T) and 2 salinity sensors (SBE4C). It also had O_2 and turbidity sensors, as well as an altimeter and fluorometer. A total of 131 samples, not including replicates, were collected for analysis of *c*(O_2) by Winkler titration in order to calibrate floats and gliders for the NAB'08 mission. In addition, 51 samples were collected from Niskin bottles for analysis of O_2 isotopologues.

The CTD on the RRS *James Cook* was a Seabird 911 plus and it was mounted on a rosette with four 20 l Niskin bottles and twenty 10 l Niskin bottles. It comprised a pressure sensor, 2 temperature sensors, 2 conductivity sensors, and had the following additional sensors: an oxygen sensor, a fluorometer, a transmissometer and a backscatter sensor. Samples were collected from the Niskin bottles to measure the salinity, and concentrations of O_2, inorganic nutrients (nitrate, phosphate and silicate), CFCs (chlorofluorocarbons), SF_6 (sulphur hexafluoride), inorganic carbon parameters (alkalinity and dissolved inorganic carbon, DIC), total chlorophyll and O_2/Ar ratios.

On JC032 a total of 17 evacuated headspace bottles (2 full depth profiles and 4 surface only stations) were taken for subsequent analysis of the O_2/Ar ratio and O_2 isotopologues ratios using an Isotope Ratio Mass Spectrometer (IRMS) at the University of East Anglia (UEA).

3.5. Sample collection and analysis

3.5.1. Winkler analysis

Samples for Winkler O_2 analysis were collected in conical glass flasks (Pyrex, Mexico) with a nominal volume of 125 cm^3. The accurate volumes at 20 °C were determined gravimetrically before the cruise. The flasks were filled directly from the USW. All the tubing used for filling the samples was soaked for at least 24 h to avoid the formation of bubbles in the tubing. Every bottle was filled by putting the tubing at the bottom of the bottle and by letting it overflow for three bottle volumes. This procedure avoids any contamination with bubbles. Once all the samples had been collected, the reagents were added and the bottles were kept for future analysis. Oxygen analyses were carried out using automated Winkler titrators. The titration unit for R/V *Knorr* was equipped with a photometric end point detector (custom built); the one for RRS *James Cook* was based on an amperometric end point detector (Winkler Ω-Metrohm, 794 DMS Titrino).

Following Dickson (1995), blanks and standards were analysed during each run. Both blanks and standards were prepared with the reference material potassium iodate (KIO_3) and were used for the calculation of the $c(O_2)$ present in the samples. Blanks are used to account for possible interference with the reagents by other species present in the water. The standards are analysed to check for drift in the standard solution of thiosulphate ($Na_2S_2O_3$). The formulas used for the calculation are presented here:

$$m_{\text{sample}} = [V_{\text{bottle}}(1 + 10^{-5}(T_{\text{fix}}/℃ - 20))/-2\ \text{cm}^3]\ \rho_{\text{sw}} \tag{3.1}$$

$$n(O_2) = \frac{1.5\ (V - V_{\text{blank}})\ V_{KIO_3}\ c(KIO_3)}{V_{\text{std}} - V_{\text{blank}}} \tag{3.2}$$

$$c(O_2) = \frac{-7.6x10^{-8}\ \text{mol}}{m_{\text{sample}}} \tag{3.3}$$

The mass of the sample (m_{sample}) is calculated from the bottle volume at 20 °C (V_{bottle}) while taking into account the change in volume due to temperature (Culberson, 1991) with T_{fix} being the Celsius temperature during sample fixation and ρ_{sw} the density of sea water at in situ temperature. The amount of O_2, $n(O_2)$, is calculated from the volume of thiosulphate used to

titrate the sample (V), the volume of the blank (V_{blank}), the volume of the standard (V_{std}), the volume of KIO_3 added in the preparation of the standards (V_{KIO3}) and the concentration of the reference material, $c(KIO_3)$. The concentration of O_2, $c(O_2)$, is calculated from $n(O_2)$, while taking into account the O_2 content of the reagents (7.6×10^{-8} mol) used for titrating the samples (sodium hydroxide NaOH, sodium iodide NaI, manganese chloride $MnCl_2$).

Calibrations for each specific cruise are given below.

For KN193-03 blanks were prepared during two titration calibration sessions with distilled water. Because both values were statistically identical 0.0033±0.0019 ml (average ± standard deviation) and 0.0019±0.0013 ml, Table 3.2-a), and the same reagents were used in both sessions, an average of 0.0026 ml was used for the whole cruise. Standards to measure the thiosulphate concentration were measured in 11 sessions (Table 3.2-b). These standards were prepared with a reference material KIO_3. This solution was prepared gravimetrically at UEA using a potassium iodate certified reference material (Fluka, 60386) before the cruise.

As seen in Table 3.2-b initially it appeared that the thiosulphate decreased in concentration over time. This is the opposite of what is expected. So once on land the cruise KIO_3 solution was compared against a set of fresh new KIO_3 solutions. It appeared that the cruise KIO_3 had increased in strength by 0.24% since before the cruise. This explained the apparent decrease in the thiosulphate during the cruise. Assuming a linear concentration change over time, the concentration of thiosulphate was stable (Table 3.2-b column 6). Therefore, it was decided to use an average of the thiosulphate concentrations for the calculation of the O_2 concentration of the samples.

Table 3.2-a: Blanks prepared for KN193-03 with information on when they were prepared, the number of replicates prepared (# rep), the average value of the replicates, the standard deviation (st dev) and the standard error (st error, expressed as the st dev over the average in %).

Date	# rep	V blank(cm^{-3})		
		average	stdev	st error
02/05/2008	4	0.0033	0.0019	57%
07/05/2008	6	0.0019	0.0013	68%

Table 3.2-b: Standards prepared for KN193-03 with information on when they were prepared, the number of replicates prepared (# rep), the average concentration of the *c*($Na_2S_2O_3$) given by the replicates, the standard deviation (st dev) , the standard error (st error, expressed as the st dev over the average) and the *c*($Na_2S_2O_3$) corrected for a change in concentration of KIO3 (corr KIO_3, see text for details).

date	# rep	*c*($Na_2S_2O_3$)/(mol l^{-1})			
		average	st dev	st error	corr KIO_3
01/05/2008	6	0.2017	2.52E-04	0.12%	0.2017
01/05/2008	4	0.2018	1.81E-04	0.09%	0.2018
03/05/2008	5	0.2017	3.20E-04	0.16%	0.2017
05/05/2008	4	0.2017	2.83E-04	0.14%	0.2018
07/05/2008	6	0.2016	4.77E-04	0.24%	0.2018
13/05/2008	3	0.2011	8.40E-05	0.04%	0.2014
14/05/2008	5	0.2015	1.17E-04	0.06%	0.2019
16/05/2008	4	0.2013	2.59E-04	0.13%	0.2017
17/05/2008	4	0.2013	1.48E-04	0.07%	0.2018
18/05/2008	6	0.2014	1.68E-04	0.08%	0.2019
19/05/2008	4	0.2014	3.37E-04	0.17%	0.2019

The reason for the apparent increase in the KIO_3 concentration is unclear, but is suspected that one of the ports on the lid of the KIO_3 reservoir was not sealed, which would have led to evaporation.

For JC032, analyses of blanks and standard calibrations were carried out jointly with the O_2/nutrients team from the National Oceanography Centre, Southampton (NOC). On the cruise a total of 149 USW water samples (329 analyses including replicates, usually duplicates and sometimes triplicates) were measured for their O_2 content in a total of 10 sessions. For each calibration one set of blanks and one set of standards were prepared following Dickson (1995). Because there was a shortage of KIO_3, all standards were prepared with 5 cm^3 instead of 10 cm^3 (except for the first session). Table 3.3 lists all the sessions with their blanks and standards. Two different solutions of thiosulphate were used: thio1 from the beginning of the cruise to 26 March and thio2 from then onwards. Session 9 calibration data was not used because the calibration result was inconsistent and had a high standard deviation (see Figure 3.3); probably due to errors during preparation of the calibration mixtures. For the calibration of the Winkler samples, the average of all the blanks from the cruise was used. For the standards, the average thiosulphate concentration for 3 different sets of sessions was used: the first set includes the first 2 sessions with the first thiosulphate solution, the second set only includes session 3 with the new thiosulphate solution that had a slightly higher concentration

than the third set, and finally the third set that included the rest of the titration sessions during which the thiosulphate concentration were roughly constant (Figure 3.3).

Regarding the precision of the measurements, the average of the standard deviations of all the replicates collected during this cruise is 0.1 µmol kg^{-1} which is smaller than the recommendation of 0.5 µmol kg^{-1} from the JGOFS protocol (Dickson and Goyet, 1994).

Table 3.3: Standard and blank sessions for JC032. In the columns are represented the number of replicates (# rep), the average volume for the blanks and the average thiosulphate concentration $c(Na_2(S_2O_3))$ with their standard deviation (st dev) and standard error (st error, which is the standard deviation divided by the average).

thio	session	blanks (ml)				$c(Na_2(S_2O_3))/(mol\ l^{-1})$			
		# rep	average	std dev	std error	# rep	average	std dev	std error
thio 1	1	5	0.0029	0.0009	31%	5	0.1981	0.0006	0.30%
	2	5	0.0030	0.0014	46%	5	0.1985	0.0006	0.30%
thio 2	3	5	0.0022	0.0022	100%	6	0.1994	0.0005	0.26%
	4	5	0.0005	0.0005	100%	6	0.2000	0.0007	0.33%
	5	5	0.0015	0.0010	67%	5	0.2002	0.0005	0.23%
	6	5	0.0019	0.0016	86%	5	0.2006	0.0005	0.26%
	7	6	0.0017	0.0004	26%	5	0.2001	0.0004	0.20%
	8	5	0.0015	0.0006	41%	7	0.2005	0.0002	0.12%
	9	5	0.0021	0.0002	11%	5	0.1980	0.0017	0.84%
	10	5	0.0019	0.0007	39%	5	0.2002	0.0002	0.12%

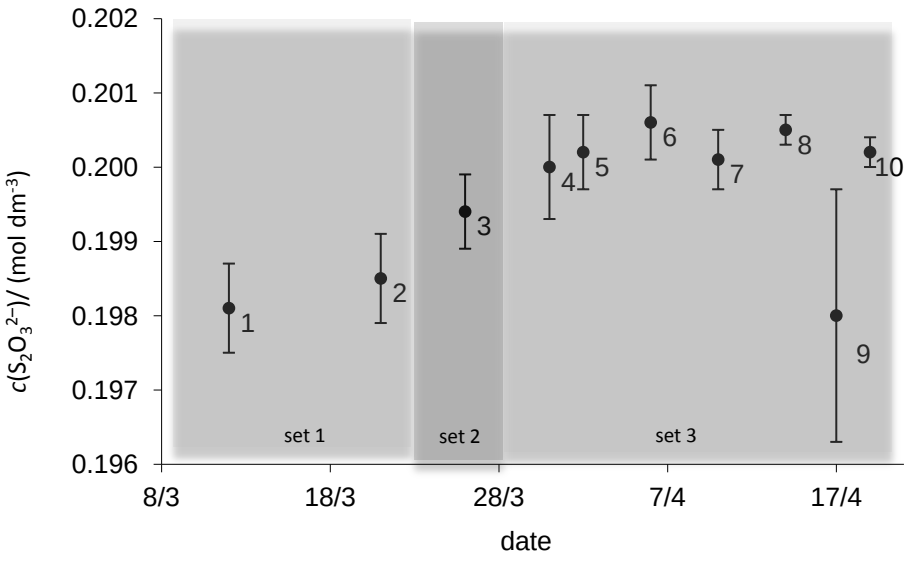

Figure 3.3: Concentration of sodium thiosulphate during cruise JC032 with error bars showing the standard deviation.

3.5.2. Optode

The aim of measuring with an optode was to have continuous measurements of the concentration of O_2 in surface waters. Combination of these O_2 concentrations with the O_2/Ar data from the MIMS allows calculation of the Ar concentrations and therefore of the physical O_2 super-saturation.

Technical description of optode measurements

The optode (Aanderaa Data Instruments, Norway, model 3835) is an instrument capable of measuring the concentration of oxygen in water. The principle behind the measurement is the special property of a substance called luminophore that changes its fluorescence and its decay time depending on the presence and concentration of certain materials. In the case of the optode the luminophore is a platinum porphyrine complex embedded in a foil that reacts with the O_2 gas molecule. This phenomenon is called dynamic luminescence quenching Tengberg *et al.* (2006) .

The platinum porphyrine is mounted on a PVC layer in a chamber inside the optode. To protect the luminophore it is separated from the outside with a gas permeable coating that eliminates possible contact with direct sunlight and separates it from the surroundings.

The optode is composed of different parts: The sensing foil, which contains the platinum porphyrine, and two LEDs. A blue LED is used for the excitation of the luminophore and the red LED is used for corrections if needed. Between the two sits a photodiode detector.

The gas present in the water passes through the coating to the chamber by diffusion. At the same time the porphyrine is excited with an intermittent pulse of the blue LED. The O_2 molecules constantly interact with the surface of the porphyrine and produce a change in the fluorescence (numerically described by the Stern-Volmer effect). The fluorescence is measured by the photodiode and saved to the computer as the D_phase, which is the change of the response time due to the presence of O_2.

Since the change of intensity in the fluorescence can drift over time, it is preferable to use the change of the fluorescence decay time, which decreases at higher concentrations of O_2 (Tengberg *et al.*, 2006).

The optode was mounted inside a bucket where tubing from the USW was seated at the bottom such that the renewal of water would be from bottom to top. The optode made continuous measurements every 10 s. The optode measurements were extracted at the times at which discrete samples for Winkler analyses were taken, such that they could be compared to identify outliers and calibrate the optode.

Analysis, calibration and comparison of different calibration methods

For KN193-03 a total of 61 USW samples for O_2 were collected (141 including replicates), the average standard deviation of the replicates was of 0.31 µmol kg^{-1}.

Calibration of the USW was done by comparing the D_phase of the discrete samples collected from the USW to the D_phase of the optode (Figure 3.4). The discrete samples concentration was converted to an equivalent D_phase by mathematically inverting the polynomial given as sensing foil calibration by the manufacturer. From this, a calibration function was derived by linear regression and used to correct the raw D_phase readings of the optode. The corrected D_phase readings were then converted back to $c(O_2)$ using again the polynomial given by the manufacturer. The average ± standard deviation of the residuals was 0.00±0.91 µmol kg^{-1}.

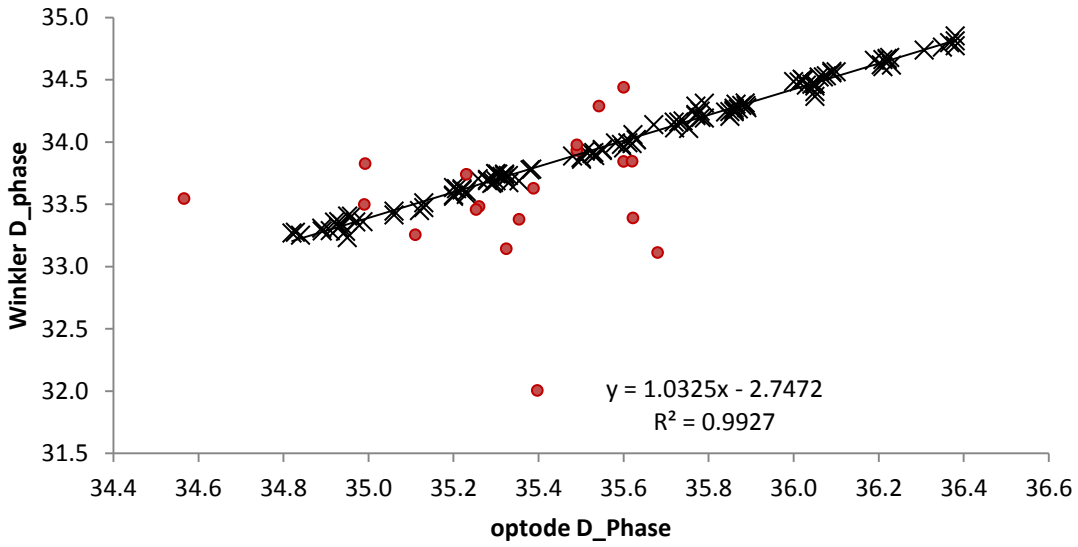

Figure 3.4: Calibration curve for O_2 optode against the discrete Winkler solved D_Phase. Black crosses depict the data used of the calibration in red are the data considered to be outliers.

To calibrate the CTD O_2 sensor a direct comparison of the sensor measurement with discrete Winkler measurements was carried out.

The data were calibrated with 3 different sets of calibration. The first set ran from the beginning of the cruise until day 125 (I), the second set included day 125 to 135 (II) and the third would be from day 135 until the end of the cruise (III). Sets I and III were calculated as a

simple linear regression of $c(O_2)$ measured by the CTD sensor vs. the $c(O_2)$ measured by discrete Winkler samples. For set II, a second-degree polynomial was used for calibration. It depended on $c(O_2)$ measured by the CTD and year-day. The standard deviation of the all the residuals from the three calibrations is 0.65 µmol kg^{-1}. The relationships are presented in Table 3.4.

Table 3.4: Calibration equations for the O_2 data from the CTD. $c(O_2)$ is the calibrated concentration of O_2, YD represents the year-day and c(O2)CTD represents the $c(O_2)$ measured by the CTD sensor. All Oxygen concentrations are in µmol kg^{-1}.

	yearday	equation	r^2
I	start-125	$c(O_2) = 1.02 \times c(O_2)_{CTD} + 7.46$	0.9992
II	125-135	$c(O_2) = 1.06 \times c(O_2)_{CTD} - 0.07 \times YD^2 + 19.54 \times YD - 1304.06$	0.9978
III	135-end	$c(O_2) = 1.07 \times c(O_2)_{CTD} - 1.22$	0.9966

For JC032 three different methods were compared for the calibration of the optode data.

The first method employed a "D_phase inversion method" where the Winkler concentrations for the USW samples were transformed to D_phase values by the equations given by the manufacturer **Aanderaa**. These manufacturer equations are expressed in equations 3.4 and 3.5, where a_0, a_1, a_2, a_3, a_4, b_{x0}, b_{x1}, b_{x2}, b_{x3}, b_{x4} are constants given by the manufacturer and shown in Table 3.5, T is the temperature in °C as measured by the optode and P is the D_phase.

$$c(O_2) = a_0 + a_1 P + a_2 P^2 + a_3 P^3 + a_4 P^4 \quad (3.4)$$

$$a_x = b_{x0} + b_{x1} T + b_{x2} T^2 + b_{x3} T^3 \quad (3.5)$$

Table 3.5: Values for the coefficients in equation 3.5 where x is substituted for 0, 1, 2, 3 and 4.

b_{00}	4945.29	b_{10}	-269.898	b_{20}	5.976379	b_{30}	-0.06181859	b_{40}	0.000245035
b_{01}	-167.764	b_{11}	8.31507	b_{21}	-0.167971	b_{31}	0.001602029	b_{41}	-5.90218E-06
b_{02}	3.41751	b_{12}	-0.174439	b_{22}	3.75245E-03	b_{32}	-3.91116E-05	b_{42}	1.59999E-07
b_{03}	-3.07691E-02	b_{13}	1.628069E-03	b_{23}	-3.6796E-05	b_{33}	4.027959E-07	b_{43}	-1.71557E-09

The Winkler D_phase was regressed linearly versus the D_phase measured by the optode in order to obtain a calibration function. The residuals calculated with the calibration function are shown in Table 3.6.

The second method was based on the Stern-Volmer equation that describes the phenomenon of dynamic luminescence quenching. In this case, $c(O_2)$ measured by the optode would be calculated from the D_phase as in equations 3.6, 3.7, 3.8 and 3.9 and then compared with the Winkler measurements.

$$c(\mathrm{O}_2) = [(P_0/P_c) - 1]/K_{sv} \quad (3.6)$$

$$P_0 = 1 + c_1 T \quad (3.7)$$

$$P_c = c_2 + c_3 P \quad (3.8)$$

$$K_{sv} = c_4 + c_5 T + c_6 T^2 \quad (3.9)$$

Where: P_0/P_c is the ratio of the phase shift in the absence of O_2 (P_0) and the phase shift in the presence of O_2 (P_c), P is the D_phase, T the temperature in °C and K_{sv} is the Stern-Volmer constant.

The values for the constants c_1 to c_6 were obtained by a non-linear parameter estimation (or unconstrained nonlinear optimisation), which finds the minimum of a scalar function of several variables, starting at an initial estimate. The initial values given to the coefficients from c_1 to c_6 were 0.017, 0, 0, 0.003, 0 and 0. The obtained best fitting set of coefficients from c_1 to c_6 are: -6.43×10^{-4}, -5.34×10^{-3}, 1.41×10^{-2}, 1.67×10^{-3}, 8.15×10^{-5} and 9.35×10^{-7}.

In the third method a multivariate polynomial dependent on temperature and the D_phase from the optode is fitted to the concentrations of O_2 measured by Winkler titration Uchida *et al.* (2008) . The polynomial was:

$$c(O_2) = d_0 + d_1 T + d_2 T^2 + d_3 T^3 + d_4 P + d_5 P^2 + d_6 TP \quad (3.10)$$

Where P expresses the D_phase, T the temperature (in °C) and the coefficients d_0 to d_6 (±standard error) are 11033 ±1566, -181.77 ±13.85, 1.3481 ±0.1096, -0.010488 ±0.001722, -503.04 ±84.18, 5.9982 ±1.1240 and 3.8344 ±0.3969. These coefficients were determined by least squares.

The residuals for each of the methods, calculated as the expected value minus the measured value, are compared in Table 3.6.

Table 3.6: Comparison of the different methods for calibrating the optode data with Winkler analysis (std dev is the standard deviation and r^2 the coefficient of determination) for JC032.

Method	std dev (µmol kg^{-1})	r^2	# data	outliers removed / number of data
1 Aanderaa all	0.99	0.943	218*	0%
1 Aanderaa ± 3 stdev	0.82	0.950	207	5%
1 Aanderaa ± 2 stdev	0.47	0.988	170	22%
2 Stern-Volmer equation all	1.68	----	218	0%
2 Stern-Volmer equation ±3stdev	1.51	----	215	1%
2 Stern-Volmer equation ±2stdev	0.5	----	181	17%
3 Multivariate polynomial all	0.99	0.962	218	0%
3 Multivariate polynomial ± 3stdev	0.69	0.965	208	5%
3 Multivariate polynomial ± 2stdev	0.48	0.987	181	17%

(*) The initial number of data is more than the number of 149 samples and less than the number of analyses including replicates (329). This is because replicates, which were collected in periods of high variability (this were identified when even the optode signal varied by more than 0.6 µmol kg^{-1} for those replicates) were considered independent.

The best fit of the data appears when we remove the outliers (distance from the regression line >2 standard deviations (σ) in all of the three methods, but a high proportion of data is lost (at least 17 %). The 3σ criterion shows an almost equally good fit and 5% or less of the data is removed. The 3σ criterion gives different standard deviations for each method, namely 1.51 µmol kg^{-1} for the Stern-Volmer fit, 0.82 µmol kg^{-1} for the manufacturer calibration and 0.69 µmol kg^{-1} for the multivariate analysis. The multivariate analysis with the 3σ criterion is used for calibration of the optode.

3.5.3. Continuous MIMS data

The O_2/Ar ratio has been measured continuously with a membrane inlet mass spectrometer as described by Kaiser et al. (2005). Similar instrument have been deployed by several other authors (Kana et al. (1994), Tortell (2005a), Guéguen and Tortell (2008), Nemcek et al. (2008) and Stanley *et al.* (2010)). The MIMS consists of a quadrupole mass spectrometer and a membrane module to extract the gases dissolved in water.

3.5.3.1. Set up of the MIMS in the shipboard laboratory

The MIMS is mounted next to a sink. It consists of 2 different parts: The first part extracts the gases from the water and comprises a water-pump, tubing and a semi-permeable membrane. The second part is a quadrupole mass spectrometer (QMS), which detects different gas species. Gases dissolved in seawater arrive through a semi-permeable membrane that allows gases through but not water (Figure 3.5).

The pump in the first part of the MIMS (Figure 3.5) brings the water to the semi-permeable membrane where another pump in the QMS creates a gradient so gases travel from the water, through the semi-permeable membrane, to the QMS. In the QMS the gas is ionized, accelerated and analysed through four parallel rods arranged as a quadrupole. One pair of opposite rods have the same direct current voltage applied while the potential difference between the other two rods oscillates and extracts ions depending on their mass-to-charge (*m/z*) ratios. This is why the instrument is capable of detecting several gases nearly simultaneously (every 10 s) by just changing the frequency. It was measured *m/z* 32 (O_2) and 40(Ar), as well as others with *m/z* 28 (N_2), 29 ($^{14}N^{15}N$), 44 (CO_2) and 18 (H_2O).

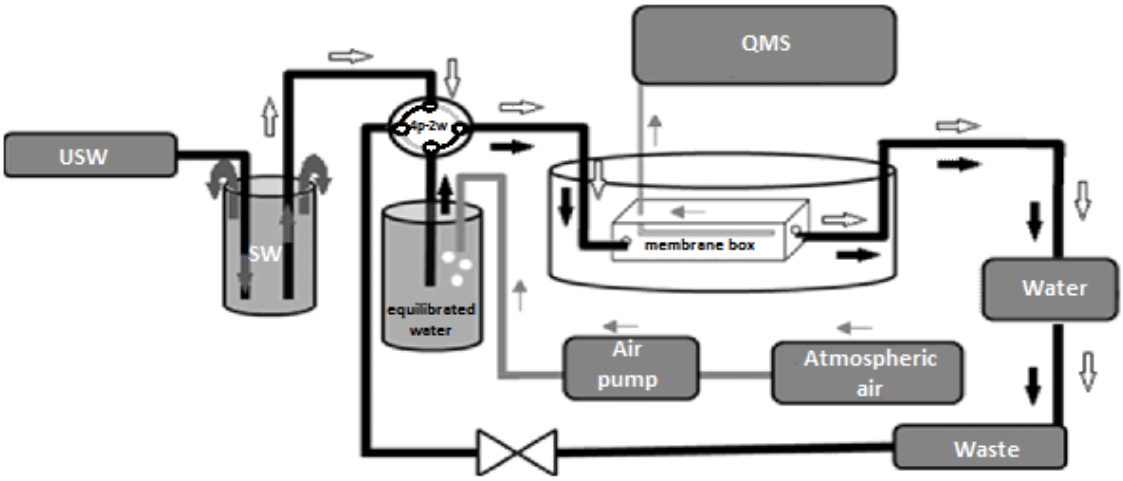

Figure 3.5: Set up of the MIMS on the cruises. USW stands for underway sea water, SW for sea water, 4p-2w four port-2 way valve and QMS is the quadrupole mass spectrometer.

For both cruises the overall setup was very similar. The only differences were: First, the membrane enclosure was different on each cruise: for KN193-03 a cartridge (Membrana Liquicel) was used and for JC032 a custom built membrane box, which contained a tubular

Teflon AF membrane (Random Technologies), was used. Second, as the data was collected during a bloom, a filter in the intake to the MIMS on KN193-03 was fitted, so the system would not become clogged up with plankton cells.

3.5.3.2. Analysis and calibration for KN193-03

No equilibrated waters were prepared for this cruise due to technical problems and the data could not be calibrated against the discrete O_2/Ar samples because it is likely that the cartridge use for this cruise kept clogging and was of slow response so there was not linear relationship between the continuous O_2/Ar and the discrete samples (Figure 3.6).

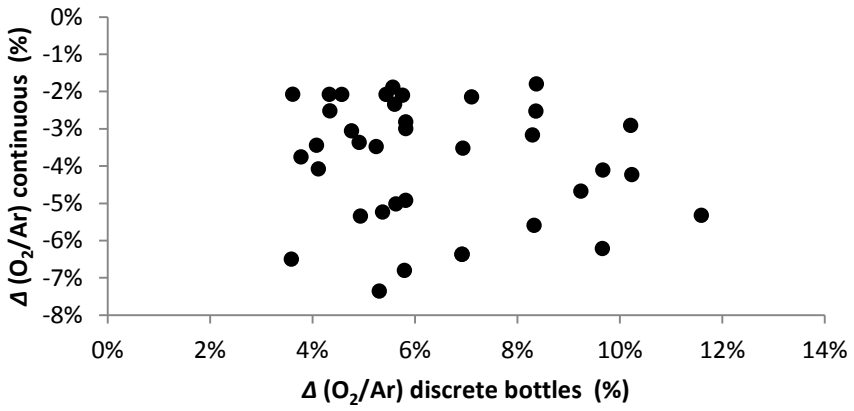

Figure 3.6: Comparison of the $\Delta(O_2/Ar)$ as measured by the IRMS versus the MIMS

3.5.3.3. Analysis and calibration for JC032

To test for drift in the mass spectrometer *m/z* 28, 32, and 40 were measured in a range of 5 different mass-to-charge ratios (*m*/*z*) separated by 0.03 (see Table 3.7). This is done to check whether the strongest signal (therefore the most accurate) is always centred on the same *m/z*.

Table 3.7: The mass to charge ratios m/z and the corresponding molecules measured on the MIMS on JC032.

molecule	m/z	molecule	m/z	molecule	m/z	molecule	m/z
O2	31.97	Ar	39.94	N_2	28.00	H_2O	18.00
	32.00		39.97		28.03	$^{14}N^{15}N$	29.03
	32.03		40.00		28.06	CO_2	44.03
	32.06		40.03		28.09	$^{13}CO_2$	45.03
	32.09		40.06		28.12	$C^{18}O_2$	46.03

This was not the case; it was proved by looking at the maximum signal for these 5 *m/z* ratios by fitting a quadratic relationship of the *m/z* versus signal response (voltage) and taking the *m/z* ratio at which the maximum value of this fit occurred. When this maximum was plotted over time, a trend was discovered showing drift in the MIMS and a shift of the strongest signal to heavier mass to charge ratios over time (Figure 3.7). The data used were these maximum intensities.

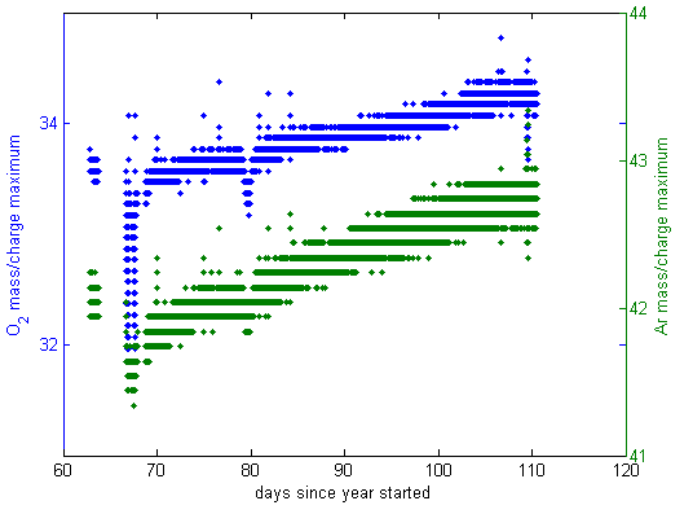

Figure 3.7: Maximum signal in the mass to charge ratios as identified by a quadratic fit to the 5 collected masses for O2 and Ar along JC032.

A second test for the stability consists of measuring “standard” air-saturated seawater twice daily, the equilibrated water inFigure 3.8. This standard is seawater that has been allowed to equilibrate with atmospheric air pump from the tallest point in the ship’s roof to

the lab by a KNF pump) for at least 12 h at a constant temperature of 15 °C (controlled by a water bath, Thermo Neslab RTE-10), such that the saturation of oxygen and argon for each of these standard solutions is constant throughout the cruise.

To run this water to the MIMS (Figure 4), first the valve to the waste is opened to remove bubbles in the tubing and then the four-port two-position valve is switched, thus allowing the equilibrated water to run to the quadrupole mass spectrometer. The valve is kept like this for 6 minutes, sufficiently long to get a stable signal for the O_2/Ar ratio of the standard. After this period the valve is switched back to resume USW sampling.

Figure 3.8 shows the O_2/Ar ratio of these equilibrated waters and it is obvious that there is a positive correlation between time and the O_2/Ar signal.

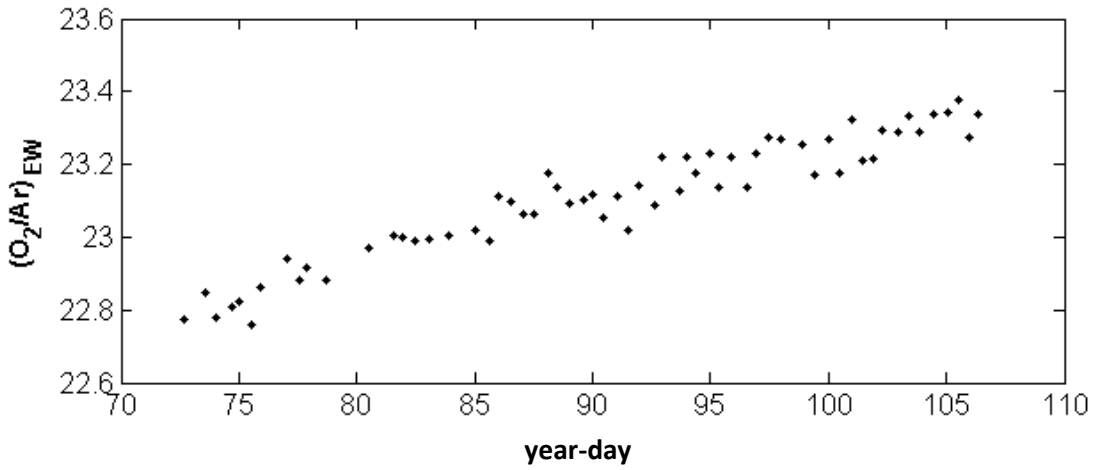

Figure 3.8: O_2/Ar ratio of the runs with equilibrated waters at 15 °C for JC032.

This drift was quantified with a linear regresson which was then applied to all the data. The correction has the equation:

$$(O_2/Ar)_{EW} = (O_2/Ar)_{raw-EW} - (0.016\,YD + 21.672) \quad (3.11)$$

Where the value for the O_2/Ar ratio for the equilibrated water is $(O_2/Ar)_{EW}$, YD is the days since "31/12/2008" and $(O_2/Ar)_{raw\text{-}EW}$ is the ratio of O_2/Ar when the equilibrated water was run. This regression had a coefficient of determination, r^2 of 0.915 (n = 60). The short term

reproducibility of the O_2/Ar ratios determined by the MIMS, expressed as a relative error (standard deviation over the average), and was 0.14 % over a period of 45 min.

With this fit the values of the continous measurements on the MIMS were corrected following this equation:

$$\Delta(O_2/Ar) = \frac{(O_2/Ar)_{raw}}{(O_2/Ar)_{EW}} \frac{(O_2/Ar)_{sat-EW}}{(O_2/Ar)_{sat-in\ situ}} - 1 \quad (3.12)$$

Where $(O_2/Ar)_{raw}$ is the value for the continous measurements, $(O_2/Ar)_{sat\text{-}EW}$ is the saturation concentration ratio of the gases O_2 (Garcia and Gordon, 1992) and Ar (Hamme and Emerson, 2004) calculated for equilibrated seawater 15°C and a salinity of 35 and the $(O_2/Ar)_{sat\text{-}in\ situ}$ is the saturation concentration calculated for in situ temperature and salinity.

3.5.4. Analysis of the O_2/Ar ratio and the O_2 isotope content by IRMS

3.5.4.1. Sampling

The samples for the O_2/Ar ratio and O_2 isotopes were taken in evacuated bottles (Figure 3.9) for analysis by IRMS. Sampling was carried out at least once a day and in most cases twice a day in order to get as much geographical coverage as possible. On KN193-03 a total of 39 samples were taken from the USW and 51 from CTD stations. For JC032 a total of 74 samples were taken with 57 samples from the USW and 17 bottles from CTD stations. The sampling was always done at the same time of the day around 05:00 and 17:00 GMT.

Samples for the O_2/Ar ratio and O_2 isotopes were collected in 400 cm^3 flasks, which had previously been evacuated and poisoned with 7.6 mg $HgCl_2$ (100 µl of a saturated solution of mercuric chloride). Thanks to the T-neck design of the flasks, it is possible to first fill only their necks and let the water overflow. Once the sample has been overflowing for a few seconds the tap is opened and seawater is allowed to enter at the bottom of the flask. Once the bottle is approximately half full, then the tap is closed and the bottle is sealed with water on its neck to minimize exchange with O_2 from the air. These bottles were stored for later analysis at UEA.

In order to avoid deterioration samples from KN193-3 were extracted 7 months after collection in glass sealed tubes, which were eventually analysed 4 years after collection. For JC032 samples were extracted and analysed 2 years after collection.

Figure 3.9: An evacuated bottle with a sample.

3.5.4.2. Isotope ratio mass spectrometry measurements

Once on land, the headspace of the bottles containing the samples was run through an extraction line for the removal of H_2O vapour, CO_2 and N_2, as these might interfere with the analysis of the O_2 isotopologues in the (IRMS) MAT 252. This extraction line, built in the stable isotope laboratory at the University of East Anglia, was based on that of Barkan and Luz (2003) and is described in Chapter 2.

Samples were run through the extraction line in sets of 5 to 6 samples and one aliquot of 2ml of reference gas per day. The reference gas was always drawn from the same tank of dry air. It was collected at UEA by Andrew Manning's lab and dried to reach a water vapour mole fraction of less than 2×10^{-6}. The purpose of this dry air was to calibrate the samples and to check how reproducible the line was. All the samples and the reference gas were collected on a collection manifold, which consisted of stainless steel fingers each protected by a valve (Swagelok 6LVV-DPS4-C) with 0.050 g of molecular sieve 5Å pellets in them. Each stainless steel finger was preconditioned for 2 min at 300 °C in order to remove all gases adsorbed to the molecular sieve pellets.

Once the gas was in the collection finger, it was analysed by IRMS the next day. For each measurement a sample and a "working reference" (O_2-Ar mixture of 4.7% of Ar in O_2 from BOC) were put in the bellows on the sample and the standard side, respectively. The bellows are two flexible receptacles where the gas is kept for analysis. They are connected to the source by independent capillaries. The flow on these capillaries is regulated by the

pressure on the bellows, thus allowing changing the flow at which the sample or the standard enters the source (Figure 3.10), such that the same signal intensity can be achieved on the collectors shown in the figure below.

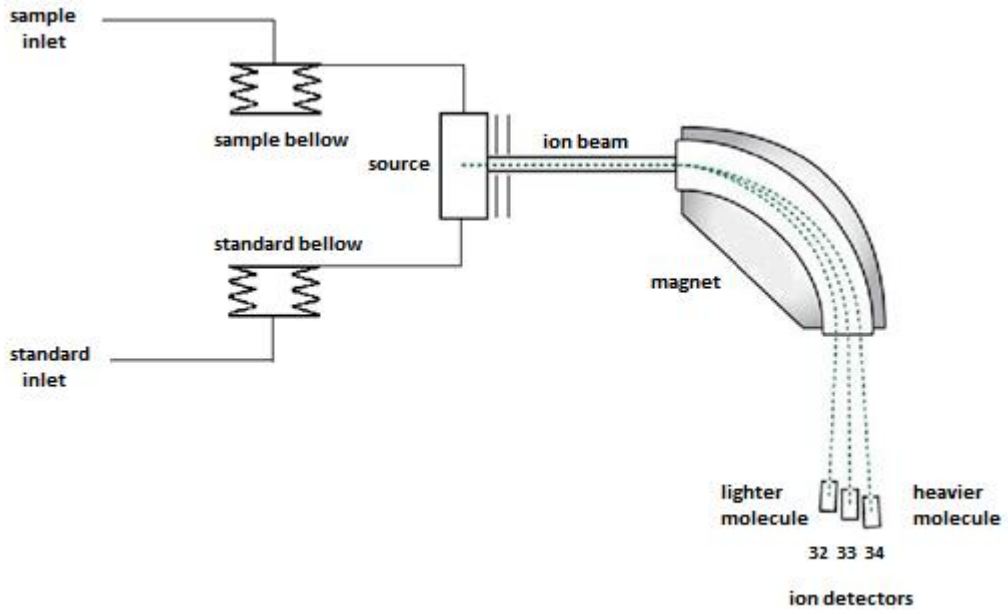

Figure 3.10: A schematic view of an IRMS mass spectrometer. Image adapted from http://serc.carleton.edu/research_education/geochemsheets/techniques/gassourcemassspec.html, December 2011.

Once the bellows are filled with the sample and working reference gas the procedure is as follows: first the gas from standard enters the source where it is ionized and accelerated to form the ion beam that goes to the flight tube. In the flight tube the magnet deviates the ions according to their mass to charge ratio. Ions are collected on the ion detectors where their intensity is recorded during the chosen set time (integration time). This procedure repeats itself with the sample. These cycles of a standard and sample run are separated by a set time (idle time), so the signal of one gas is not mixed with the other. This procedure is repeated for 30 cycles. Measurements from the mass spectrometer for the oxygen (O) isotopes are the average of these 30 cycles and are calculated as follows:

$$^{*}\delta = {}^{*}R_{\mathrm{sample}}/{}^{*}R_{\mathrm{ref}} - 1 \quad (3.13)$$

$$^{*}R_{\mathrm{sample}}/{}^{*}R_{\mathrm{ref}} = \frac{(n(^{*}\mathrm{O})/n(^{16}\mathrm{O}))_{\mathrm{sample}}}{(n(^{*}\mathrm{O})/n(^{16}\mathrm{O}))_{\mathrm{ref}}} \quad (3.14)$$

Where * stands for 17 and 18 for the $^{17}O^{16}O$ and $^{18}O^{16}O$ isotopes of O_2. ^{16}O in the formula stands for O_2 formed by the two light isotopes ^{16}O and ref refers to the reference.

IRMS measurements were performed according to the following daily routine: First, zero enrichment is used to test the performance of the mass spectrometer, which is done by putting the working reference gas with the O_2-Ar mixture in both bellows (standard and sample side). Then the dry air standard plus the 6 samples all prepared the previous day in the extraction line follow (see Chapter 2).

Each gas sample was run for 3 blocks of measurements containing 30 cycles each. The integration time was 16 s, the idle time 5 s and the measurement intensity 3.5 V with a 3 x 10^8 Ω feedback resistor. At the beginning of each block a peak centre for the standard was performed at *m/z* 32 in order to find the maximum intensity for the signal. Then, both bellows (standard and sample side) were adjusted to 3.5 V in the major cup. Interfering masses were measured at the end of the third block and were run in the *m/z* order of: 32, 40 and 28. Mass to charge ratio 32 (O_2) and 40 (Ar) were measured in the same major collector, whereas the *m/z* 28 (N_2) was measured in a minor detector capable to detect 1/300 times smaller concentrations than in major detectors.

3.5.4.3. Calculation of O_2/Ar ratios by IRMS

O_2 and Ar were measured as *m/z* 32 and 40 respectively for a sample and the working reference (work_ref). The initial $\delta_{\mathrm{sample/work\_ref}}$ (O_2/Ar) was calculated as:

$$\delta_{\mathrm{sample/work\_ref}}\,(O_2/Ar) = \left(\frac{(^{32}/_{40})_{\mathrm{sample}}}{(^{32}/_{40})_{\mathrm{work\_ref}}}\right) - 1 \quad (3.15)$$

Dry air is used as a standard for the O_2/Ar and isotopologues analysis. Dry air is used as the standard, because the O_2/Ar ratio in the atmosphere is well known and is constant

(Glueckauf, 1951), while at the same time dry air is an internationally accepted reference for O_2 isotopologues (Barkan and Luz (2003); Wieser (2007)). The use of atmospheric O_2 is preferred to Vienna Standard Mean Ocean Water (VSMOW), firstly because the isotope ratios of dissolved O_2 samples are closer to atmospheric O_2 than to VSMOW and secondly because atmospheric air is readily available. Any processes fractionating atmospheric O_2 are likely to occur on timescales greater than 1000 years and are therefore negligible for the purposes of this study.

Then the $\delta_{\text{sample/dry air}}$ (O_2/Ar) is:

$$\delta_{\text{sample/dry air}}\,(O_2/Ar) = \frac{\delta_{\text{sample/work\_ref}}\,(O_2/Ar) - \delta_{\text{dry air}}\,(O_2/Ar)}{1+\delta_{\text{dry air}}\,(O_2/Ar)} - 1 \tag{3.16}$$

To obtain the final O_2/Ar of the sample it is necessary to correct for the distribution of gases between the gas phase and the water phase. This correction factor Q described by Luz et al. (2002) was applied as per the following equation:

$$\delta_{\text{sample}}(\text{O}_2/\text{Ar}) = Q\;\delta_{\text{sample/dry air}}\,(\text{O}_2/\text{Ar}) \tag{3.17}$$

$$Q = \frac{1 + \alpha(O_2)\;{V_{\text{gas}}}/{V_{\text{water}}}}{1 + \alpha(Ar)\;{V_{\text{gas}}}/{V_{\text{water}}}} \tag{3.18}$$

Where $\alpha(^{16}O_2)$ is the Ostwald solubility and V_{gas} and V_{water} are the volume of the headspace and water. The supersaturation of O_2 as in equation 3.16 can be calculated from $\delta(O_2/Ar)_{sample}$.

3.5.4.4. O_2 isotopologues by IRMS

The IRMS values for $^{17}O^{16}O$ and $^{18}O^{16}O$ were obtained from the *m/z* measurements 33 and 34, respectively, from two of the minor cups. The software from the IRMS gave the $^{33}\delta$ and $^{34}\delta$ which are assumed to be exactly the same as $^{17}\delta$ and $^{18}\delta$ since the conversion correction is very small (Kaiser and Röckmann, 2008).

The $\delta(N_2/O_2)$ correction was evaluated by combining the O_2-Ar working reference with 7 different gas mixtures containing different amounts of N_2.

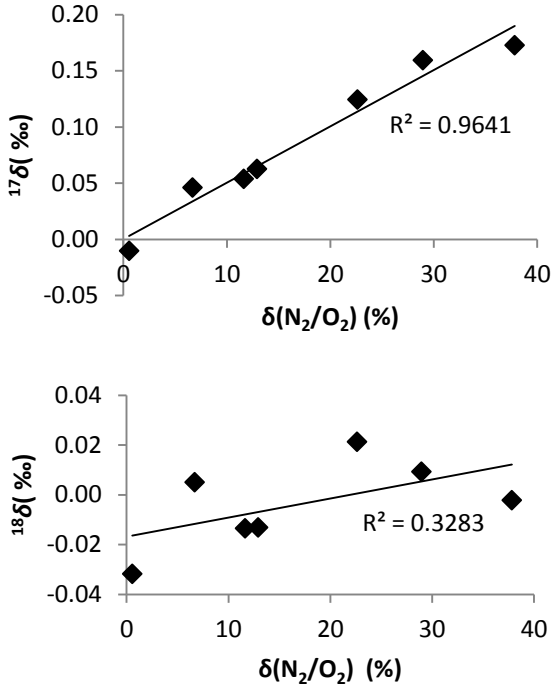

Figure 3.11: Calibration curves for $^{17}\delta$ and $^{18}\delta$ versus $\delta(N_2/O_2)$.

Just as in previous studies (Castro-Morales, 2010) I found a relationship between $\delta(N_2/O_2)$ and $^{17}\delta$, but not with $^{18}\delta$ (Figure 3.11), probably due to interaction in the ion source of the N_2 with the O_2. Therefore only $^{17}\delta$ was corrected for this effect. No correction was applied to $^{18}\delta$, as there is no significant dependence on N2/O2. A linear fit was calculated and the $^{17}\delta$ values were corrected with the equation below.

$$^{17}\delta_{\mathrm{N_2 corr}} = {}^{17}\delta_{\mathrm{meas}} - (0.0050\ \delta(\mathrm{N_2/O_2}) + 0.0003) \qquad (3.19)$$

The measurements were also referenced against the dry air standard in a similar way as done for $\delta(O_2/Ar)$. To calculate the δ referenced to dry air we use this equation:

$$^{i}\delta_{\text{sample/dry air}} = \frac{^{i}\delta_{\text{sample/work\_ref}} - ^{i}\delta_{\text{dry air}}}{1 + ^{i}\delta_{\text{dry air}}} - 1 \quad (3.20)$$

Where i stands for 17 or 18 depending on which oxygen isotope is being calculated, ^{17}O or ^{18}O.

Finally, $^{18}\delta$ was corrected for the fractionation between the gas and water phase in the storage bottle. Such fractionation mostly affects ^{18}O and to a lesser extent ^{17}O. The correction was typically:

$$^{*}\delta = {}^{*}\delta_{\text{sample/dry air}}\ Q \quad (3.21)$$

$$Q = \frac{1 + \alpha(^{*}O\ ^{16}O)\ {V_{\text{gas}}}/{V_{\text{water}}}}{1 + \alpha(^{16}O_2)\ {V_{\text{gas}}}/{V_{\text{water}}}} \quad (3.22)$$

Where * stands for 17 or 18 referring to ^{17}O or ^{18}O. The Ostwald solubility coefficient for oxygen is $\alpha(^{16}O_2)$. The $\alpha(^{18}O^{16}O)$ was calculated as follows:

$$\alpha(^{*}O^{16}O) = \alpha(^{16}O_2)(1 + {}^{*}\delta_{\text{sat}}) \quad (3.23)$$

The headspace correction was 0.002% for $^{18}\delta$ and 0.001% for $^{17}\delta$.

3.6. Gas exchange parameterizations and wind speed

The gas transfer coefficient is crucial for the estimation of the net community production and gross oxygen production (*N* and *G*). There are several parameterizations of *k*, e.g. Liss and Merlivat (1986), Wanninkhof (1992), Nightingale et al. (2000) and Sweeney (2007). In this study we decided to use the parameterization by Nightingale et al. (2000), because it is based on real measurements and it is between the estimates of Wanninkhof and Liss and Merlivat. The k defined by Nightingale *et al.* is:

$$k_i = \frac{24}{100}(0.333\ U_{10} + 0.222\ U_{10}^2)\ \left(\frac{Sc}{600}\right)^{-0.5} \quad (3.24)$$

Where k_i is the instantaneous gas transfer coefficient (m d^{-1}), U_{10}, is the wind speed at 10 m height (m s^{-1}), and *Sc* the (dimensionless) Schmidt number for O_2 defined by Wanninkhof (1992) for salinity 35 and temperatures T between 0 °C and 30 °C:

$$Sc = 1953.4 - 128.00\ T + 3.9918\ T^2 - 0.050091\ T^3 \quad (3.25)$$

In this work I use the weighting technique of *k* according to the history of the wind speed for up to 60 days prior to sampling k_w (Reuer *et al.*, 2007). The weighting factors are calculated from the mixed layer depth z_{mix} as well as the gas transfer velocities. z_{mix} was calculated from CTD profiles on JC032 and defined as the depth where the change in the density relative to the surface value (≈ 10 m) was greater than 0.125 kg l^{-1} compared to that of surface waters (average of 0-10 m). This calculation assumes that z_{mix} has not changed during the weighting period. Arbitrarily, ω_1 is set to 1.

$$k_w = \frac{\sum_{i=1}^{60} k_i\ \omega_i}{\sum_{i=1}^{60} \omega_i} \quad (3.26)$$

$$\omega_i = \omega_{i-1}(1 - f_{i-1}) \quad (3.27)$$

$$f_i = k_i \frac{0.25\ \mathrm{d}}{z_{mix}} \quad (3.28)$$

Where, f_i is the fraction of the mixed layer ventilated throughout 6 h (0.25 days) and ω_i is the weighting factor. *k* is a major source of uncertainty in the calculation of F_{bio}.

Leaving the uncertainty due to the different parameterizations of *k* aside, a 15 % relative error in the wind speed causes an error of up to 30 % in *N,* because of the quadratic term in the Nightingale *et al.* (2000) parameterisation. The exact error depends on the value of the wind speed. Therefore it was identified which wind dataset best matched the measured ship winds.

Wind speeds were measured on the *RRS James Cook* with a Gill Windsonic anemometer located in the foremast of at 19.9 m above sea level. These wind speeds were corrected to a height of 10 m using the wind profile power law expressed here (Peterson and Hennessey, 1978):

$$\frac{U_{10}}{U_m} = \left(\frac{z_{10}}{z_m}\right)^{\alpha} \tag{3.29}$$

Where U_{10} is the wind speed in m s^{-1} at 10 m (z_{10}) and U_m is the wind speed in m s^{-1} at the measurement location of 19.9 m (z_m).

The wind products were from the National Centre for Environmental Prediction (NCEP, Kalnay *et al.* 1996), the European Centre for Medium-Range Weather Forecasts (ECMWF, 2009) and the Cross-Calibrated Multi-Platform Ocean Surface Wind Velocity Product (CCMP, Atlas *et al.* 2009). A comparison of the different wind products and the wind speed measured on the ship was carried out, as shown in Figure 3.12. All the wind products had a time resolution of 6 h, but varied spatially from 1° latitude by 1° longitude for NCEP and ECMWF to 0.25° latitude by 0.25° longitude for CCMP. The root mean square difference (RMSD) between the shipboard wind speed and the three products was calculated. I got a difference of 1.89 m s^{-1} for NCEP, 1.14 m s^{-1} for ECMWF and 1.00 m s^{-1} for CCMP. Thus, CCMP was closest to the shipboard wind in this region of the ocean.

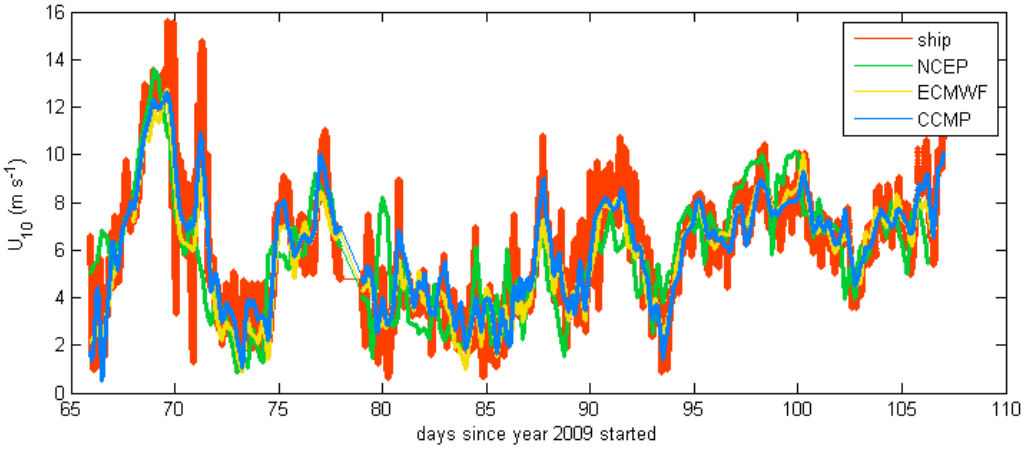

Figure 3.12: Wind speed (in m s-1) at 10 m above sea level during cruise JC032 from the shipboard sensor and from wind products from NCEP, ECMWF and CCMP.

Chapter 4. Oxygen production in the subtropical South Atlantic from O_2/Ar ratios and O_2 isotopologues

4.1. Introduction

The South Atlantic gyre (SATL) is a vast, undersampled region covering 25 % of the Atlantic Ocean. It is known as an oligotrophic region where nutrient inputs are small; therefore, biological production rates are low (Longhurst, 2007). However, despite its low production rates, the size of the gyre makes this area relevant for global carbon budgets, and it is important to know whether the metabolic balance represents a net carbon sink or source to the atmosphere.

Earlier studies of the metabolic balance in the SATL include Atlantic Meridional Transect (AMT) cruises (Gist *et al.*, 2009; González *et al.*, 2002; Serret *et al.*, 2006). These studies have examined the metabolic state of the gyre *in vitro* by using bottle incubations of oxygen (O_2). This method can produce biased results due to changes in the phytoplankton community composition during bottle enclosure, e.g. a reduction in autotrophs during the incubation time (Calvo-Díaz *et al.*, 2011; Fernández *et al.*, 2003), an increase in heterotrophs (Calvo-Díaz *et al.*, 2011) or the exclusion of grazers (Bender *et al.*, 1999).

Using this method, González *et al.* (2002) found that the gyre was net heterotrophic (community respiration greater than production), based on the data average for austral autumn and spring of the same year (May and October 1997). However, their measurements were made at the western edge of the gyre and it is not clear whether they can represent the whole of the gyre. In contrast to González *et al.* (2002), Serret *et al.* (2002), using the same techniques, found that the central region of the gyre was net autotrophic in spring. More recently, Gist *et al.* (2009) found that the SATL was in balance in spring and net heterotrophic in autumn (average of three spring and autumn cruises each).

An alternative method to measure the metabolic balance consists of measuring the O_2/Ar ratio, e.g. with a membrane inlet mass spectrometer (Kaiser, 2005). This enables continuous measurements of net oxygen production in the mixed layer along a ship transect (see chapter 1).

Biological gross production by autotrophs can also be measured by bottle incubations, e.g. based on ^{14}C-labelled bicarbonate uptake rates or changes in O_2 concentration in dark/light experiments. Here, are used *in situ* measurements of the isotopic composition of dissolved O_2 in the mixed layer to estimate biological gross O_2 production (see chapter 1).

4.2. Methods

For this study, the South Atlantic was crossed on board of RSS *James Cook* cruise JC032 in early austral autumn of 2009, departing from Montevideo (Uruguay) 7th March and arriving to Walvis Bay (Namibia) on the 21st April (Figure 4.1). Samples from the mixed layer were analysed for their O_2/Ar and O_2 isotopologue ratios. The results were used for the calculation of net community (*N*) and gross oxygen production (*G*), respectively.

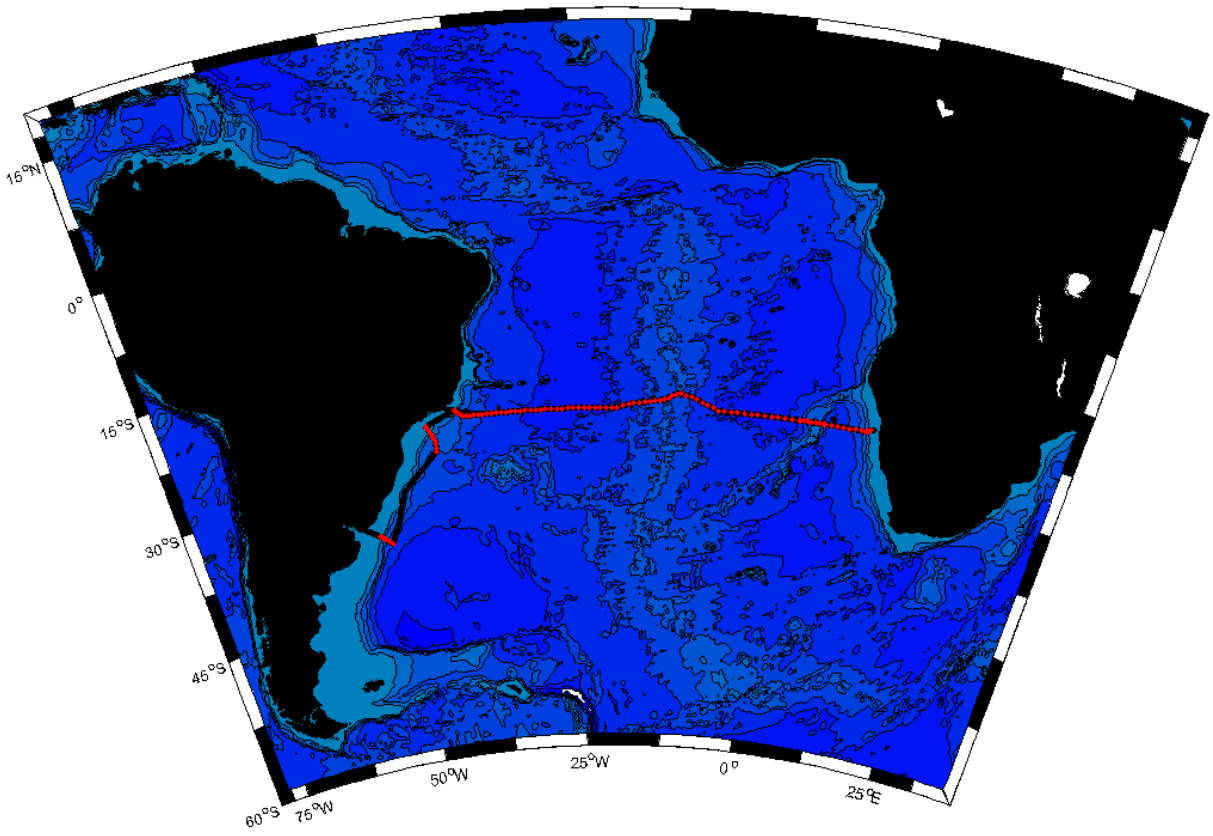

Figure 4.1: Map showing the location of the cruise-track (black line) and CTD stations (red dots).

The cruise JC032 was composed of three sections across the Brazil current at 37° S, 25° S and 24° S (8th to 20th March 2009) and a main section along 24° S (21st March to 20th April 2009), starting from the coast of Brazil at 40° W and ending in Africa at 12° E.

O_2/Ar ratios and oxygen concentrations, $c(O_2)$, were measured continuously using MIMS and an O_2 optode in the underway sea water supply (USW) every 10 s, corresponding to about 50 m spatial resolution. Discrete samples were collected from the USW to measure the

isotopic composition of dissolved O_2 for the quantification of the gross oxygen production (*G*). Additionally, F_v/F_m ratios in the USW were measured using fast rate repetition fluorescence (FRRF). O_2 concentrations in the USW were measured using Winkler titrations (Dickson, 1995) at regular intervals, as described in the cruise report (King et al., 2010), and used to calibrated the optode measurements.

A more detailed description of the individual measured parameters is given in the following sections. Some ancillary measurements and calibrations were done by different groups: A team led by Sinhué Torres (National Oceanography Centre, Southampton, NOCS) performed additional dissolved O_2 as well as nutrient measurements in Niskin samples from rosette hydrocasts. Mark Moore (NOCS) measured chlorophyll *a* concentrations, nitrogen isotope ratios ($\delta^{15}N$) in particulate organic nitrogen and, at selected stations, nitrogen fixation rates (using ^{15}N-labelled N_2). Lorna McLean and Ben Moat (NOCS) calibrated the underway and CTD temperature and salinity measurements, see the cruise report for details (King et al., 2010).

4.2.1. Temperature and salinity measurements

A FSI remote temperature module FSI OTM (serial number 1370) was used for sea surface temperature (ϑ_0) measurements near the USW intake. It was calibrated using CTD temperatures from 118 stations. Sea surface salinity (S_0) was measured using an FSI OCM conductivity sensor (serial number 1333) located in the rosette sampling room of the *RRS James Cook*. Salinity measurements were calibrated against 242 discrete salinity samples measured with a Guildline Autosal 8400B (serial number 68426) and the surface salinity measurements done at 118 CTD stations.

4.2.2. Continuous measurements of O_2 in the surface waters

$c(O_2)$ was measured in the USW with an O_2 optode (*Aanderaa*, Norway; model 3835, serial number 329). The calibration procedure is detailed in Chapter 3. In brief, the O_2 signal of the sensor (DPhase) was compared with 218 (plus 111 replicates) discrete Winkler samples collected from the USW (Figure 4.2). To accomplish this, the Winkler O_2 concentrations were converted to equivalent DPhase values by inverting the optode-specific, temperature and concentration-dependent calibration function.

There were some periods with bubbles in the USW. These are identified by sudden changes of the order of 2-15 µmol kg^{-1} in $c(O_2)$ over less than 1 min. They occurred during year-

day 69.5-71.5 and 99-105 and corresponded to periods when the ship speed was under 4.6 kn and wind speeds greater than 5 m/s. In contrast, the sudden increase of $c(O_2)$ on year-day 75.5 is associated with a decrease in salinity and temperature most likely associated with a different water mass than the surrounding Brazil current. Excluding these bubble periods, repeatability of the optode measurements is high, with only 0.02% difference between samples over 30 min, calculated as the standard deviation divided by the mean.

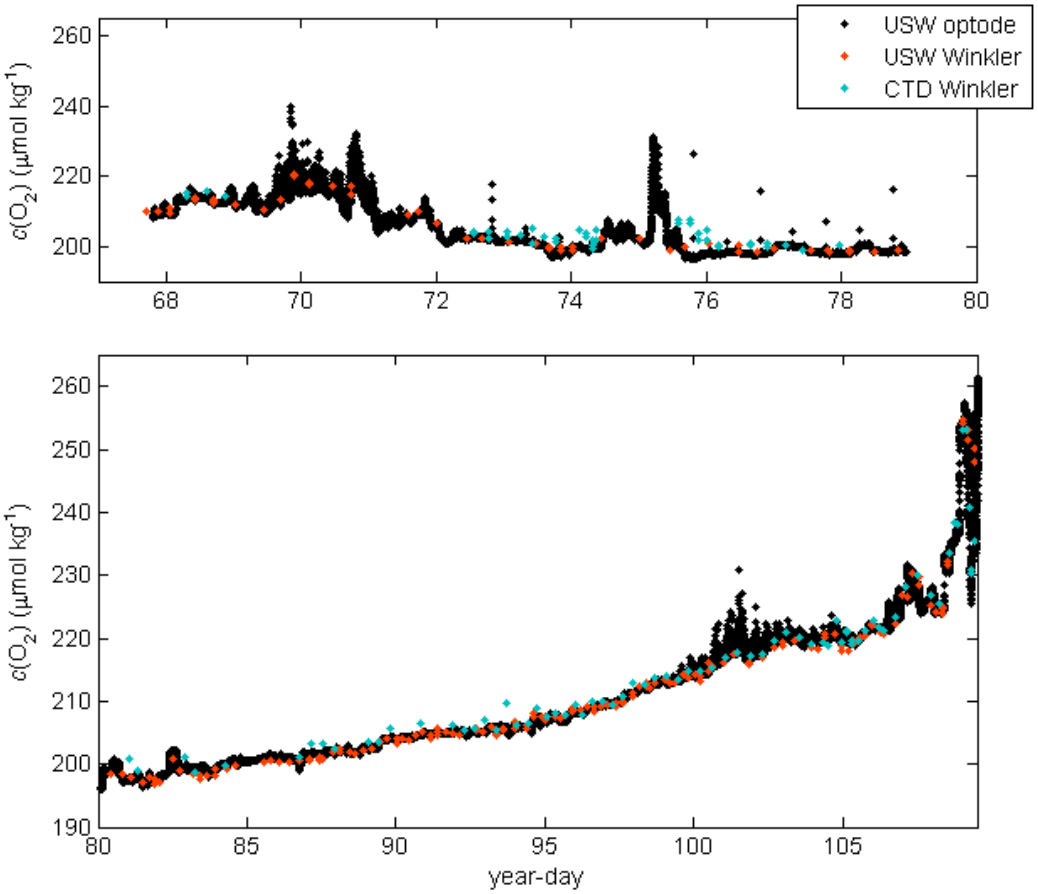

Figure 4.2: O_2 concentrations, $c(O_2)$ measured by the optode (black points) in the underway sea water (USW) versus time (year-day represents the days since year 2009 started, day 1= 1st January). Red dots represent the discrete samples used to calibrate the optode. Turquoise dots represent O_2 concentrations as measured from discrete surface Niskin samples. Panel a) shows the data from the Brazil current section only, while panel b) presents the data from the main section of the cruise at 24° S from west to east. Note that in panel b) the y-axis has been magnified to visualise the variability in $c(O_2)$.

Because a disagreement between the $\Delta(O_2)$ and $\Delta(O_2/Ar)$ data with the $\Delta(O_2/Ar)$ showing values always above saturation whereas $\Delta(O_2)$ showed mostly undersaturation it was raised the alarm of a problem with the calibration in the $c(O_2)$ measured by the Winkler

titration. To check the quality of the Winkler O_2 concentrations, Oliver Legge (UEA) compared them to previous cruises using the CARINA database and a Matlab tool-box available in the CDIAC website (http://cdiac.ornl.gov/oceans/2nd_QC_Tool) (Tanhua, 2010). JC032 data were compared to two cruises (CLIVAR A16S 2005 [CARINA record no. 49NZ20031106] and CLIVAR/Carbon A10 [33RO20050111]) that crossed the path of cruise JC032 in the Brazil current section at 44° E and at 25° E. Samples within a specific distance (222 km x 222 km; latitude x longitude) were selected, from depths greater than 1500 m to avoid any seasonal or interannual variations. $c(O_2)$ for JC032 data was found to be 3 % (±0.6%) lower than those of the previous two cruises. I therefore applied a correction of +3% to the Winkler O_2 data. This correction has already been taken into account in Figure 4.2. It brings the O_2 saturation anomalies, $\Delta(O_2)$, into much better agreement with the O_2/Ar saturation anomalies, $\Delta(O_2/Ar)$, see below.

Previous studies (Juranek *et al.*, 2010) found evidence of O_2 consumption in USW lines. Therefore, I compared $c(O_2)$ from the surface Niskin bottle with $c(O_2)$ measured by the optode and the discrete Winkler samples taken from the USW, which were taken at the same time as the surface Niskin bottle was fired (Figure 4.3). The average difference between the oxygen concentration from the USW and the upper Niskin are negative, indicating a loss of O_2 in the USW pipes of the ship, probably due to respiration. For the Winkler bottles, the average depletion of O_2 was -0.9±0.9 µmol kg^{-1}, while the more complete optode dataset gave a depletion of -1.2±1.4 µmol kg^{-1}.

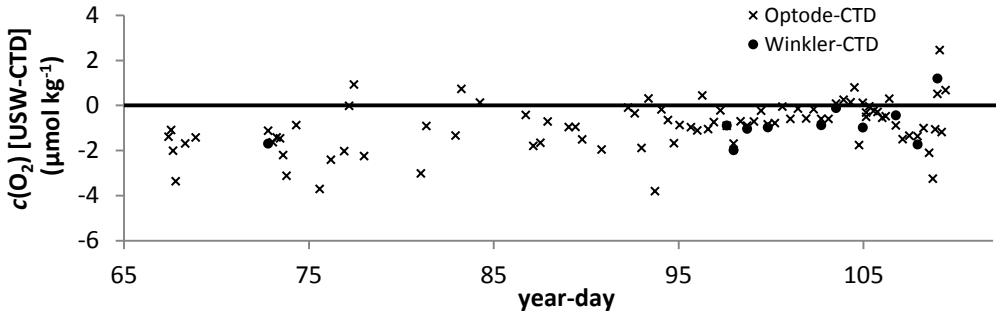

Figure 4.3: Oxygen consumption in the USW pipes of the RSS James Cook calculated as $c(O_2)$ measured in the USW minus $c(O_2)$ measured in the surface bottle of the CTD (from 5 m depth). Crosses (x) were calculated from $c(O_2)$ measured by the optode and black circles (●) measured by the Winkler titration.

Using the calibrated and corrected O_2 concentrations from the optode, the O_2 saturation anomaly was calculated as:

$$\Delta(O_2) = \frac{c(O_2) + \Delta c(O_2,\ R_p)}{c_{sat}(O_2)} - 1 \quad (4.1)$$

where $\Delta c(O_2, R_p)$ = 1.2 µmol kg^{-1} corrects for respiration in USW pipes and $c_{sat}(O_2)$ is the saturation concentration of O_2 at *in situ* temperature, salinity and atmospheric pressure (corrected to sea level).

4.2.3. Calculation of air-sea O_2 fluxes

The air-sea flux of O_2, $F(O_2)$, was calculated as

$$F(O_2) = \Delta(O_2)\, k_w\, c_{sat}(O_2) \quad (4.2)$$

where k_w is the gas transfer coefficient calculated following a similar procedure as Reuer *et al.* (2007) and is described in Chapter 3. Essentially, the gas transfer coefficient is calculated as a weighted gas transfer coefficient that takes into account the historical wind speed of the area (k_w). The wind-speed gas exchange parameterisation of Nightingale *et al.* (2000) was used together with CCMP winds as explained in Chapter 3.

Mixed layer depths (z_{mix}) were calculated as the depth at which there was a change of density of 0.125 kg/m^3 from a reference depth of 10 m.

4.2.4. Calculation of diapycnal O_2 fluxes between mixed layer and thermocline

The euphotic zone in the gyre was deeper than the mixed layer. This led to the formation of an O_2 maximum just below the mixed layer (Figure 4.4), with a flux of O_2 that depends on the O_2 concentration gradient. This flux of O_2 ($F_v(O_2)$) was estimated using:

$$F_v(O_2) = \frac{\Delta c(O_2)}{\Delta z} K_v \quad (4.3)$$

where the oxygen concentration gradient over depth is $\Delta c(O_2)/\Delta z$ and K_v is the vertical eddy diffusivity. As no direct measurements of K_v, were available the flux was calculated with $K_v = (1.7 \pm 0.2) \times 10^{-5}$ m^2 s^{-1}, the quantity measured by Ledwell *et al.*(1998) during a tracer release experiment in the North Atlantic Gyre.

This flux was calculated to estimate the leakage of signal from below the mixed layer.

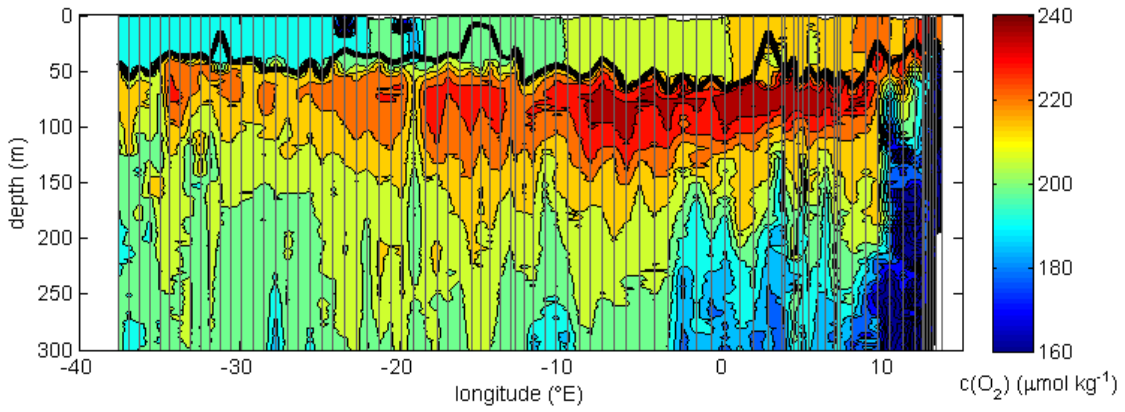

Figure 4.4: $c(O_2)$ for the section at 24°S. The black line represents the mixed layer depth (z_{mix}) and the vertical grey lines the sampling locations.

4.2.5. Continuous measurements of O_2/Ar ratios for determination of *N*

O_2/Ar ratios in the surface waters were measured continuously with a membrane inlet mass spectrometer (MIMS). The MIMS was calibrated twice daily using equilibrated water; this procedure is explained in detail in Chapter 3. The calibrated data were used to calculate the biological saturation anomaly of O_2, $\Delta(O_2/Ar)$, which is:

$$\Delta(O_2/Ar) = R(O_2/Ar) \,/\, R_{sat}(O_2/Ar) \; - 1 \quad (4.4)$$

where $R(O_2/Ar)$ and $R_{sat}(O_2/Ar)$ are the ratios of the O_2 and Ar concentrations, at *in situ* conditions and at air saturation, respectively.

$\Delta(O_2/Ar)$ was used to calculate the biological air-sea flux of O_2 to the atmosphere as

$$F_{bio}(O_2/Ar) = \Delta(O_2/Ar)\, k_w\, c_{sat}(O_2) \quad (4.5)$$

where k_w is the weighted gas transfer coefficient, calculated using a weighted historical wind speed value for the previous 60 days of sampling.

Assuming only vertical diffusion of O_2 from the mixed layer to the waters below (F_v) and no horizontal exchange, net community production (N), would be calculated as:

$$N(O_2/Ar) = F_{bio}(O_2/Ar) - F_v \quad (4.6)$$

The Ar saturation anomaly can be calculated from $\Delta(O_2)$ and $\Delta(O_2/Ar)$ to estimate the relevance of physical processes as:

$$\Delta(Ar) = \frac{\Delta(O_2) - \Delta(O_2/Ar)}{1 + \Delta(O_2/Ar)} \quad (4.7)$$

4.2.6. Gross oxygen production measured using O_2 isotopologues

Discrete samples from USW and selected CTD stations were taken to measure their isotopic content; 57 samples were collected along with 17 samples from the CTD at different depths. Samples were measured on land in the Stable Isotope Laboratory (SIL, UEA). The analysis of $^{17}\delta$ and $^{18}\delta$ is described in Chapter 3. $^{17}\delta$ and $^{18}\delta$ were used to calculate the ratio between gross O_2 production and the O_2 flux from the atmosphere (g) (Kaiser, 2011b):

$$g = \frac{(1 + \Delta(O_2))({}^{17}\varepsilon_E - \gamma_R\,{}^{18}\varepsilon_E) - \frac{{}^{17}\varepsilon_I - {}^{17}\delta}{1 + {}^{17}\delta} + \gamma_R \frac{{}^{18}\varepsilon_I - {}^{18}\delta}{1 + {}^{18}\delta}}{\frac{{}^{17}\delta_P - {}^{17}\delta}{1 + {}^{17}\delta} - \gamma_R \frac{{}^{18}\delta_P - {}^{18}\delta}{1 + {}^{18}\delta}} \quad (4.8)$$

Where $\Delta(O_2)$ is the saturation anomaly of O_2; ${}^{17}\varepsilon_E$ and ${}^{18}\varepsilon_E$ are the kinetic ${}^{17}O/{}^{16}O$ and ${}^{18}O/{}^{16}O$ fractionation during O_2 evasion from sea to air; γ_R is the ${}^{17}\varepsilon_E/{}^{18}\varepsilon_E$ ratio of respiratory ${}^{17}O/{}^{16}O$ and ${}^{18}O/{}^{16}O$ fractionation; ${}^{17}\varepsilon_I$ and ${}^{18}\varepsilon_I$ are the kinetic ${}^{17}O/{}^{16}O$ and ${}^{18}O/{}^{16}O$ fractionation during O_2 invasion from sea to air; ${}^{17}\delta$ and ${}^{18}\delta$ relative ${}^{17}O/{}^{16}O$ and ${}^{18}O/{}^{16}O$ differences between measured O_2 and air O_2; and ${}^{17}\delta_p$ and ${}^{18}\delta_p$ relative ${}^{17}O/{}^{16}O$ and ${}^{18}O/{}^{16}O$ differences between photosynthetic O_2 and air O_2.

Gross oxygen production, *G*, was then calculated using:

$$G = g\, k_w c_{sat}(O_2) \quad (4.9)$$

where *g* is calculated by Eq. 4.8; k_w is the weighted gas transfer coefficient and $c_{sat}(O_2)$ is the saturation concentration of O_2 at *in situ* conditions.

4.2.7. Fast Repetition Rate Fluorometer

Variable fluorescence (F_v/F_m) was measured in the USW by Fast Repetition Rate Fluorometer (Chelsea Instruments Ltd.). *F*v/*F*m measures the effective absorption of light by Photo System II (PSII), and it has been used as an indicator of light stress or nutrient limitation (Cassar *et al.*, 2011; Huang *et al.*, 2012). It is an indirect measurement of the efficiency with which light is used to fix carbon, with low values indicating low carbon fixation due to high stress by either lack of nutrients or light excess. For this study, we fed a FRRF instrument with a continuous flow of USW and recorded one F_v/F_m value every 10 s. Only night-time data were used, as during the day PSII is saturated, which makes it impossible to discriminate between light and nutrient stress. For the discussion here only the minimum F_v/F_m measured during a given night is retained.

4.2.8. Nitrogen-related measurements

Nitrate concentrations were used to calculate a nutrient limitation index (z_{lim}) following Behrenfeld et al. (2002):

$$z_{\mathrm{lim}} = z_{\mathrm{NO_3}} - z_{\mathrm{mix}} \tag{4.10}$$

where z_{NO_3} is the first depth at which the concentration of nitrate is above the detection limit (0.15 µmol kg^{-1}) and z_{mix} is the mixed layer depth. The higher z_{lim}, the higher the nutrient stress.

Samples for $\delta(^{15}N)$ analyses of particulate organic nitrogen were collected at 32 different locations from the USW and filtered and frozen for analysis (Mark Moore, NOCS). The nitrogen isotope ratio is used as a tracer of nitrogen sources. $\delta(^{15}N)$ between 0 and 1 ‰ correspond to N_2 fixation, whereas higher values around 5 ‰ indicate nitrate-based production (Karl *et al.*, 2002).

Depth profiles of nitrogen fixation rates were also measured by Mark Moore at 36 CTD stations. Samples were collected from the Niskin bottle into Nalgene polycarbonate bottles and sealed to avoid contamination with bubbles. The samples were then enriched with 3-4 ml of $^{15}N_2$ gas and incubated on deck for 24 h, simulating "in situ" conditions. Afterwards, these samples were filtered and frozen for later analysis at NOCS.

4.3. Results

The results from the main section across the oligotrophic gyre are described first because the gyre was the focus of this study, followed by the sections across the Brazil current.

Results for the main section pertain to data collected between 37° W and 14° E, beginning on 20th March 2009, en route to the first station off the coast of Brazil. Data collected within this section were composed of two different physical-chemical regimes (explained below): a more homogenous part (hereafter, gyre section, 37° W to 8° E), and the part influenced by the Benguela current (hereafter Benguela section, 8° E to 14° E).

4.3.1. Temperature, salinity and oxygen concentration variations

Sea surface temperatures ranged from 16 °C to 28 °C (Figure 4.5a). Higher temperatures were found at the western edge of the gyre and decrease steadily at a rate of –0.14 °C per degree longitude towards the African coast where temperatures of 22 °C were reached at 8° E. From 8° E until the transect end at 14° E, in the Benguela section the temperatures varied sharply and decreased to a minimum of 16 °C. Salinity (Figure 4.5b) ranged from 34 to 37, with values decreasing steadily towards the African coast. Salinity also presented more pronounced changes close to Brazil, influenced by coastal processes.

The calibrated optode oxygen concentration $c(O_2)$ varied from 197 µmol kg^{-1} to 258 µmol kg^{-1} (Figure 4.5c). $c(O_2)$ in the gyre was of 209±7 µmol kg^{-1}, although it increased with proximity to the African coast at a rate of 0.55 µmol kg^{-1} per degree longitude and reached a maximum of 227 µmol kg^{-1} at 8° E. This rate of change corresponds to the observed rates of change of ϑ_0 and S_0. Between 8° E and 14 ° E, $c(O_2)$ varies more sharply and reaches values as high as 258 µmol kg^{-1}, which is probably associated with the Benguela upwelling. Bubbles appeared in the USW between 6° W and 5° E and, as explained in the methods, were present whenever the ship speed was under 4.6 kn and wind speed greater than 5 m/s.

The O_2 saturation anomaly (Figure 4.5d) shows a consistent supersaturation along the whole of the gyre with an average ± standard deviation value of 2.6±0.3 %. High values occur between 6° W to 5° E consistent with the observed $c(O_2)$ in that area. For the Benguela section, the $\Delta(O_2)$ varies much more than in the gyre with values ranging from -5% to 10%, which are out of scale (Figure 4.5d), with an average ± standard deviation 3.3±2.1 %.

The air-sea O_2 flux $F(O_2)$ was positive everywhere, showing outgassing of O_2 to the atmosphere. The highest $F(O_2)$ values are associated with the bubble period, but if data from

this period are ignored, $F(O_2)$ for the gyre section was 16±4 mmol m^{-2} d^{-1}, whereas for the Benguela section the flux was 29±4 mmol m^{-2} d^{-1}.

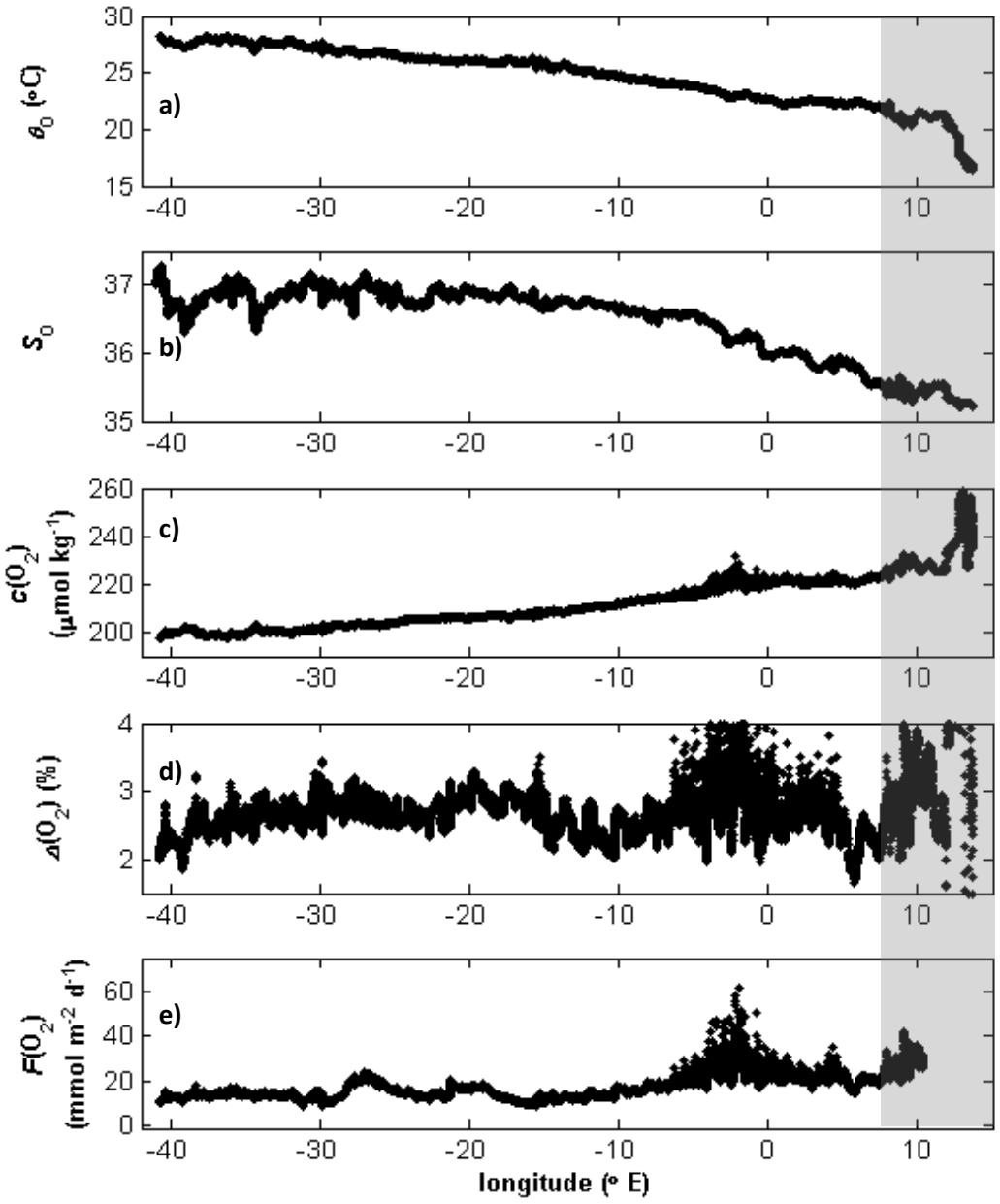

Figure 4.5: Five measured variables versus longitude travelled during the main section on cruise JC032. The white portion represents the gyre region, and the shaded grey region represents data from within the Benguela current (see text). Panels show: a) sea surface temperature; b) sea surface salinity; c) the calibrated and corrected optode oxygen concentration; d) O_2 saturation anomaly; and e) air-sea flux of O_2.

4.3.2. Mixed layer depth and nutrient limitation

Mean mixed layer depth (z_{mix}) along the gyre section was 47±12 m (range 10 m –70 m); within the Benguela section, it was 34±13 m. The nutrient limitation index (z_{lim}) varied little from -38° E to -15° E but decreased with the proximity to the African coast. The mean value was 48±36 m for the gyre and -20±14 m for the Benguela section. The data shows the gyre to be under nutrient stress, which decreases within the Benguela upwelling and eventually disappears.

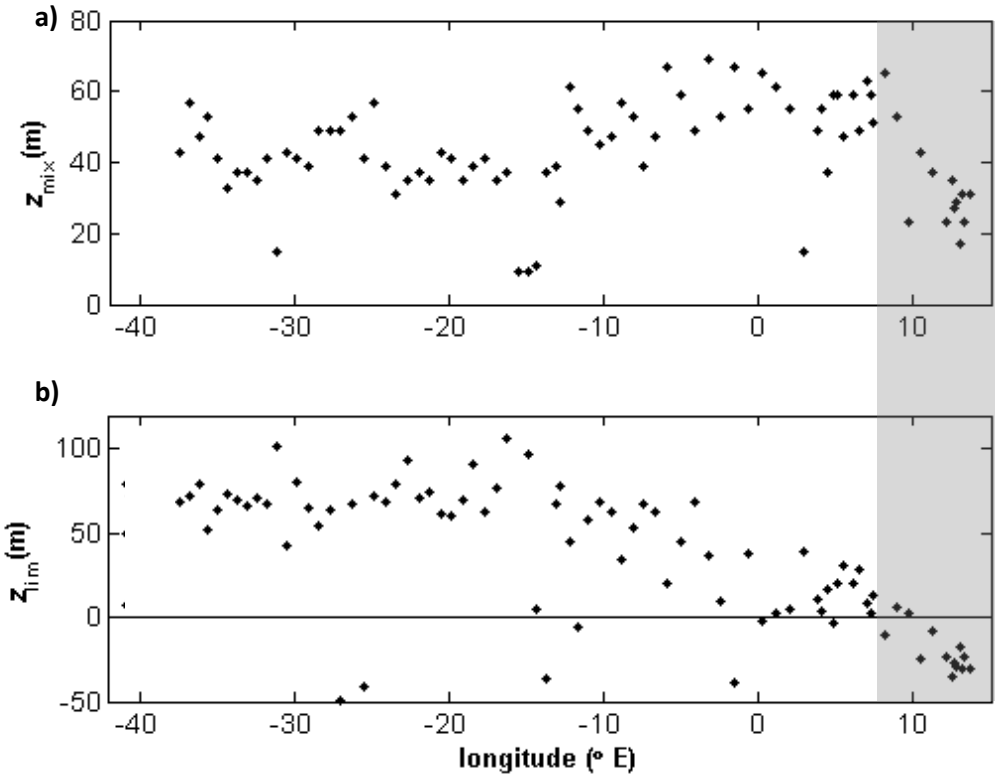

Figure 4.6: a) Mixed layer depth calculated with a criterion difference of 0.125 kg m^{-3} from a reference depth of 10 m versus longitude. b) Nutrient limitation index calculated as the difference between the first depth at which NO_3^- concentrations are above detection limit minus mixed layer depth. Positive values indicate stations where the mixed layer is shallower than the nitracline, whereas negative values are stations where NO_3^- is above detection limit and thus not nutrient limited. The vertical panel in grey shows the Benguela section, and the white represents the gyre section.

4.3.3. Net community production

N was calculated according to Eq. (4.6)

The biological oxygen saturation anomaly, $\Delta(O_2/Ar)$, (Figure 4.7c) was positive across the gyre section, averaging 1.9±0.4 %. There was little variation overall, although the values decreased from west to east at a rate of -0.02 percentage points per degree longitude. Values for $\Delta(O_2/Ar)$ in the Benguela section were higher (mean 2.5±1.9 %) but also more variable with values ranging from -7% at 13.3° E to 7% at 13.0° E. Overall, the O_2/Ar measurements had a standard deviation of 0.12 % over 1 min.

The weighted gas transfer coefficient (k_w, Figure 4.7d) averaged 3.1±0.7 m d^{-1} (range 1.7 m d^{-1} to 4.5 m d^{-1}) in the gyre section and 4.3±0.1 m d^{-1} in the Benguela section.

$F_v(O_2)$ (Figure 4.7a) is homogenous for the gyre section with an average value of 2..5±1.3 mmol m^{-2} d^{-1}, corresponding to a diffusive flux of the O_2 into the mixed layer. For the Benguela section, $F_v(O_2)$ averaged -1.3±3.1 mmol m^{-2} d^{-1}, a negative value indicating a diffusion of O_2 out of the mixed layer.

N values (Figure 4.7e) ranged from 1 to 21 mmol m^{-2} d^{-1} for the gyre section with an average value of 10±3 mmol m^{-2} d^{-1}, indicating a net flux of biological O_2 to the atmosphere. Variation in *N* was generated mainly by the variability in k_w (Figure 4.7-d) given the observed overall pattern, the peaks in both variables at 27° W, and the low variability in $\Delta(O_2/Ar)$. Regression analyses showed that 37 % of the variability in *N* was caused by the variability in k_w, whereas $\Delta(O_2/Ar)$ accounts for 16 % of the variability in *N*. An exception to this relationship between k_w and *N* occurs between 38° W and 34° W and for the Benguela section, where wind speeds are stable and $\Delta(O_2/Ar)$ shows some variability. Moreover, from 5° W to the edge of the Benguela section, *N* is decoupled from wind speed; this is explained by $\Delta(O_2/Ar)$ decreases from 5° W eastwards, which are partially compensating wind speed changes.

$\Delta(Ar)$ is indicative of the physical saturation in O_2, this was calculated from the $\Delta(O_2/Ar)$ and $\Delta(O_2)$ (Figure 4.7-b). Its values are negative mainly on the western margin of the gyre section and gradually increased towards the Benguela section. Overall, mean $\Delta(Ar)$ was 0.6±0.4 % for the gyre section (excluding the data with bubbles), and 1.2±0.7 % for the Benguela section.

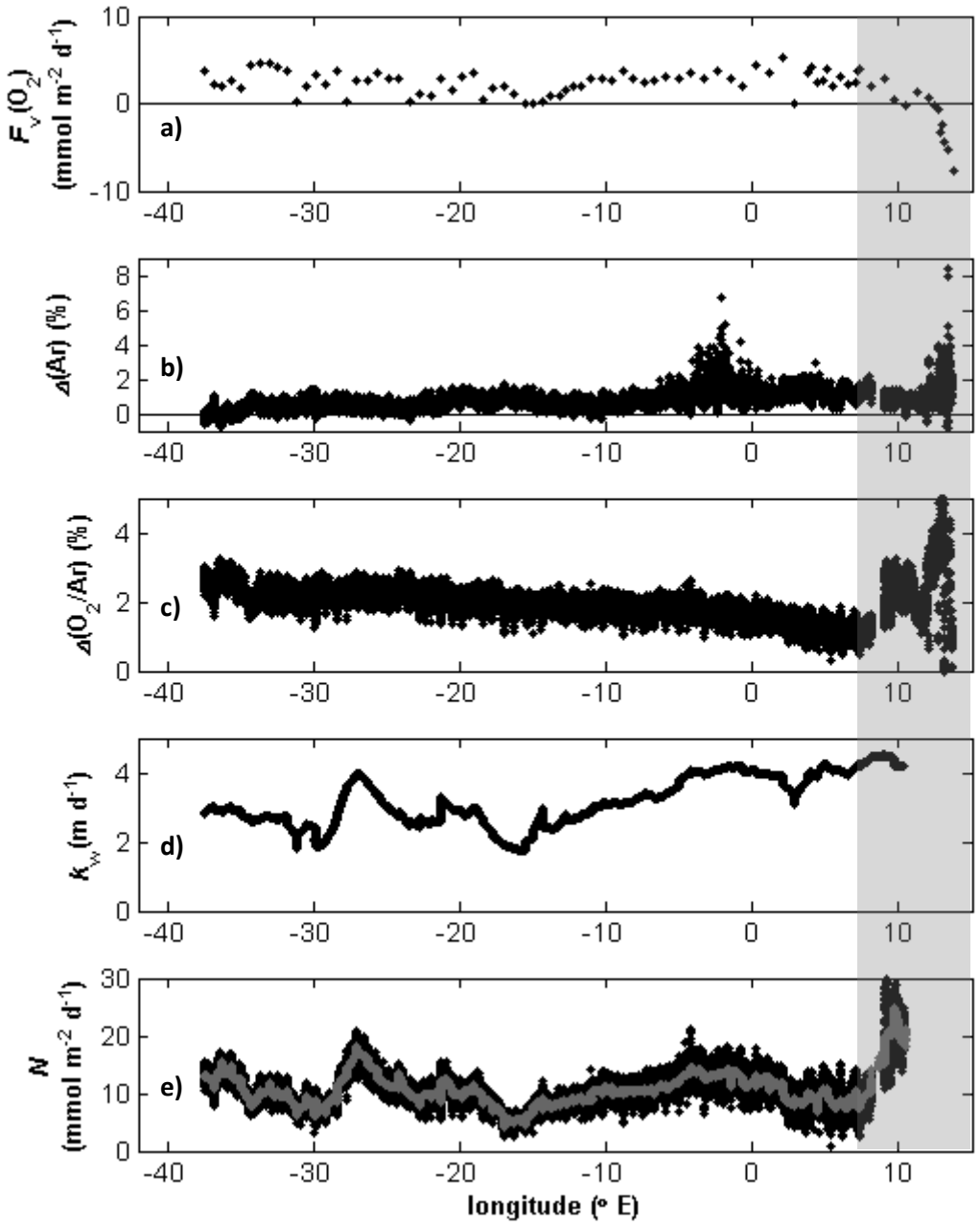

Figure 4.7: a) Expected vertical diffusion flux into the mixed layer calculated using K_v = 1.7 x 10^{-5} m^2 s^{-1}, the black line separates positive values (indicating an entrainment of O_2 into the mixed layer) and negative fluxes (indicating a diffusion out of the mixed layer); b) Ar saturation anomaly ; c) biological saturation anomaly; d) weighted gas transfer coefficient calculated similarly to Reuer *et al*. (2007); e) net community production, black points represent the raw data and the grey line represents the data smoothed with a moving average with a span of 3.33 h. Areas in white correspond to the gyre section and those in grey to the Benguela section.

4.3.4. Gross oxygen production

The ratio of gross oxygen production to gross oxygen uptake (*g*, Figure 4.8c) was higher in the gyre section (mean 0.28±0.13) than in the Benguela section 0.15±0.22. Gross oxygen production (*G*, Figure 4.8d) in the gyre section was 173±97 mmol m^{-2} d^{-1} (range: 13 mmol m^{-2} d^{-1} at 4.5° E to 381 mmol m^{-2} d^{-1} at 18.4° W). Average *G* in the Benguela section was 153±56 mmol m^{-2} d^{-1}, (range: 101 mmol m^{-2} d^{-1} at 11.3° E to 229 mmol m^{-2} d^{-1} at 13.05° E). Unlike the variability observed in *N*, which was due mostly to k_w, 77% of variability in *G* was due to *g* and only 16 % was due to the k_W.

The entrainment calculated for the isotopes, F_v for O_2 isotopologues, was calculated similarly as for the O_2/Ar. Here I used samples with data in the mixed layer and below at two stations, one at 6 °E and one at 11 °E. Using K_v is 1.7×10^{-5} m^2 s^{-1} and the gradient to the mixed layer the entrainment flux was calculated to be about 4% and 17% of G for stations at 6° E and 11° E, respectively. Given the similarity of the gradient of the c(O_2) across the gyre between 38° W and 10°E (see Figure 4.4), I assumed that the entrainment at 6°E was similar to that at the rest of the stations.

Surface concentrations of chlorophyll *a*, *c*(chl *a*), (Figure 4.8a) varied very little along the gyre section. *c*(chl *a*) averaged 0.07±0.02 µg l^{-1}, with the lowest values in the centre of the gyre around 12° W (0.04 µg l^{-1}) and higher values near the edges (0.11 µg l^{-1}). Values were higher in the Benguela section, where *c*(chl *a*) averaged 0.7±1.2 µg l^{-1}, with the easternmost point reaching 2.8 µg l^{-1} at 13.7° E (out of scale, not shown on the graph).

The photosystem quantum efficiency (F_v/F_m) varied from 0.26 to 0.42 (Figure 4.8-b) for the gyre section (mean 0.36±0.04) and 0.28 to 0.44 (mean 0.33±0.79) for the Benguela section.

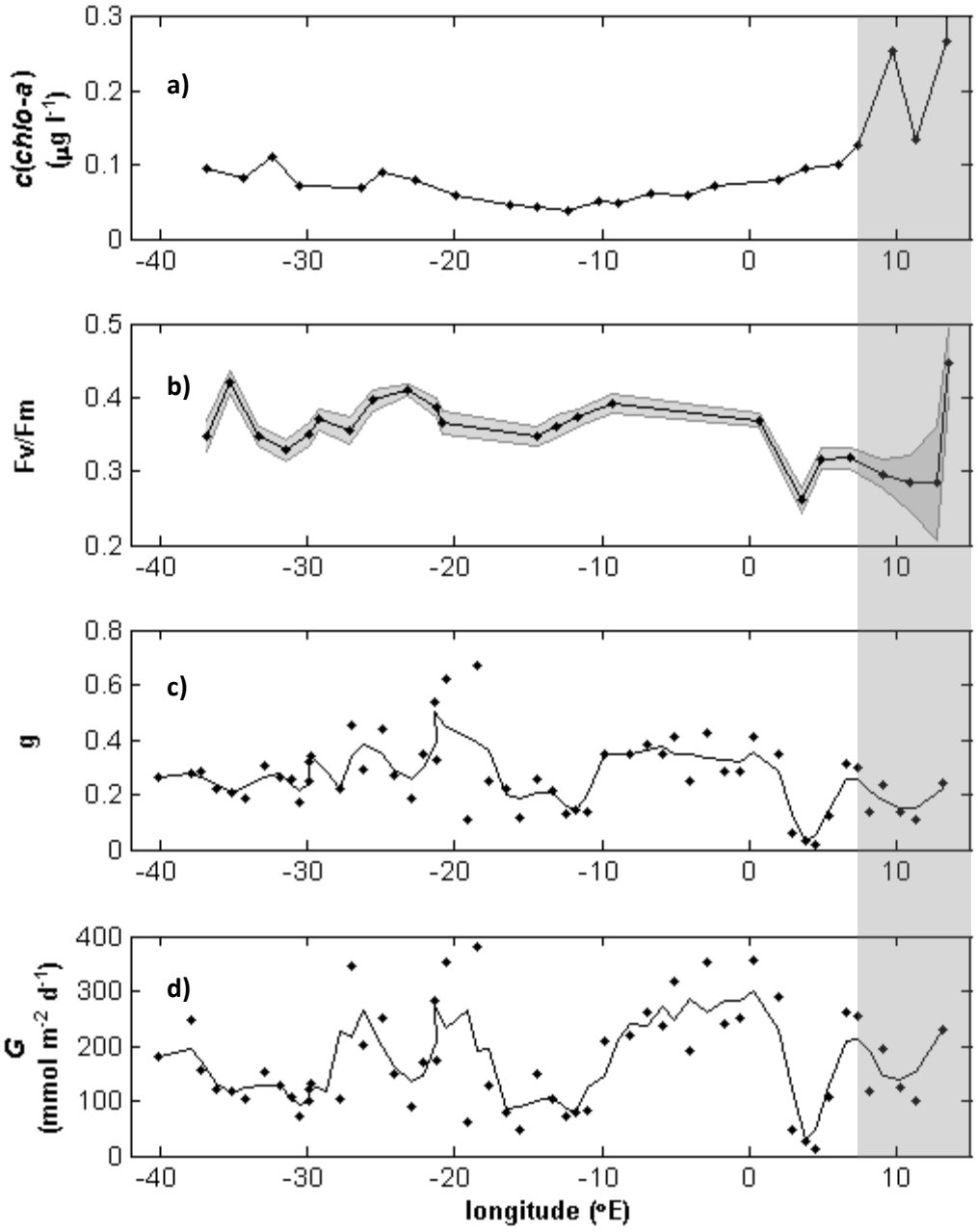

Figure 4.8: Various variables versus longitude areas in white correspond to the gyre section and those in grey to the Benguela section. Panels show: a) chlorophyll *a* concentration; b) Photosystem II quantum efficiency (night-time minima, with the shaded gray area representing the standard deviation for the entire night; c) *g* calculated with $^{*}\delta_{VSMOW}$ as measured by Kaiser and Abe (2012) and using the exact equation of Kaiser (2011b) the black line representing the 4 point-moving average; d) gross oxygen production, with 4-point moving average.

4.3.5. Nitrogen sources (data from Mark Moore, NOCS)

Nitrogen fixation rates in the surface water (<10 m) of the gyre averaged ± standard deviation 2.1±8.2 nmol l^{-1} d^{-1}, with the highest rates (42.8 nmol l^{-1} d^{-1}) at the westernmost edge. N fixation rates decreased towards the east where values of 0.0 nmol l^{-1} d^{-1} were common. No surface data were collected for the Benguela section.

In the gyre section, the isotopic composition of particulate organic nitrogen, $\delta(^{15}N$, PON), averaged ± standard deviation 2.2±3.1 ‰ (Figure 4.9b). Values were lowest (as low as -2.1 ‰) between 40° W and 18° W and increased from 18° W until the end of the section, reaching a maximum of 8.6 ‰. The lower values in the western portion of the gyre and the higher nitrogen fixation rates (Figure 4.9a) suggest that the source of N is likely to be atmospheric N_2, with the processes converting atmospheric N_2 gas into organic matter through nitrogen fixation. Higher $\delta^{15}N$ PON values to the east suggest that the source of N to the ecosystem comes from below the mixed layer as NO_3^-, given the decreases in z_{lim} (Figure 4.6b) and the low N_2 fixation rates in this area (Figure 4.9-a).

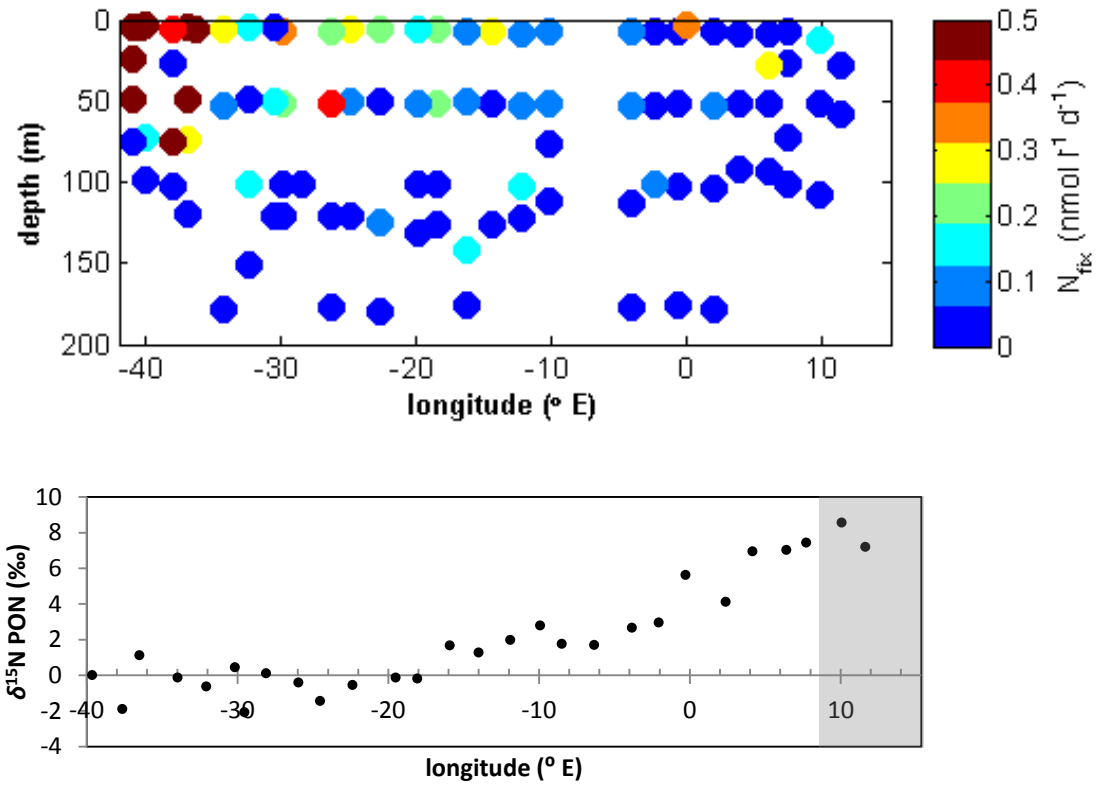

Figure 4.9: a) N_2 fixation rates. Rates > 0.5 nmol l^{-1} d^{-1} were coloured dark red in order to be able to appreciate the small change in N_2 fixation in the middle of the gyre; b) Abundance of the ^{15}N isotope in the particulate organic nitrogen expressed as $\delta^{15}N$ and represented here versus atmospheric N_2.

4.3.6. Brazil current

The region of the Brazil Current was subdivided into three areas, labelled from south to north as Brazil Current 1 (BC1), BC2, and BC3. In this region, the biological O_2 supersaturation ($\Delta(O_2/Ar)$) ranged from 0.8 to 2.6 % (Figure 4.10a). The highest values of $\Delta(O_2/Ar)$ were found at the beginning of the cruise. Values reaching 2.4 % were recorded between 32° S and 29° S and were associated with the highest gas transfer coefficient (9 m d^{-1}) of this section and thus the highest estimates of N (50 mmol m^{-2} d^{-1}), which indicate net autotrophy. This is supported by the input of nutrients from below, as z_{lim} in BC1 had values below 0 (Figure 4.10d).

Moving northwards from 32 to 28° S, while the $\Delta(O_2/Ar)$ value remained high (1.8% to 2.4%), k_w was low (4 to 7 m d^{-1}) which leads to lower N values between 10 and 30 mmol m^{-2} d^{-1}. Also, the nutrient limitation indicates a gradient from non-stressed areas in the BC1 to nutrient-limited areas in BC2.

The area of BC2 and up to 24° S shows the lowest $\Delta(O_2/Ar)$ observed in this section. Here, $\Delta(O_2/Ar)$ values ranging from 0.8 % to 1.8 %, together with low k_w (2 to 5 m d^{-1}), resulted in the lowest N, with values between 5 to 10 mmol m^{-2} d^{-1}. These low N values might be explained by the nutrient limitation observed for BC2.

In section (BC3), located between 40° W and 36° W, $\Delta(O_2/Ar)$ ranged from 2 to 2.4 %, but because k_w was only 5 m d^{-1}, N did not exceed 25 mmol m^{-2} d^{-1}. This is higher than in the 29°to 23° S range of section BC2, despite showing a similar nutrient limitation index.

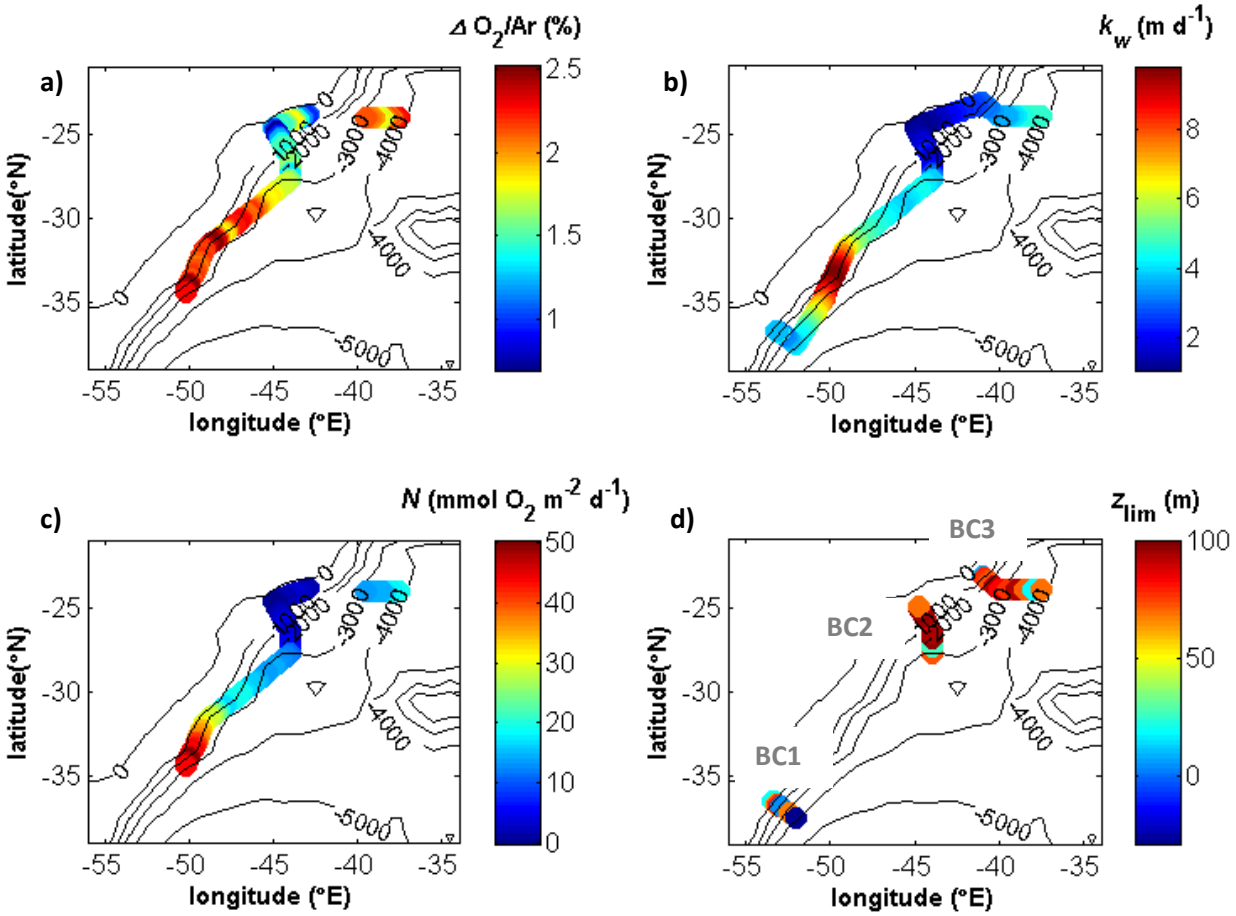

Figure 4.10: Brazil Current Section: a) biological saturation anomaly of oxygen; b) the weighted gas transfer coefficient; c) the net community production (*N*); d) nutrient limitation index, superimposed are the locations of the three Brazil current sections (BC1, BC2 and BC3).

4.4. Discussion

This discussion relates only to the data within the gyre section between 38° W and 8° E, as this is the focus of this study.

As described in the results we observed a consistent supersaturation of O_2 with respect to Ar (Figure 4.7c), which means that production exceeded respiration across the whole gyre. When accounting for the entrainment of O_2 from below the mixed layer the net community production of O_2 was, on average ± standard deviation, 10±3 mmol m^{-2} d^{-1} (Figure 4.7e).

4.4.1. Net community production

(1) To understand what was driving net production in the gyre, I compared the nutrient limitation index and other variables to *N* (Figure 4.11). I found no relationship between sea surface temperature, salinity or chlorophyll *a* and *N*. In all three cases, the correlation coefficient of determination (r^2) for a linear relationship was smaller than 0.01. Overall, salinity across the gyre showed no relationship to *N*, but when I considered only data with lower salinities (between 35.5 to 36.6), which corresponded to data east of 10° W until the edge of the Benguela section, the relationship was strong (r^2 = 0.74). This lower salinity signal is a tracer of the Benguela upwelling (see low salinities in the Benguela section in Figure 4.5b) and so it is the availability of nutrients as seen in the lower values of z_{lim} (indicating available nutrients), and thus the high values of *N* in the surface water. Although I expected to find a positive relationship between the surface concentrations of chlorophyll *a* and *N*, no clear relationship existed, based on the data available.

The correlation between nutrient limitation index, z_{lim}, and *N* was weak (r^2 = 0.15). However, I observed different trends within each of three discrete sections of nutrient limitation index: the first for $-50 < z_{lim}/m \leq 0$ (not nutrient limited), the second for $0 < z_{lim}/m \leq 50$ (nutrient limited) and the third for $z_{lim}/m > 50$ (highly nutrient limited). When the relationship with *N* was re-analysed within each section category, no clear relationship was found for $0 < z_{lim}/m \leq 50$, but r^2 were of 0.29 and 0.30 were found for $-50 < z_{lim}/m \leq 0$ and $z_{lim}/m > 50$, respectively. Such negative relationships were expected for the whole of the gyre.

A possible reason for the weak relationships between *N* with *c*(chl *a*) and z_{lim} could be due to the difference in integration times of c(chl *a*) and z_{lim}. While they are measurements of the conditions at the specific time of sampling, *N* integrates over the oxygen gas exchange between mixed layer and atmosphere, which was approximately 15 days.

To investigate the relationship between *N* and wind speed, it would not have been appropriate to compare *N* with k_w because F_{bio} (as a component of *N*) directly depends on k_w. Therefore, I compared $\Delta(O_2/Ar)$ with k_w. A negative relationship was found with greater values of $\Delta(O_2/Ar)$ corresponding to lower values of k_w, with r^2 = 0.34. The opposite relation was expected because stronger winds were thought to increase turbulence and introduce nutrients into the mixed layer. It appears instead that the increased wind tends to lead to more outgassing, which reduces $\Delta(O_2/Ar)$ for constant *N*.

A useful comparison here is also the *f* ratio. The *f* ratio was first proposed by Eppley and Peterson (1979) and was calculated as the ratio of new production measured by incubation of a sample with ^{15}N-labelled nitrate over net primary production as measured by ^{14}C incubations. This term would give information of the amount of organic matter available for export. Hendricks *et al.* (2004) proposed the use of *f* ratios expressed by the *N*/*G* as measured by $\Delta(O_2/Ar)$ and O_2 isotopologues.

No relationship was found between *f* and *N* (r^2 <0.01), despite the fact that *f* is calculated from the ratio *N*/*G*, highlighting that *N* = 10±3 mmol m^{-2} d^{-1} was not very variable whereas the variation in *G* = 173±97 mmol m^{-2} d^{-1} was 56%.

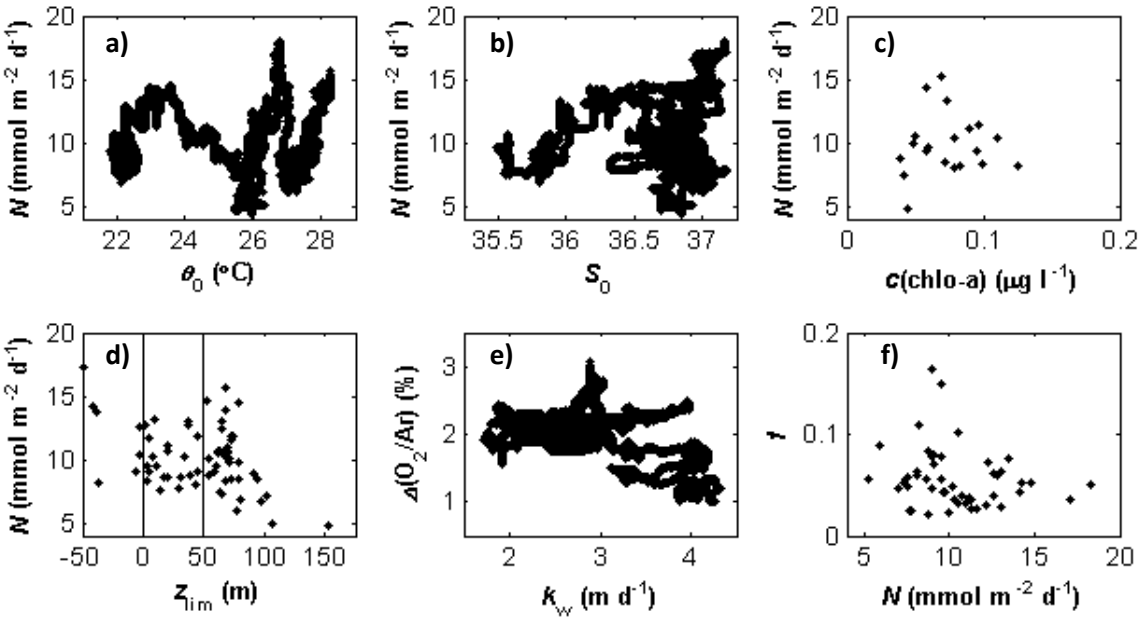

Figure 4.11: Comparison smoothed (moving average of 3.3 h) net community production (*N*) and smoothed biological oxygen saturation anomaly, $\Delta(O_2/Ar)$ with other parameters: a) *N* versus sea surface temperature (ϑ_o); b) *N* versus sea surface salinity S_0; c) *N* versus surface concentration of chlorophyll *a*; d) *N* versus nutrient limitation index (z_{lim}); e) $\Delta(O_2/Ar)$ versus gas transfer (k_w) f) $f = \Delta(O_2/Ar)/g$ versus *N*.

(2) Regarding the origin of the nutrients feeding net phytoplankton production, it seems that the gyre section can be considered to consist of two different sections according to N_2 fixation rates and $\delta(^{15}N, PON)$ (Figure 4.9): one west of 10° W and one east of 10° W. The section to the west had high N_2 fixation rates, ranging from >0.5 to 0.1 nmol l^{-1} d^{-1}, and $\delta(^{15}N, PON)$ < -2 ‰, both of which indicate that N_2 fixation is an important process in the western portion of the gyre. The section east of 10° W had low N_2 fixation rates, <0.1 nmol l^{-1} d^{-1}, and higher $\delta(^{15}N, PON)$ >2 ‰. This longitudinal separation seems to match that of the z_{lim} (Figure 4.6-b). West of 10° W, z_{lim} was generally greater than 50 m (thus making this region NO_3^- limited or high nutrient stressed), whereas moving east of 10° W, z_{lim} starts to decrease. While areas in the western portion were nutrient limited (specifically NO_3^- limited), the edge with the Benguela section had areas with no nutrient limitation. Therefore, it seems that production east of 10° W is based more on NO_3^- and to the west based more on N_2 fixation. Atmospheric nutrient deposition may play a role in both parts.

4.4.2. Previous measurements on *N* and *G* in the SATL

(3) Previous studies of the metabolic balance of the South Atlantic Tropical Gyre (SATL) have been carried out by using light and dark O_2 incubation techniques (Gist *et al.*, 2009; González *et al.*, 2002; Serret *et al.*, 2001). All three studies measured instantaneous rates of net community production; therefore this methodology was restricted to just the production and respiration during the incubation period in the bottle (7 or 24 h). Measuring the rates of O_2 /Ar presents an advantage over this earlier technique for several reasons: it has no bottle effects; O_2/Ar evaluates the *N* over periods of weeks, the time that takes to ventilate the mixed layer, which in this case was of about 15 days; and, finally, the rate of measurements is higher than in any of the previous studies, as it measures continuously in the mixed layer.

Among previous studies (Table 4.1), the lowest levels of *N* were recorded by González *et al.* (2002). These values, which differed substantially from those of the other studies, were recorded from measurements taken at locations at the western edge of the gyre, so it is possible that these data may not have been collected strictly within the gyre. Serret *et al.* (2006) defined the gyre as net autotrophic in the two springs that he was there. Gist *et al.* (2009) recorded a similar pattern but with values of *N* that were very close to a net balance, with 5 mmol m^{-2} d^{-1}. In autumn, Gist *et al.* (Gist *et al.*, 2009) found the gyre to be net heterotrophic, with a rate of -14 mmol m^{-2} d^{-1}.

Measurements of O_2/Ar showed a supersaturation, indicating that at least at the time of sampling all of the gyre was net autotrophic. Because the O_2/Ar method averages *N* over time of the exchange of O_2 with the atmosphere this means that the gyre was net autotrophic for the period between sampling and 15 days before (the time it takes to exchange the mixed layer calculated as the ratio of z_{mix}/k_w).

Table 4.1: Results of net community production (*N*) from previous studies and this one in the South Atlantic gyre. Columns represent: the reference source of the data; the number of stations for which the study reported values; the season with "S" and "A" standing for spring and autumn; the value of *N* as the net community production; the technique used; and latitude and longitude of the locations of the measurements.

Reference	no. of stations	season	*N* (mmol m^{-2} d^{-1})	Technique used	lat (° N)	lon (°E)
González *et al.* 2002*	2	S	-44.5 ± 130	O_2 in vitro 7 h	5 to 32	-26 to -44
González *et al.* 2002*	2	A	-117 ± 135	O_2 in vitro 7 h	5 to 32	-26 to -44
Serret *et al.* 2006	5	S	20 ± 3	O_2 in vitro 24 h	10 to 34	-16 to -54
Gist *et al.* 2009	28	S	5 ± 26	O_2 in vitro 24 h	10 to 35	-3 to -35
Gist *et al.* 2009	28	A	-14 ± 26	O_2 in vitro 24 h	10 to 35	-3 to -35
This study	continuous	A	13 ± 3	O_2/Ar in situ	24	-50 to 11

(*) as reported by Serret *et al*. 2006

Bottle incubation techniques aim to measure net community production (*N*) by enclosing a water sample in bottles and recording the change of O_2 concentration under dark and light conditions. *N* is defined as the difference in concentration between the light condition and the dark condition. This technique assumes that the trophic composition of the water sample is and will remain the same as that of the sample from which it was taken.

Gieskes *et al.*(1979) and Harris (1986) found high rates of photochemical pigment destruction in enclosed samples, and this destruction was higher in smaller water samples (30 ml) than in larger samples (4 l), in which the reduction in photochemical pigment was nearly negligible. Fernández *et al.* (2003) found that the concentrations of important phytoplankton species in oligotrophic Atlantic waters – *Prochlorococcus spp*. and picoeukaryotes (Marañón *et al.*, 2000) – declined dramatically (>50 %) after only two hours of incubation. Moreover, Calvo-Díaz *et al.* (2011), examining the abundance of the representative community for oligotrophic waters, observed not only a decreased in *Prochlorococcus* and picoeukaryotes over the time of incubation but also, in some experiments, an increase in the total concentration of heterotrophic bacteria.

On the other hand, measurements in other gyres using the same technique of measuring O_2/Ar ratios that was used in this study have found similar results to the ones presented here. For instance, Quay *et al*. (2010) at station ALOHA near Hawaii found an average *N* of 14±4 mmol m^{-2} d^{-1} during a time series spanning from March 2006 to February 2008. Luz and Barkan (2009) found at BATS near Bermuda values of *N* ranging from 6 to 8.3 mmol m^{-2} d^{-1} over a time series between May-October 2000. Juranek *et al.* (2012) collected data during 4 different cruises in the North Pacific Gyre in the spring 2003 and 2006 and summer 2003 and 2008 and recorded an average *N* of 8.3±1.3 mmol m^{-2} d^{-1}. All these results for *N* ranging from 6 to 14 mmol m^{-2} d^{-1} compared well with these estimates of 10±3 mmol m^{-2} d^{-1}.

Therefore, it is likely that measurements of *N* made by bottle incubation techniques might be overestimating the respiration of these communities, at least in oligotrophic regions, due to a decrease of the autotrophic components of the community. Hence, it is preferable to derive *N* from *in situ* measurements such as O_2/Ar data.

4.4.3. Gross oxygen production

(4) Using the isotopic composition of dissolved O_2, I estimated gross oxygen production (*G*), calculated using the dual delta method proposed by Kaiser (2011b) and using $^*\delta_{VSMOW}$ as reported by Kaiser and Abe (2012). Following from this an average *g* = 0.28±0.13 and *G* = 173±97 mmol m^{-2} d^{-1} was obtained for the gyre.

As explained in Chapter 1, *g* can be calculated using the dual delta method or the older approximate method by Luz and Barkan (Luz and Barkan, 2000) based on the ^{17}O excess, $\Delta(^{17}O)$. Here I present results using both approaches:

$$g_{\mathrm{LB}} = \frac{{}^{17}\Delta_{\mathrm{dis}} - {}^{17}\Delta_{\mathrm{sat}}}{{}^{17}\Delta_{\mathrm{p}} - {}^{17}\Delta_{\mathrm{dis}}} \tag{4.11}$$

$$g_{\mathrm{K}} = \frac{(1+\Delta(\mathrm{O}_2))({}^{17}\varepsilon_{\mathrm{E}} - \gamma_{\mathrm{R}}\,{}^{18}\varepsilon_{\mathrm{E}}) - \frac{{}^{17}\varepsilon_{\mathrm{I}} - {}^{17}\delta}{1+{}^{17}\delta} + \gamma_{\mathrm{R}}\frac{{}^{18}\varepsilon_{\mathrm{I}} - {}^{18}\delta}{1+{}^{18}\delta}}{\frac{{}^{17}\delta_{\mathrm{P}} - {}^{17}\delta}{1+{}^{17}\delta} - \gamma_R\frac{{}^{18}\delta_{\mathrm{P}} - {}^{18}\delta}{1+{}^{18}\delta}} \tag{4.12}$$

The value of *g* not only varies according to the formula used to calculate it, but is also strongly influenced by the choice of parameters needed to calculate it (Kaiser, 2011b; Prokopenko *et al.*, 2011). Among these parameters are $^{17}\delta p$ and $^{18}\delta p$, which hereafter are referred to as $^{*}\delta p$ – where "*" stands for 17 or 18. This $^{*}\delta p$ is calculated from the isotopic composition of the source water ($^{*}\delta_{VSMOW}$) and the photosynthesis fractionation ($^{*}\varepsilon_p$). As explained in Chapter 1, there is disagreement on the values of $^{*}\delta_{VSMOW}$, with values reported by Kaiser and Abe (2012), K&A) of $^{17}\delta_{VSMOW}$ = -12.102 ‰ and $^{18}\delta_{VSMOW}$ =-23.647 ‰, and the values reported by Luz and Barkan (2011), L&B) of $^{17}\delta_{VSMOW}$ = -11.883 ‰ and $^{18}\delta_{VSMOW}$ = -23.324 ‰. Values reported by Barkan and Luz (2005) are similar to those of Kaiser and Abe (2012), once corrected for mass-dependent fractionation effects. Therefore, I examine how *G* is impacted by using the approximate equation and the choice of $^{*}\delta_{VSMOW}$ reported by two previous studies, K&A (2012) and B&L (2011).

Figure 4.12 show that the bias due to the approximate calculation method would have been small for the present dataset. Greater differences were encountered when comparing the results using the $^{*}\delta_{VSMOW}$ reported by K&A and the one from B&L (2011). On average, *G* based on $^{*}\delta_{VSMOW}$ K&A value was 30% higher than if based on L&B. This relative difference ranged from 26 % to 37 %.

In view of this comparison, the choice of $^{*}\delta_{VSMOW}$ appears much more relevant than the choice of formulae and would therefore generate greater uncertainty than the selection of the formula to calculate *g*, the influence of which can be considered negligible for this dataset.

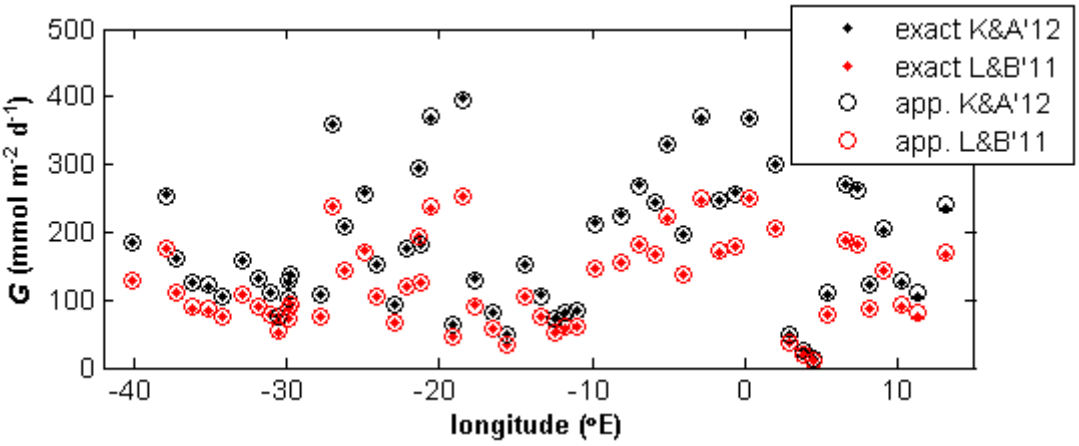

Figure 4.12: Comparison of *G* using different approaches indicated in the legend. These differences are due to: using the exact formula (dual delta method) proposed by Kaiser (2011b) (closed diamonds) or the approximated formula proposed by Luz and Barkan (2000) (open circles) and the choice of $^{*}\delta_{VSMOW}$ of by Barkan and Luz (2011) or by Kaiser and Abe (2012), in red and black, respectively.

(5) As for *N* and $\Delta(O_2/Ar)$ in Figure 4.11, we compared *G* and *g* to different potential predictor variables (Figure 4.13). We observed no relationship (r^2 never > 0.06) between *G* or *g* and ϑ_0, S_0 or surface chlorophyll *a* concentrations. The lack of a relationship between *c*(chl-*a*) and *G* could be due to the different integration times of the measurement: *G* integrates over the residence time of O_2 over the mixed layer (15 days for the gyre) and *c*(chl *a*) more closely reflects the shorter lifetime of the phytoplankton community.

Overall, the relationship between z_{lim} and G was very weak (r^2 = 0.05). When the z_{lim} was subdivided into three different depth sections, r^2 increased to 0.11 for data from above 50 m, while no better relationship was found for the z_{lim} between 0 and 50 m. Only two data points were available for areas with no nutrient limitation (z_{lim}<0), so no regression was done. In any case, the lowest values of G were associated with mixed layer under low to high nutrient limitation, whereas the high values of G were associated with low to no nutrient limitation. Also, no relationship was found between *g* and k_w (r^2=0.01).

What was striking was an unexpected strong inverse relationship between *G* and *f* (r^2=0.83) (Figure 4.13f). The expected outcome was that for high values of *G*, *f* would also be high. Instead, the highest *f*, up to 0.8, was found in samples with the lowest *G*, and in samples with high *G* (above 300 mmol $m^{-2}d^{-1}$), *f* was < 0.05. This relationship was not linear, but hyperbolic, and it explains 83% of the variability in *G* present in the data. Due to the low variability of the $\Delta(O_2/Ar)$ compared to *g*, *f* can be approximated by 6 mmol m^{-2} d^{-1} / *G* .

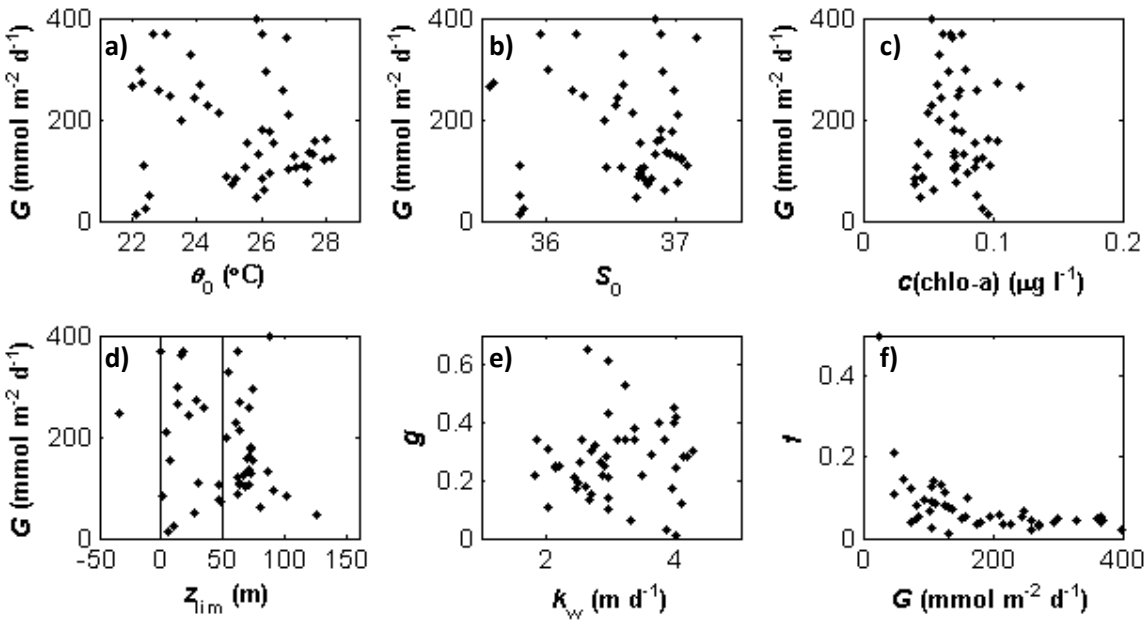

Figure 4.13: Comparison of different predictor variables to gross oxygen production (*G*) and *g*. a) *G* versus sea surface temperature (ϑ_o); b) *G* versus sea surface salinity; c) *G* versus surface concentration of chlorophyll *a* –*c*(chlo-a)-; d) *G* versus nutrient limitation (z_{lim}, lines in the figure added to help visualize three different relationships between *G* and z_{lim}); e) *g* versus gas transfer (k_w);and f) *G* versus the *f* ratio (f=*Δ*(O_2/Ar)/*g*).

(6) Regarding the analysis of FRRF data presented as photosystem quantum efficiency (F_v/F_m, Figure 4.8-b), it appears that the area to the west of the Greenwich meridian has a more stable F_v/F_m and the area to the east is more variable. I hypothesize that this difference across different regions of the gyre is due to a different phytoplankton species composition. Traditionally, F_v/F_m was interpreted as an indicator of nutrient or light stress (Huang *et al.*, 2012) (Cassar *et al.*, 2009). On the other hand, Sugget *et al.*(2009), proposed that F_v/F_m was not only an indicator of nutrient stress but also was dependant on the taxonomic composition of the sampled area. If this is correct, the ecosystems in the two sections of the gyre should be differentiated by their respective nutrient availabilities – poorer in nutrients to the west and higher concentrations of nutrients to the east, which is influenced by the Benguela current (Figure 4.8-b). That is why my findings – cells to the west seemed less stressed, with F_v/F_m values of 0.45 to 0.6, while the lower values of 0.3 to 0.5 recorded in the east – were unexpected. This might be explained by higher activity of Photosystem II (PSII) to the west, where cells are adapted to low nutrient concentrations and manage the excess of light by mechanisms like the Mehler reaction in order to alleviate damaging effects of high rates of

photon absorption by PSII (Grossman *et al.*, 2010). One explanation of this unexpected result could be that to the east the autotrophic organisms are typical of high-nutrient ecosystems and when entering the gyre they experience high stress leading to low values of F_v/F_m. On the other hand, Sugget *et al.*(2009) found in laboratory experiments that when cells growing in nutrient-poor conditions were fertilized with N, their F_v/F_m decreased; therefore, it is possible that cells from the gyre, when exposed to higher concentrations of nitrogen from the upwelling, might experience a decrease in F_v/F_m.

4.4.4. Previous measurements of gross production

(7) The ***G* measurements** recorded by different authors (Table 4.2), were also measured in different seasons and different years, which is important to remember when comparing them. Marañón *et al.*(2003) found an average for two spring and two summer seasons of 38 mmol m^{-2} d^{-1} O_2, which is a lower value than the average of the two seasons as measured by Gist *et al.*(2009) of 57 mmol m^{-2} d^{-1} O_2. Data for a single season recorded by Serret *et al.*(2009) and Gist *et al.*(2009) seem to be much more similar to each other than either is to those of Marañón. Considering that all those studies integrated production within the euphotic layer, their values of *G* are very small compared to the results of the present study, which do not integrate the entire euphotic layer and were restricted to the mixed layer. The fact that the method used here considered only production within the mixed layer implies that I could, if anything, have underestimated production. However, my values of 177 mmol m^{-2} d^{-1} were nearly four times greater than those measured by Gist *et al.*(2009). My findings for *G* have a greater uncertainty than those for *N* so a comparison with previous data has to be much more cautious.

Several factors increase the uncertainty for valuing *G*: (1) it is possible that the differences observed could be attributed to inter-annual variability. (2) The entrainment from below the mixed layer might enhance the difference in *G* values, and, as discussed earlier, this is probably at about 4% assuming a constant mixed layer; if this is the case then it is unlikely to have caused the difference with the measurements of previous studies. But if the mixed layer has deepened then O_2 from below the mixed layer has entrained, this process was modelled by Nicholson *et al*. (2012) and was accounted to be of 60% and 80 % of the observed values at BATS and HOT respectively.

(3) As with the variability in *g* values, depending on the parameters used to calculate it, I showed that a difference of up to 30 % between *G* calculated with the $*\delta_{VSMOW}$ reported by

L&B (122 mmol O_2 m^{-2} d^{-1}) and that calculated by K&A (177 mmol O_2 m^{-2} d^{-1}). (4) The wind speed parameterisation accounts for 30 % of the error in G.

Finally, (5) it is plausible that the Mehler reaction might be an important mechanism regulating to the light stressed cells in this area (Grossman *et al.*, 2010). This reaction might show an increase in the *G* of up to 10-60% when actually there is no real fixation of C or release of O_2 (Kana, 1990; Kana, 1992). This reaction happens in the PSII, which would increase the likelihood that it would produce the high values of the F_v/F_m seen (Figure 4.8-b).

Table 4.2: Results reported for *G* (gross oxygen production) from previous studies and data from this study in the South Atlantic Gyre. Columns represent: the reference source of the data; the number of stations for which the study reported values; the season with "S" and "A" standing for spring and autumn; the value of *G* as the gross oxygen production; the technique used; and latitude and longitude of the locations of the measurements.

Reference	no. of st	season	*G* (mmol m^{-2} d^{-1})	Technique used	lat (° N)	lon (°E)
Marañón *et al.* 2003	25	S & A	38 ± 18	Integrated production rate (^{14}C 7 h), *PQ=2.7	-8 to -32	-28 to -44
Serret *et al.* 2006	5	S	60 ± 8	O_2 in vitro incubation for 24 h (GP)	-10 to -34	-16 to -54
Gist *et al.* 2009	28	S	72 ± 26	O_2 in vitro incubation for 24 h (GP)	- 10 to -35	-3 to -35
Gist *et al.* 2009	28	A	42 ± 26	O_2 in vitro incubation for 24 h (GP)	- 10 to -35	-3 to -35
This study	50	A	177 ± 98	isotopic composition of dissolved O_2	-24.00	-40 to 10

(*) Photosynthetic Quotient (PQ) used here is taken from Marra (2002).

When the effect that the Mehler reaction might have on *G* is considered, it is very likely that it is this reaction that is responsible for the abnormal relationship between *f* and *G* depicted in Figure 4.13-d. This relationship would initially suggest that greater *f* ratios occur at very low values of *G*, which is counterintuitive. This relationship relies mainly on the variability in *G*. It is very likely that the more light stressed the cell might be, the smaller the $\Delta(O_2/Ar)$ (thus *N*), and, in opposing behaviour, the greater the value of *G*, though probably due to Mehler reaction as a mechanism for coping with excess of light as opposed to C fixation. The relevance of the Mehler reaction in oligotrophic areas is assumed to be higher than in other areas where there are higher nutrient concentrations and less light, but the magnitude of variability in the influence of this reaction is unknown, with reported values of Mehler reaction ranging from 10% to 60% of all the apparent C fixation (Kana, 1990; Kana, 1992).

There are studies in other oligotrophic regions using O_2 isotopologues. Juranek *et al.* (2012) recorded *G* values of 89±9 mmol m^{-2} d^{-1} for the North Pacific subtropical gyre during six different cruises. Juranek *et al.* (2010) recorded G values of 98±8 and 115±7 mmol m^{-2} d^{-1} for the North and South Pacific gyre, respectively, during 2 cruises. Quay *et al.* (2010) from a time series at the ALOHA site obtained an average of 81±39 mmol m^{-2} d^{-1} during the Northern summer. These measurements are far from my estimate of 177±98 mmol m^{-2} d^{-1}, but if I calculate *G* using L&B values for $*\delta_{VSMOW}$ (as previous studies have used, albeit implicitly) I obtain 122±63 mmol m^{-2} d^{-1}, a value within the standard deviation of the other studies.

4.5. Conclusions

(1) A gradient from west to east was observed in ϑ_0, S_0 and associated with it there was a gradient in $c(O_2)$ and $\Delta(O_2/Ar)$. The sea-to-air flux of O_2 was 16±4 mmol m^{-2} d^{-1}.

(2) The biological O_2 saturation anomaly derived from continuous measurements showed a consistent supersaturation across the gyre. When accounting for entrainment into the mixed layer, this gave an average *N* of 10±3 mmol m^{-2} d^{-1}.

(3) No clear relationship was found between ϑ_0, S_0, *c*(chl *a*) or *f* ratio and *N*. A weak correlation (r^2 = 0.30) was found between *N* and z_{lim} for highly stressed cells with z_{lim} > 50 m, with higher values of *N* associated with less severe nutrient stress. Also a higher r^2 = 0.34 was found when comparing $\Delta(O_2/Ar)$ to k_w but unexpectedly the relationship was negative.

(4) Based on the $\delta^{15}N$ of particulate organic nitrogen and N_2 fixation rates the gyre seemed to be separated in 2 distinct areas one west of 10 °W where N_2 fixation was higher and low values of $\delta^{15}N$. To the east, N_2 fixation rates were negligible and $\delta^{15}N$ indicates that the source of nitrogen is likely to be NO_3^-, with a gradient from 10° W to the Benguela section, probably influenced by upwelling.

(5) Other metabolic studies of the south Atlantic gyre were all done by light and dark bottle incubations and all *N* estimates were lower than mine. This difference is attributed to bottle effects for which studies have reported a change in the community when enclosed in bottles. Our measurements matched well with other measurements in other similar regions using the O_2/Ar measurements.

(6) Gross oxygen production was estimated to be 177±98 mmol m^{-2} d^{-1} (*n* = 50) when using the dual delta method proposed by Kaiser (2011b) and using $*\delta_{VSMOW}$ as reported by

Kaiser and Abe (2012). *G* calculated with $*\delta_{VSMOW}$ as reported by Luz and Barkan (2011) is 30 % lower. The formula used for the calculation of *g* did not have a great impact on *G*.

(7) Compared with other published data in the south Atlantic gyre our estimates of *G* were higher. The difference could be attributed to several causes. One of these uncertainties lies in k_w which has an impact on *G* of ±30%. Another possibility is entrainment, which can be by eddy diffusion or by mixed layer deepening. For eddy diffusion, this was estimated to be 4 % for one station for which isotope samples were collected at 6° E. If deepening of the mixed layer has occurred then past signals in photosynthesis in the O_2 would enhance the *G* measured in the mixed layer. Whether these mechanisms are relevant we cannot know, but Nicholson modelled it to be between 60 to 80% for BATS and HOT respectively. Finally but not least important it is likely that Mehler reaction might be playing a role in increasing the isotopic measurements made from the isotopes and F_v/F_m (Grossman *et al.*, 2010; Kana, 1990; Kana, 1992) but not the real C fixation, the range of this reaction is unknown and has been reported to be between 10 % to 60 %.

(8) Despite these uncertainties our measurements compared well with those in the literature for other gyres using the isotopic composition of the O_2 dissolved in the mixed layer if using $*\delta_{VSMOW}$ of Luz and Barkan (2011) as the other studies have similar results.

Chapter 5. Measurements of production in a North Atlantic Bloom

5.1. Introduction

Despite its relatively small area, covering 15% of the global ocean, the North Atlantic region absorbs 23% of the total anthropogenic carbon (C) uptake by the oceans (Sabine *et al.*, 2004). This is due to the cooling of the surface waters during northward transport, which increases CO_2 solubility, and the drawdown of CO_2 by biological activity (Takahashi *et al.*, 2009).

This biological activity is most intense during the spring bloom. The mechanisms that trigger this bloom are still under debate. The first theory was put forward by Sverdrup (1953), who hypothesised that the initiation of the bloom would occur when spring warming would decrease the depth of the mixed layer to less than the critical depth. Since then, several studies have challenged this hypothesis, suggesting different mechanisms for the triggering of the spring bloom. Waniek (2003) postulated that episodic events of stratification intercalated with storms allowing the input of nutrients to sustain the blooms. On the other hand, Behrenfeld (2010) put forward that the initiation of the bloom would start when growth and grazing of phytoplankton are decoupled, so that the bloom would start in winter time when the mixed layer is deeper than the euphotic zone and predators and prey have less chances to meet. In 2011, Taylor and Ferrari (2011) suggested that a weakening of turbulent mixing would enable the accumulation of phytoplankton growth. More recently, Mahadevan *et al.* (2012) presented a different hypothesis tested with the data of the bloom in spring 2008. It states that the horizontal gradient of density between the colder north and warmer south would generate mixed layer eddies where stratification would occur and where phytoplankton blooms would develop.

The evolution of the bloom was described by Sieracki *et al.* (1993) for the North Atlantic Bloom Experiment (NABE) in 1989. Initially, the bloom is formed mainly by diatoms, which prosper until they consume most of the silicate. It is then that there is a shift in the community which changes to small phytoflagellates. Towards the end of the diatom bloom, Sieracki *et al.* (1993) found a large amount of detritus in the water column ("*calculated as the difference between the total particulate elemental carbon measured on glass-fiber filters and the sum of the carbon in all the biomass components"*), which was absent in the second stage with the phytoflagellates and they attributed this increase in the detritus to material produced by the diatoms that did not sink with them.

Primary productivity has been measured during several studies. One of the first was in the NABE experiment as part of Joint Global Ocean Flux Study (JGOFS). In spring 1989 and 1990 net primary production was found to be between 48 to 105 mmol m^{-2} d^{-1} C (with a standard deviation of the four different studies of 18 mmol m^{-2} d^{-1} C) by means of ^{14}C uptake in bottle incubations (Bender *et al.*, 1992; Bury *et al.*, 2001; Joint *et al.*, 1993; Martin *et al.*, 1993).

Previous estimates of net community production (*N*) have been derived by several methods, including; ^{234}Th budgets, daily changes in O_2 and CO_2, NO_3^- drawdown, DIC drawdown, PO_4^{3-} drawdown, O_2 budget and POC budget (Bender *et al.*, 1999; Buesseler *et al.*, 1992; Chipman *et al.*, 1993; Robertson *et al.*, 1993; Sambrotto *et al.*, 1993). Such studies for NABE in May 1989 experiment measured a range of *N* from 5-90 mmol m^{-2} d^{-1} C with a mean of 47 mmol m^{-2} d^{-1} C.

In this chapter is described the biological flux of O_2 from the sea to the atmosphere during a spring bloom in the North Atlantic in 2008. Based on O_2 observations is shown the highly variable nature of the North Atlantic Bloom. As described in earlier studies, it is common to find different water masses with different biological conditions in close proximity.

This study was part of a project studying the bloom from a Lagrangian float which followed the same water mass, here is described the biological O_2 flux produced by this water mass, as measured on a ship, and compare it to the float measurements. Also, is discussed, based on flow cytometry (Mike Sieracki), biological O_2 production in two different stages of the bloom, the first one dominated by diatoms, followed by a second stage dominated by nanophytoplankton.

5.2. Methods

The data used for this study were collected on board of RV/Knorr in an area Southwest of Iceland centred at 61.4° N 26° W between 1 and 22 May 2008 (Figure 5.1). Data were collected for the analysis of O_2 and O_2/Ar concentrations in surface waters for quantification of net community productivity (*N*). In addition, the isotopic composition of the O_2 dissolved in the water was measured for the determination of the gross production in terms of O_2 (*G*).

Continuous measurements from the underway sea water (USW) of O_2 and O_2/Ar were collected, as well as discrete samples for the analysis of their $c(O_2)$ and evacuated bottles for O_2/Ar and isotopic composition of the O_2 dissolved in the water. From the Niskins on the CTD,

discrete samples for the measurement of O_2 concentration were collected to calibrate the O_2 sensor on the CTD. Discrete evacuated bottle samples were also taken for Paul Quay and for me from both the CTD and the USW for analysis of their O_2 isotopic composition and O_2/Ar concentrations.

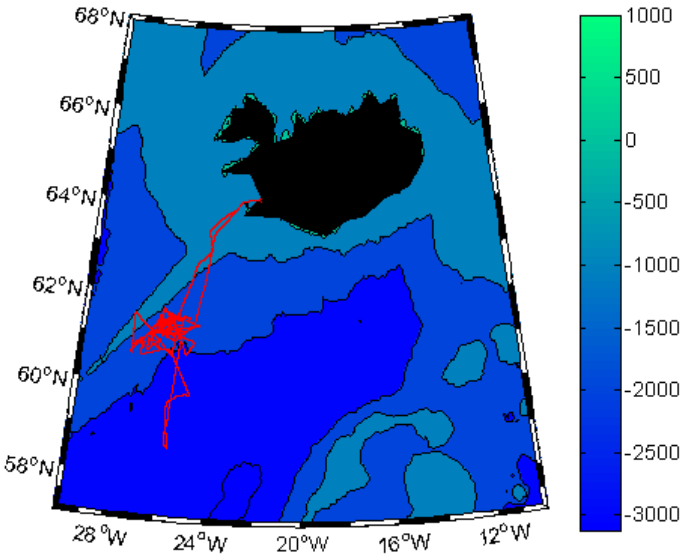

Figure 5.1: Map showing the location of the study. Blue colours represent depths in m as indicated by the colourbar. The black colouring represents depths above sea level, in this case Iceland. The red line represents the cruise track.

Ancillary continuous measurements taken in the underway sea water supply (USW) were the sea surface temperature (ϑ_0), salinity (S_0) and the concentration of chlorophyll *a* (c(chl *a*)). Sea surface temperature from the USW was calibrated against the temperature measured by the CTD sensor in surface waters. This procedure was repeated for the salinity. Chlorophyll *a* concentrations were measured continuously by Giorgio Dall'Olmo and Toby Westberry by hyperspectral absorption-attenuation meter (ACs) (Westberry *et al.*, 2010). The phytoplankton species composition was studied at selected CTD stations (Mike Sieracki with a Becton Dickinson FACScan flow cytometer (Sieracki and Poulton, 2011)).

O_2 optode USW concentrations - $c(O_2)$ - were calibrated against discrete Winkler samples taken from the USW (Figure 5.2). The O_2 calibration is explained in detail in Chapter 3. In brief, the raw signal from the optode (DPhase) was compared to the discrete Winkler measurements. To do so, the $c(O_2)$ obtained by the discrete sampling were converted to

DPhase using the inverted manufacturer-provided sensing foil calibration equation. From all the optode $c(O_2)$ data, approximately 36% were disregarded, because of problems with bubbles or shut-down of the USW. The periods with bubbles display abnormal variability with very high values of O_2 concentration alternated with lower $c(O_2)$ values, which were more in line with expectations. During the USW shut-down the O_2 concentration decreased over time on 4 May 2008 (year-day 125). The four periods with bubbles were 3-5 (year-day 124-126), 9-10 (year-day130-131), 17-18 (year-day 138-139) and 19-22 (year-day 140-143) May, 2008. These periods were recognized when the $c(O_2)$ of samples from the CTD was lower than that of the USW by more than 2.65 µmol kg^{-1}. These periods were not used for the study presented here.

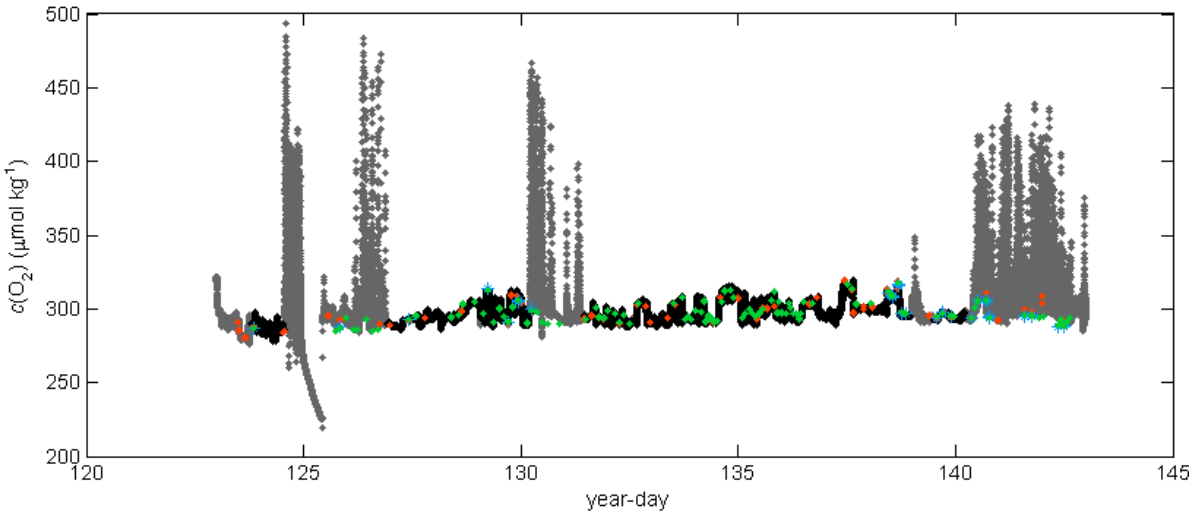

Figure 5.2: All calibrated O_2 concentrations ($c(O_2)$) over time (measured as year-day; year-day represents the days since year 2008 started, day 1= 1st January) are represented as grey points. Black points represent data considered to be good without influence of bubble periods in the USW and a temporal closure of the USW from year-day 124.5 to year-day 125.5. Orange points show the discrete Winkler samples from the underway sea water (USW) used to calibrate the continuous data from the optode. Green points are the $c(O_2)$ as measured by the CTD sensor at the surface and which were calibrated against the Winkler samples collected from the surface Niskin depicted in turquoise points on the graph.

The CTD O_2 sensor was calibrated by direct comparison with the discrete Winkler samples versus the sensor O_2 concentration reading. The O_2 data from the CTD was used for calculation of the change of $c(O_2)$ in the pipes of the ship. On average there was net consumption of O_2 in the pipes of the R/V Knorr (Figure 5.3). This consumption was -0.6±1.0

µmol kg^{-1} (mean±standard deviation) as measured by the discrete Winkler measurements from the Niskins and -0.91±1.12 µmol kg^{-1} as measured by the sensor on the CTD. All data combined gave a net consumption of O_2 of -0.87±1.11 µmol kg^{-1},. This net consumption of O_2 in the pipes (R_p) accounted for 0.3% of the mean O_2 saturation concentration and was corrected for when calculating $\Delta(O_2)$, the oxygen saturation anomaly.

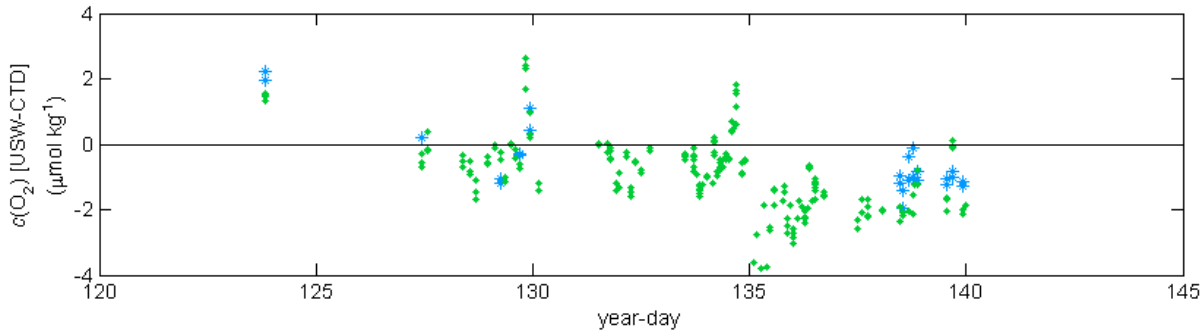

Figure 5.3: Change in calibrated O_2 concentration ($c(O_2)$) in the pipes measured as USW - CTD. Turquoise stars represent the calibrated $c(O_2)$ measured by the optode minus discrete $c(O_2)$ from samples collected from surface Niskin bottles . Green points correspond to the calibrated $c(O_2)$ measured by the optode minus surface measurements of the CTD sensor.

The **oxygen saturation anomaly, $\Delta(O_2)$** was calculated using the continuous measurements of $c(O_2)$ in the USW with the equation below:

$$\Delta(O_2) = \frac{c(O_2)}{c_{sat}(O_2)} - 1 + R_p \quad (5.1)$$

Where $c(O_2)$ and $c_{sat}(O_2)$ are the concentration and saturation concentration at in situ conditions of O_2, respectively, and R_p is the term that accounts for the 0.3% of respiration in the pipes.

The **mixed layer** depth (z_{mix}) was calculated as the depth at which the density was different by 0.01 kg m^{-3} from that at a reference depth of 10 m. The euphotic depth (z_{eu}) was calculated as the depth at which there is 1% of the surface irradiance.

The **gas transfer coefficient** was calculated as a weighted gas transfer coefficient (k_w) accounting for the wind speed history 60 days previously to the sampling, similarly as described by Reuer (2007) and explained in Chapter 3.

A gradient of O_2 occurred below the mixed layer, with generally lower $c(O_2)$ below the mixed layer, causing the O_2 in the mixed layer to diffuse downward to deeper waters (Figure 5.4-b). To calculate the "loss" of O_2 across the mixed layer, it was used a vertical eddy diffusivity (k_v) of 10^{-4} m^2 s^{-1} (Moum and Osborn, 1986). The flux was calculated as:

$$F_v = \frac{d(O_2)}{dz}\, k_v \qquad (5.2)$$

Where $d(O_2)/dz$ is the change of $c(O_2)$ over depth between the bottom of the mixed layer and 10 m below the mixed layer and K_v is the vertical eddy diffusivity.

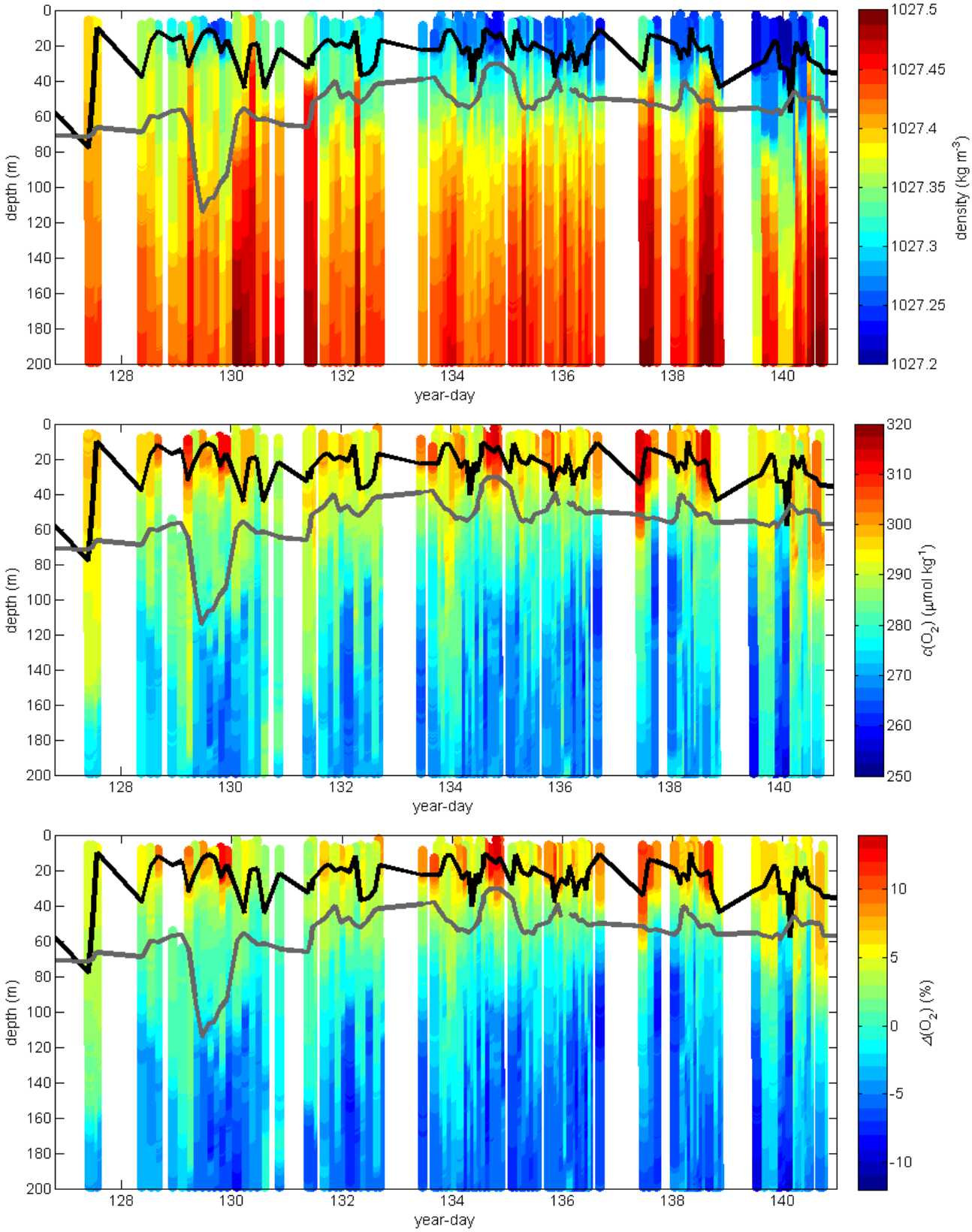

Figure 5.4: Depth profiles of the density (a), $c(O_2)$ (b) and $\Delta(O_2)$ (c) as measured by the CTD over time. The solid black line is the mixed layer depth (z_{mix}) according to the 0.01 kg m^{-3} depth density difference criterion. The gray line is the euphotic zone depth defined as the depth at which the irradiance is 1% of that at sea surface.

The biological O_2 saturation anomaly, $\Delta(O_2/Ar)$, and the isotopic composition of dissolved O_2 ($^{17}\delta$ and $^{18}\delta$) were measured back on land in UEA's Stable Isotope Laboratory for 53 discrete samples (37 from the USW and 16 from the CTD). In addition 32 samples for Paul Quay were collected which he measured independently at the University of Washington. For a comparison between these two laboratories for this study were collected 6 replicates at the same location and time. The samples were collected in 500 cm^3 pre-evacuated flasks, poisoned with $HgCl_2$. The analytical procedures are described in detail in Chapter 3. The analysis determined $\Delta(O_2/Ar)$ and $^{17}\delta$ and $^{18}\delta$ of the samples, which were used to calculate *N* and *G* respectively. Below is described how to calculate $\Delta(O_2/Ar)$ and *N.* Afterwards is explained how g was calculated, from $^{17}\delta$ and $^{18}\delta$ values, as well as from *G*.

For the calculation of $\Delta(O_2/Ar)$:

$$\Delta(O_2/Ar) = \frac{(O_2/Ar)}{(O_2/Ar)_{sat}} - 1 \tag{5.3}$$

Where (O_2/Ar) and $(O_2/Ar)_{sat}$ are the ratio of the O_2 and Ar concentrations, as measured at *in situ* conditions and at saturation.

A comparison of the $\Delta(O_2)$, as calculated from the continuous measurements of O_2 from the USW, and $\Delta(O_2/Ar)$ from the discrete samples, is presented in Figure 5.5. The slope of this relationship gives information on whether $\Delta(O_2)$ is mainly influenced by biological processes or not. In such relationship, a slope of 1 and an intercept of 0 with a high r^2 implies that all the supersaturation observed in the $\Delta(O_2)$ is due to biological processes. It was obtained a slope of 1.11±0.03 (slope±standard error) and an intercept of -0.23±0.24 % (intercept± standard error) with a high correlation (r^2=0.93, Figure 5.5), meaning that the $\Delta(O_2)$ deviates little from the $\Delta(O_2/Ar)$. Thus the biological processes affecting the $c(O_2)$ are large compared to the physical processes. Therefore O_2 alone can be used as a proxy for biological activity.

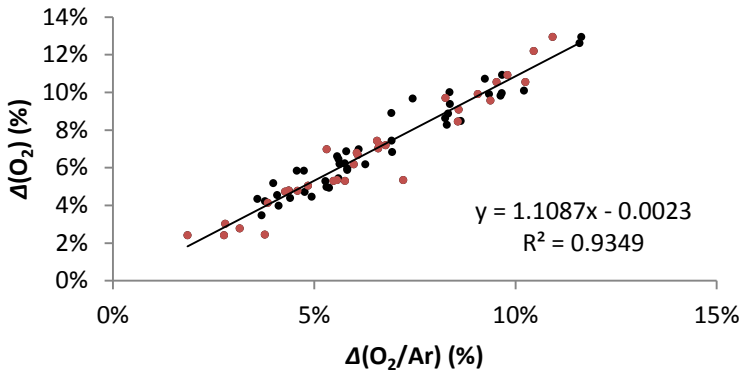

Figure 5.5: Comparison of the discrete $\Delta(O_2/Ar)$ ratios with the $\Delta(O_2)$ from the USW collected at the same time. Red dots represent the data from Paul Quay and black dots represent the data analyzed at UEA.

To estimate the physical contribution to the $c(O_2)$ observed, we calculated the Ar saturation anomaly, $\Delta(Ar)$, from the discrete measurements of $\Delta(O_2/Ar)$ and $\Delta(O_2)$ as:

$$\Delta(\mathrm{Ar}) = \left(\frac{\Delta(\mathrm{O_2}) - \Delta(\mathrm{O_2/Ar})}{1 + \Delta(\mathrm{O_2/Ar})}\right) \tag{5.4}$$

The mean $\Delta(Ar)$ was 0.44±0.67 % (mean±standard deviation) and it ranged from -1.54% to 5.70%. This means that overall the physical processes contributed 0.44% to the total $\Delta(O_2)$, which was subtracted from the $\Delta(O_2)$ using the analogous equation:

$$\Delta(\mathrm{O_2/Ar}) = \left(\frac{\Delta(\mathrm{O_2}) - \Delta(\mathrm{Ar})}{1 + \Delta(\mathrm{Ar})}\right) \tag{5.5}$$

The results from the direct comparison of $\Delta(O_2/Ar)$ and $\Delta(O_2)$ (Figure 5.5) show that $\Delta(O_2)$ can be used for calculating the biological O_2 air-sea flux, if a correction is made for the 0.44% of the O_2 anomaly that is due to physical processes (as obtained from $\Delta(Ar)$).

The biological air-sea flux of O_2 was calculated as:

$$F_{\mathrm{bio}}(\mathrm{O_2/Ar}) = \Delta(\mathrm{O_2/Ar})\, k_{\mathrm{w}}\, c_{\mathrm{sat}}(\mathrm{O_2}) \tag{5.6}$$

Where k_w is the weighted gas transfer coefficient, calculated using a weighted historical wind speed value for the previous 60 days of sampling (as explained in Chapter 3).

Assuming only vertical diffusion of O_2 from the mixed layer to the waters below (F_v) and no horizontal exchange, *N*, would be calculated as:

$$N(\mathrm{O_2/Ar}) = F_{\mathrm{bio}}(\mathrm{O_2/Ar}) - \mathrm{F_v} \tag{5.7}$$

The ratio (g) between gross O_2 production and gross O_2 influx from the atmosphere can be calculated with g (which is the ratio of gross oxygen production (*G*) over $k_w\, c_{sat}(O_2)$) with the equation described by Kaiser (2011b):

$$g = \frac{(1+\Delta(\mathrm{O_2}))(^{17}\varepsilon_{\mathrm{E}} - \gamma_R\, ^{18}\varepsilon_{\mathrm{E}}) - \frac{^{17}\varepsilon_{\mathrm{I}} - {}^{17}\delta}{1+{}^{17}\delta} + \gamma_R \frac{^{18}\varepsilon_{\mathrm{I}} - {}^{18}\delta}{1+{}^{18}\delta}}{\frac{^{17}\delta_P - {}^{17}\delta}{1+{}^{17}\delta} - \gamma_R \frac{^{18}\delta_P - {}^{18}\delta}{1+{}^{18}\delta}} \tag{5.8}$$

Where $\Delta(O_2)$ is the saturation anomaly of O_2; $^{17}\varepsilon_E$ and $^{18}\varepsilon_E$ are the kinetic $^{17}O/^{16}O$ and $^{18}O/^{16}O$ fractionation during O_2 evasion from sea to air; γ_R is the $^{17}\varepsilon_E/^{18}\varepsilon_E$ ratio of respiratory $^{17}O/^{16}O$ and $^{18}O/^{16}O$ fractionation; $^{17}\varepsilon_I$ and $^{18}\varepsilon_I$ are the kinetic $^{17}O/^{16}O$ and $^{18}O/^{16}O$ fractionation during O_2 invasion from sea to air; $^{17}\delta$ and $^{18}\delta$ relative $^{17}O/^{16}O$ and $^{18}O/^{16}O$ differences between measured O_2 and air O_2; and $^{17}\delta_p$ and $^{18}\delta_p$ relative $^{17}O/^{16}O$ and $^{18}O/^{16}O$ differences between photosynthetic O_2 and air O_2.

Gross oxygen production, *G*, was then calculated using :

$$G = g\, k_{\mathrm{w}} c_{sat}(O_2) \tag{5.9}$$

Where g is defined in equation 5.8; k_w is the weighted gas transfer coefficient and $c_{sat}(O_2)$ the saturation concentration of O_2 at *in situ* conditions.

5.3. Results

The mean $c(O_2)$ for the surface waters throughout the whole cruise was of 296.9±6.8 µmol kg^{-1} with a minimum of 278.0 µmol kg^{-1} and a maximum of 319.7 µmol kg^{-1} (Figure 5.6-a). Sharp changes in $c(O_2)$ like on year-day 129 from 295 to 310 µmol kg^{-1} over a distance of 0.7 nm show the high variability in the area. Sea surface temperature (ϑ_0) ranged between 8.0°C to 9.8°C with sharp changes of up to 1°C over distances of less than 0.5 nm (Figure 5.6-b). Salinity varied from 35.2 to 35.3 (Figure 5.6-c), but as for ϑ_0 displayed very sharp changes over short distances. Chlorophyll *a* concentrations, *c*(chlo-*a*), (Figure 5.6-d) in surface waters ranged from 0.1 to 4 mg m^{-3} and were on average 1.33±0.78 mg m^{-3}. The *c*(chlo a) also presents high variability, in particular between year-day 127 up to year-day 135.

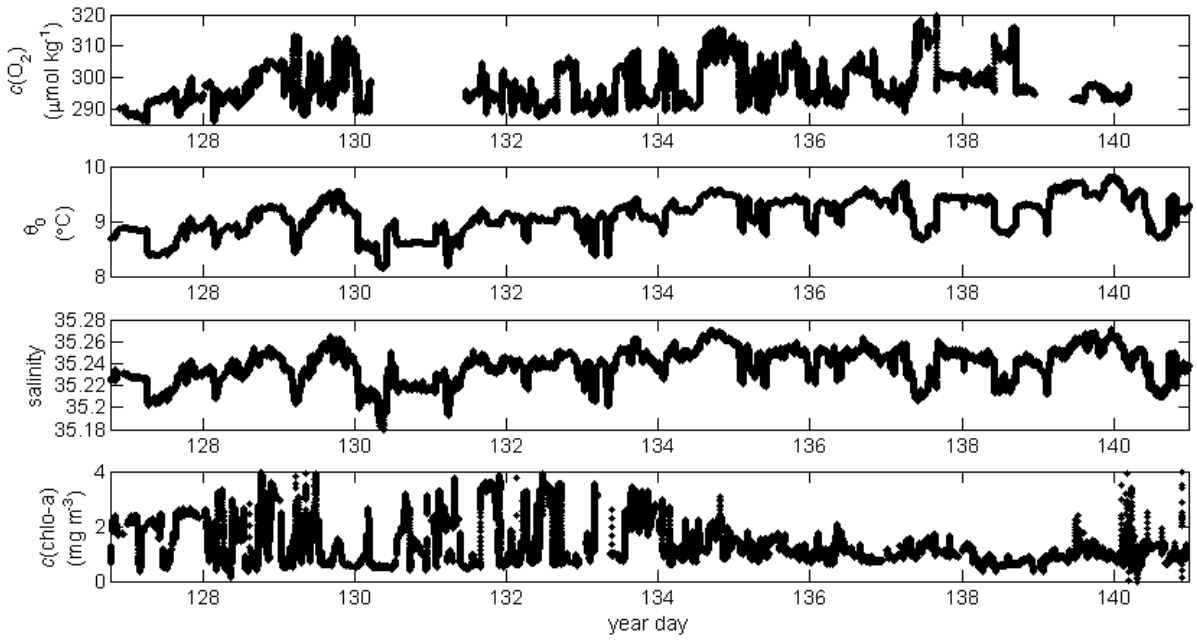

Figure 5.6: Calibrated O_2 concentrations ($c(0_2)$), sea surface temperature (θ_0), salinity and chlorophyll-a concentration (*c*(chlo-a)) in surface waters over time (year-day).

Mixed layer depths (z_{mix}) are relatively deep (78 m) at the beginning of the cruise. This is probably associated with a storm on year-day 124 (3 May 2008), which shows as a high k_w on

year-day 127 (Figure 5.7). After this storm event, the water column appears more stratified, with z_{mix} ranging from 10 to 66 m until the end of the cruise.

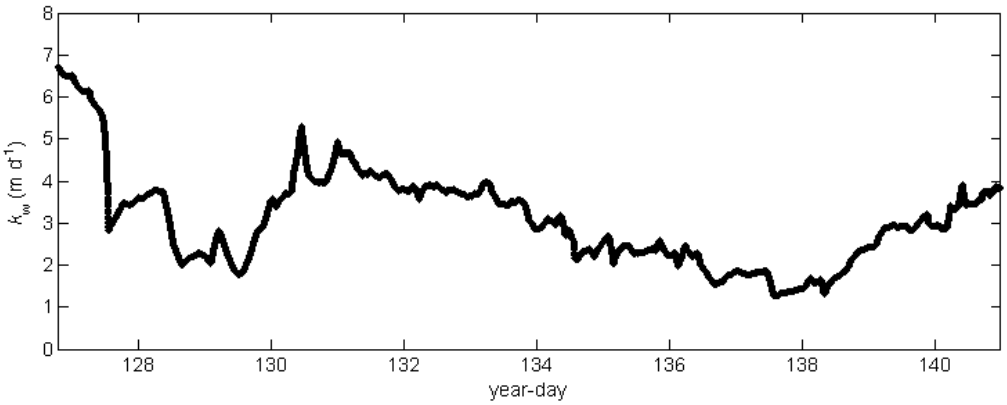

Figure 5.7: Weighted gas transfer coefficient calculated after Reuer *et al.* (2007) which integrates wind speeds from 60 days previous to the measurements. Wind speed data was extracted from the cross-calibrated multi-platform, CCMP, wind product reanalysis (Atlas *et al.*, 2009).

5.3.1. Net community production from continuous O_2 measurements and discrete O_2/Ar.

The oxygen saturation anomaly was 6.3±2.5 % (Figure 5.8) during the cruise with values ranging from 1.1% to 13.7%. Its spatial variability was high, similar to the $c(O_2)$, with changes of up to 4% over just 0.4 nm distances, as for example on 17 May (year-day 138, Figure 5.8). These sharp changes can also be observed in the centre of the grid between 27° W to 25.7° W and 61.2° N to 61.6° N (Figure 5.9). Removal of the physical effect as given by Δ(Ar) (using equation 5.5) provides a mean $\Delta(O_2/Ar)$ of 5.93%.

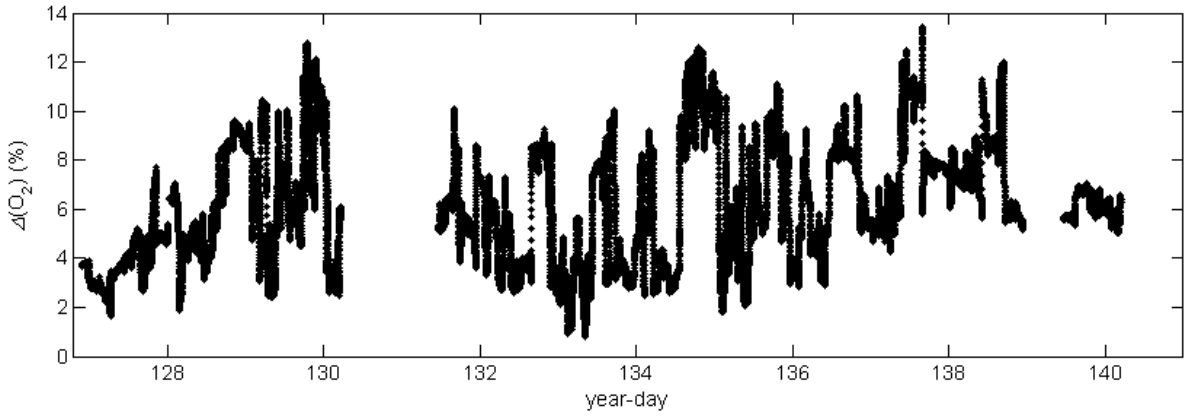

Figure 5.8: Oxygen saturation anomaly, $\Delta(O_2)$, in surface waters over time. Note the rapid changes in $\Delta(O_2)$.

The **vertical diffusive flux (F_v)** (equation 5.2) is presented in Figure 5.10, with positive fluxes indicating diffusive mixing of O_2 into the mixed layer and negative fluxes indicating diffusion of O_2 out of the mixed layer. Overall the flux was negative, meaning diffusion of O_2 from the mixed layer to the water below. The mean diffusive flux was -2.41±4.06 mmol m^{-2} d^{-1}.

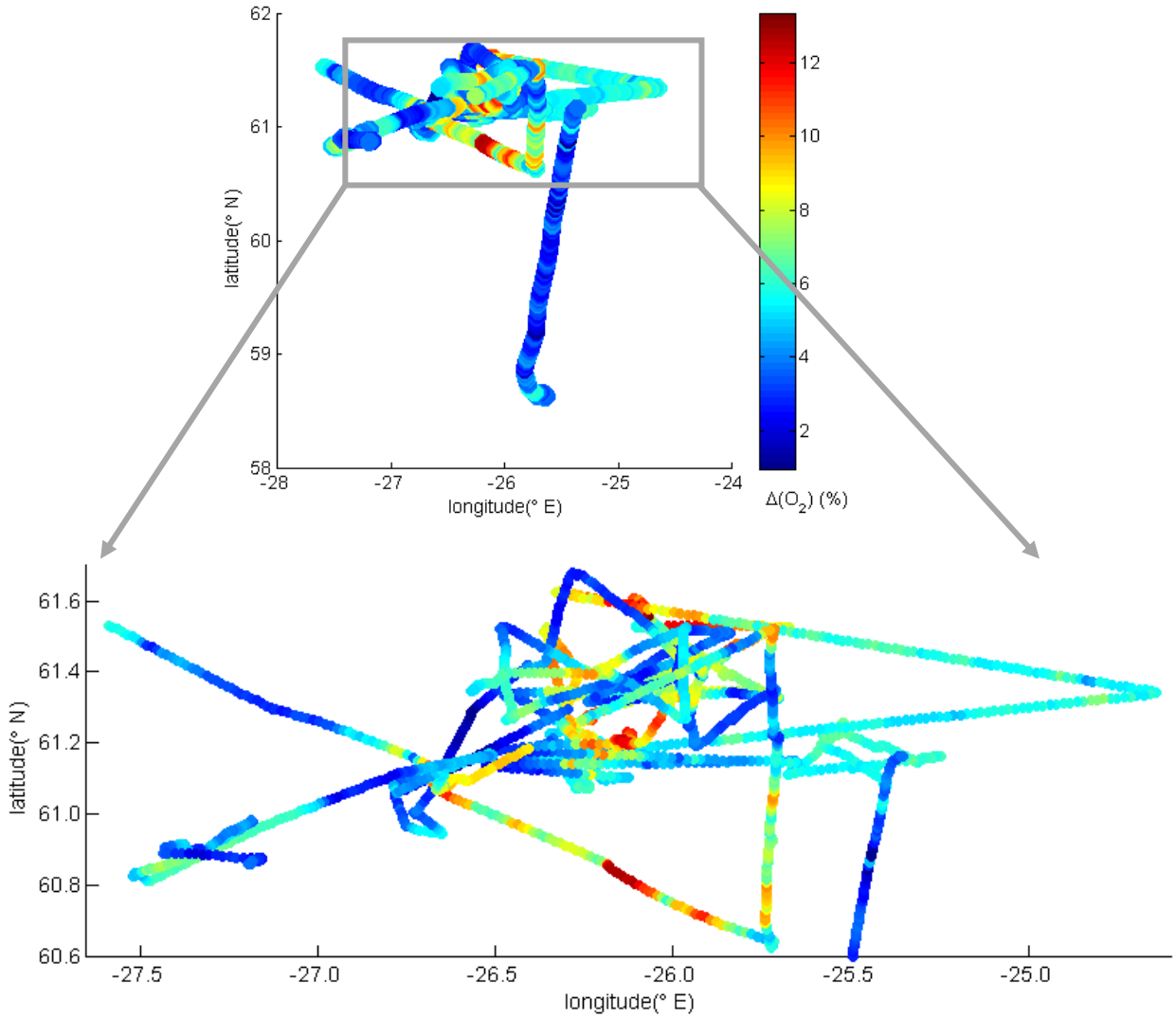

Figure 5.9: The oxygen saturation anomaly, $\Delta(O_2)$, in surface waters. Colour indicates the $\Delta(O_2)$. The top panel represents $\Delta(O_2)$ of all data collected, and the bottom panel is the inset of the area inside the box in the top panel.

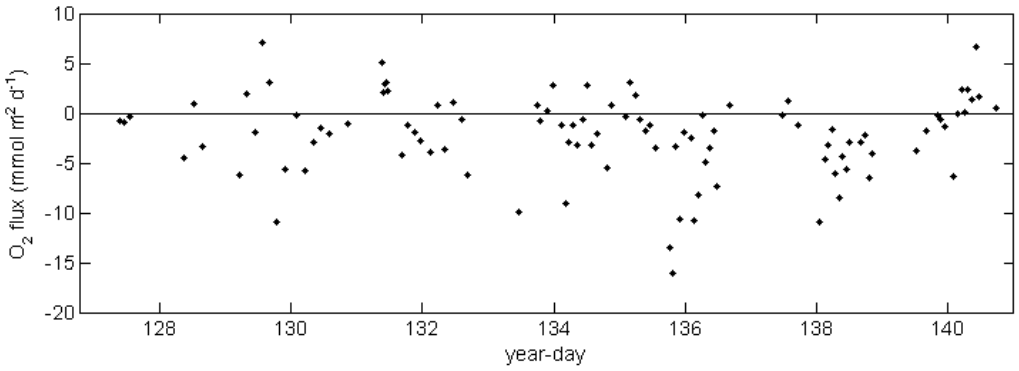

Figure 5.10: The vertical diffusive flux of O_2 calculated using the gradient of O_2 between the bottom of the mixed layer and a depth 10 m below the z_{mix} and a k_v of 10^{-4} m d^{-1}. Positive fluxes indicate diffusive mixing of O_2 into the mixed layer from waters below, negative fluxes indicate a loss by diffusion from the mixed layer to the deeper layers.

Taking into account respiration in the ship's pipes, the physical contribution on $\Delta(O_2)$ and the losses of O_2 by vertical diffusion to the waters below is calculated a $N(O_2/Ar)$ of 48.5±18.1 mmol m^{-2} d^{-1} with equation 5.7. For this estimate horizontal mixing was neglected. This would not be very realistic for individual data points in the light of the large spatial variability in the other parameters, for example ($\Delta(O_2)$, ϑ_0, S_0, c(chlo-a). However, since horizontal mixing influences cancel out for this spatial average value, in this study was nevertheless considered to be representative for the biological community in the region of interest.

A similar value of $N_{discrete}$ (O_2/Ar) of 56.0±16.6 mmol m^{-2} d^{-1} is obtained, if only the discrete O_2/Ar data from the evacuated bottles are used and a correction is made for the respiration in the pipes

5.3.2. Net community production for the water mass identified by the Lagrangian float

The spatial heterogeneity for ϑ_0, S_0 and other parameters in this region (Figure 5.6), challenges the assumption of steady state, which is necessary for $N(O_2/Ar)$ to fully represent net community production. For the assumption of steady state to be true, the calculation of $N(O_2/Ar)$ was repeated for the NAB'08 bloom waters, as identified by the Lagrangian float (Alkire *et al.*, 2012). This float surfaced every day, which provided a daily location which was

used as a proxy to identify the same water mass. Thus for this analysis it was considered only data that was within a distance d from the float. The distance *d* was defined as the minimum distance at which a sharp change in the $\Delta(O_2)$ values occurred. The value of "*d*" was observed to be 0.4 nm with a change of 3.9% in the $\Delta(O_2)$ on year-day 138.42, or 07 May 10:14 (Figure 5.8). In practice most data with *d* smaller than 0.4 nm were only observed when the float surfaced (Figure 5.12).

The data within distance "*d*" always presented high values of $\Delta(O_2)$, which indicates that these points were in an area inside the bloom. $\Delta(O_2)$ values ranged from 7 to 12% and were of 9%±1% on average, resulting in an $N(O_2/Ar)$ of 67.2±23.3 mmol m^{-2} d^{-1}.

None of the discrete O_2/Ar collection times corresponded to a distance of less than 0.4 nm; therefore, only continuous O_2 data could be used.

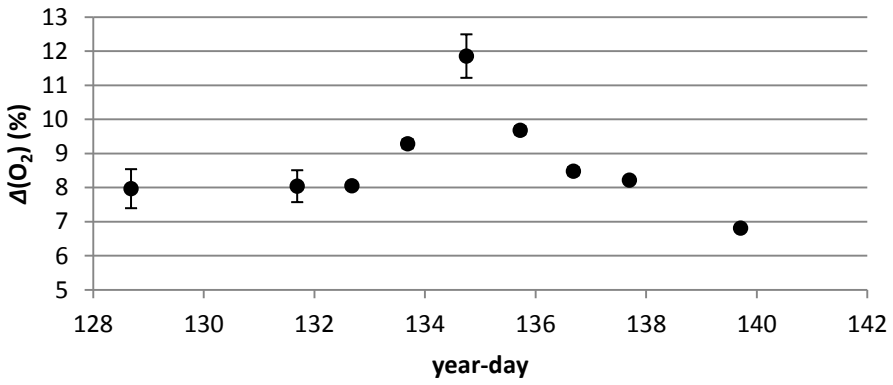

Figure 5.11: $\Delta(O_2)$ over time (year-day) for the data within 0.4 nm of the float-track. The data here represents the averages, with standard deviation as the error bars, of each of the periods when the float surfaced.

5.3.3. Comparison to Paul Quay's findings

Six discrete samples were taken in duplicate in 6 different locations for an intercomparison of isotopic and O_2/Ar analyses by the laboratories of Paul Quay and UEA. A comparison of $\Delta(O_2/Ar)$ values from these discrete samples resulted in a mean of the differences of $\Delta(O_2/Ar)$ = 0.30±0.41 % (Table 5.1, average±standard deviation). This standard deviation is smaller than the standard deviation of this study samples replicates (0.36%) and of

those analysed by Paul Quay (0.76%), suggesting agreement between the two sets of analyses for $\Delta(O_2/Ar)$.

There is not such agreement between the analyses of the isotopic compositions of these two groups of samples: The difference between this study samples and Quay's samples for $^{17}\delta$ and $^{18}\delta$ was 0.542±0.042 ppm and 0.997±0.076 ppm, respectively. These differences are much greater than the mean standard deviation of the measurements by either Paul Quay or the present study, with highest values of 0.085 and 0.163 for $^{17}\delta$and $^{18}\delta$, respectively, for the analyses by Paul Quay. For $^{17}\Delta$, the mean difference of this study samples minus Quay's is 25±24 ppm, which is twice the standard deviation of samples analysed by Quay and similar to the standard deviation for the present study samples. Therefore, although the difference of the $\Delta(O_2/Ar)$ analyses by the two laboratories is not significant, the analyses of the isotopic compositions are different.

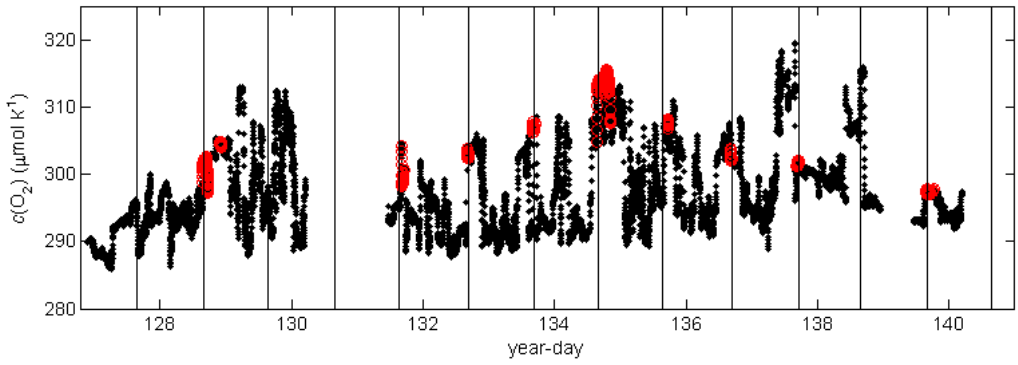

Figure 5.12: The oxygen concentration in surface water over time. Black points represent all available data, and red points represent data within 0.4 nm of the float-track. Black lines represent the timings at which the float was surfacing.

Table 5.1: Summary of the results of a comparison of 7 seawater samples. In the first row is presented the mean ± standard deviation of the difference between this study data (UEA) and Paul Quay's. The second and third row shows the mean standard deviation of the samples by Paul Quay and UEA, respectively.

	$\Delta(O_2/Ar)$	$^{17}\delta$ (‰) (ppm)	$^{18}\delta$ (‰) (ppm)	$^{17}\Delta$ (ppm)
[UEA-Quay] mean ± stdev	0.30% ± 0.41%	0.542 ± 0.042	0.997 ± 0.076	25 ± 24
Quay's stdev	0.76%	0.085	0.163	11
UEA's stdev	0.36%	0.013	0.071	22

5.3.4. Gross O_2 production in the North Atlantic Bloom

Calculation of the gross oxygen production was done from the discrete evacuated bottle samples collected from the USW and the surface CTD. From them it was obtained a g_{KA} of 0.8±1.3 which resulted in an average gross oxygen production G_{KA} of 542±804 mmol m^{-2} d^{-1}, if the $^{i}\delta_{SMOW}$ (where "i" is 17 or 18) as reported by Kaiser and Abe (2012) is used. For the $^{i}\delta_{SMOW}$ as reported by Barkan and Luz (2011) it was obtained a g_{BL} of 0.4±0.5 and a G_{LB} of 304±316 mmol m^{-2} d^{-1}. Calculating the f ratio as $f=\Delta(O_2/Ar)/g$ (Bender, 2000) it was obtained a f_{KA} 29% and f_{BL} 39%.

5.4. Discussion

(1) Several surface water parameters, temperature, salinity, c(chlo-a), $c(O_2)$ and $\Delta(O_2)$,—showed high variability with very sharp changes across small distances. This variability was expected, as earlier studies had described the heterogeneity of this area with its scattered submesoscale eddies.

(2) From continuous surface measurements of $c(O_2)$, discrete measurements of Δ(Ar) and estimates of air-sea exchange of O_2, here is reported a first-order (first order because horizontal mixing is ignored) estimate of $N_{cont}(O_2/Ar)$ for this area of 48.5±18.1 mmol m^{-2} d^{-1} and a first-order estimate $N_{discrete}(O_2/Ar)$ from the discrete O_2/Ar data of 55.0±16.6 mmol m^{-2} d^{-1}. $N_{discrete}(O_2/Ar)$ estimates from the discrete bottles were higher than those of the continuous data. This difference was expected because $N_{cont}(O_2/Ar)$ included regions of lower productivity like the leg South of 60.6° N where $\Delta(O_2)$ were much smaller than the central area where all the discrete samples of O_2/Ar were collected (Figure 5.9). This is also evident from the larger standard deviation for the continuous measurements of 18.1 mmol m^{-2} d^{-1}, relative to 16.6 mmol m^{-2} d^{-1} for the discrete measurements.

(3) Based on a set of 32 samples collected from the same 3-week bloom study, Paul Quay reported a mean $N(O_2/Ar)$ of 87±12 mmol m^{-2} d^{-1} (Quay *et al.*, 2012). Using his raw data, it was obtained a mean of 55.0±16.6 mmol m^{-2} d^{-1}. Quay *et al.* (2012) and this study used the same wind speed parameterization (Nightingale *et al.*, 2000); therefore this difference could only be explained by the different approach to calculating z_{mix}, used for the calculation of k_w (Reuer *et al.*, 2007), and the different wind data product used for the calculation of k. Quay *et al.* (2012) defined their z_{mix} by a difference of 0.03 kg m^{-3} relative to 10 m depth; in this study was used a difference of 0.01 kg m^{-3} because this criterion seemed to correspond more closely

to the changes in O_2 in the water column. Moreover, others have used this same criterion (Alkire *et al.*, 2012). The effect of the choice of z_{mix} criterion on *N* was tested and that it was found to represent 9% of the value of $N(O_2/Ar)$.

The other parameter that differed between the two estimates of N was the wind speed product used to calculate k_w. While Quay *et al.* (2012) used QuickSCAT data for which he reported a difference of 1 m s^{-1} from buoy data, for the present study it was used cross calibrated multi-platform, CCMP (Atlas *et al.*, 2009) wind product, which differed from the ship's wind speed by 1 m s^{-1}. Using only the data of this study, it was calculated that a change of ±2 m s^{-1} in the wind speed would cause $N(O_2/Ar)$to vary by as much as ±50%.

Both the mixed layer depth z_{mix} and the choice of wind speed product, affect the calculation of *N*. The different assumptions for z_{mix} and the wind speed product, or just the choice of wind speed alone can explain the difference between the *N* values reported by Quay et al. (2012) and UEA. If $N(O_2/Ar)$ is calculated for Quay's samples for the same parameters that were used for treating the data of this study it was obtained: $N(O_2/Ar, Quay)$ = 55.0±16.8 mmol m-2 d^{-1}. This value is very close to this study from 53 bottles: $N_{discrete}(O_2/Ar, UEA)$ = 56.0±16.6 mmol m^{-2} d^{-1}. Combining the results from the discrete samples by Quay and UEA, $N_{discrete}(O_2/Ar)$ = 55.6±16.6 mmol m^{-2} d^{-1} is obtained.

(4) The laboratory intercomparison (Table 5.1) has shown that $\Delta(O_2/Ar)$ for both Quay and myself are very similar. This is not the case for the $^{17}\delta$ and $^{18}\delta$. The higher values of this study samples are due most likely to a mass dependent fractionation of the samples, which results in removal of the lighter isotopes and leaving behind the heavier molecules. But this cannot be the only explanation as if it was only mass dependant fractionation *G* would be not so affected. Probably some error while transferring the samples might have occurred.

(5) Given the heterogeneity of this region, it would be more correct to give an individual *N* value for each of the different water masses. By studying the same water mass, it can be assumed steady state. When using only the data that was within the same water as the Lagrangian float, which is considered to be always in the same water mass, a $N(O_2/Ar)$ of 67.2±23.3 mmol m^{-2} d^{-1} was found. This value was higher than the earlier $N_{cont}(O_2/Ar)$ of 43.46±17.82 mmol m^{-2} d^{-1} and $N_{discrete}(O_2/Ar)$ of 55.6±16.6 mmol m^{-2} d^{-1}. A higher value for N in the productive bloom waters than for the region as a whole is expected, as relatively high values of $\Delta(O_2)$ and $c(O_2)$ were also found in the patch of water identified by the float (Figure 5.12 and Figure 5.13).

(6) When examined only the data collected from the water mass in close proximity (0.4 nm) to the float, I obtained a value for $N(O_2/Ar)$ of 67.2±23.3 mmol m^{-2} d^{-1}. This estimate was higher than two previous estimates by 31% and 18%, generated from continuous and discrete samples, respectively. This higher value is attributed to the distinctively higher production, indicated by higher concentrations of O_2 (Figure 5.12 and Figure 5.13) in the water mass nearest to the float than that in neighbouring water masses.

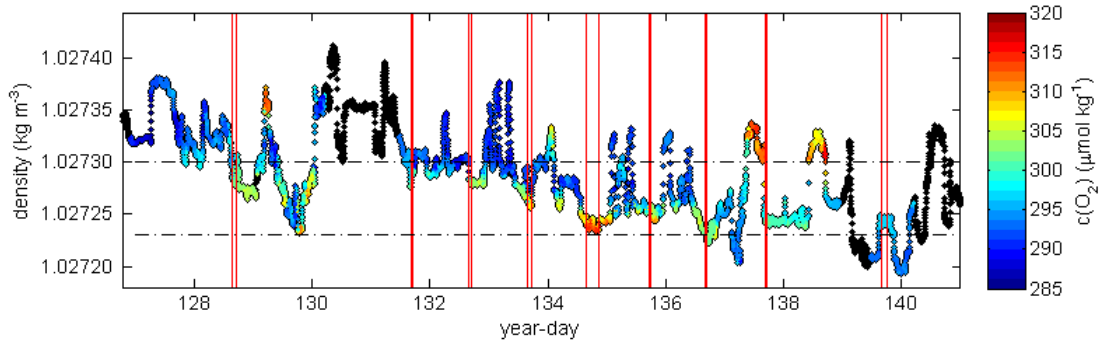

Figure 5.13: Density as calculated from θ_0 and salinity measured in the surface waters versus time. Coloured points represent the $c(O_2)$. Areas in black denote locations where O_2 data is unavailable. The data points between the vertical, closely spaced red lines depict data within 0.4 nm of the float used for the analysis of N by means of an oxygen budget $N(O_2$ budget). Horizontal black dashed lines depict the density limits of the data analyzed for the study of $N(O_2$ budget).

The water mass, which the float was following, had a relatively low density and was warmer than the neighbouring water masses (Figure 5.13). This may indicate that the warmer, more strongly stratified waters enabled the development of the bloom (Mahadevan *et al.*, 2012).

Observing the data obtained close to the float over time, the O_2 concentration increases from 300 µmol kg^{-1} to 312 µmol kg^{-1} over a 6-day period (year-day 128.7-134.7), then decreases again to its initial values of around 300 µmol kg^{-1} over a 5-day period (year-day 134.7-139.7, Figure 5.12). This tendency was also shown by Alkire *et al.* (2012) for the data acquired with the float. They studied the bloom dynamics over time with budget calculations of O_2, NO_3^- and particulate organic carbon (POC). Based on the O_2 budgets, they separated the bloom into several stages and calculated net community production (in terms of O_2 and using a PQ=1.45, as they report in the paper): an early bloom (96±51 mmol m^{-2} d^{-1}); the main bloom

(167±74 mmol m^{-2} d^{-1}); the termination (-270±120 mmol m^{-2} d^{-1}) and post-bloom (3±32 mmol m^{-2} d^{-1}). The ship was on location only for the main bloom and the early stages of the post-bloom.

Below is calculated net community production based on O_2 budgets in the mixed layer for short periods of several days. These *N* values for short periods differ from my previous estimates of *N* ($N_{cont}(O_2/Ar)$, $N_{discrete}(O_2/Ar)$, which integrate relatively long time periods of several weeks. Here it will be *N* estimates based on O_2 budgets in the mixed layer with the float estimates of *N* by Alkire *et al.* (2012) for the main bloom and the early stages of the post-bloom.

Net community production based on O_2 budgets was calculated as the change over time of the $c(O_2)$ inventory (I, mmol m^{-2}) in the mixed layer accounting for air-sea gas exchange:

$$I_{(i)} = \int_0^{z_{mix}} c_{(i)}(\mathrm{O_2})\,\mathrm{d}z = c_{(\mathrm{i})}(\mathrm{O_2})\,z_{\mathrm{mix}} \tag{5.10}$$

$$F_{\mathrm{ASE(i)}} = k_{\mathrm{w(i)}}[\,c_{(i)}(\mathrm{O_2}) - c_{\mathrm{sat(i)}}(\mathrm{O_2})\,] \tag{5.11}$$

$$N(\mathrm{O_2\ budget}) = \frac{I_{(\mathrm{i+1})} - I_{(\mathrm{i})}}{t_{(\mathrm{i+1})} - t_{(\mathrm{i})}} + \frac{(F_{\mathrm{ASE(i)}} + F_{\mathrm{ASE(i+1)}})}{2} \tag{5.12}$$

Where $I_{(i)}$ is the inventory in the mixed layer at the time i, $c_{(i)}(O_2)$ is the concentration of O_2 at time i, z_{mix} is the mixed layer depth, $c_{sat(i)}(O_2)$ is the saturation concentration of O_2 at time i, $F_{ASE(i)}$ is the air sea flux at time i and $k_{w(i)}$ the weighted gas transfer coefficient at the time i. z_{mix} was of 18±5 m which was the mean of the z_{mix} of the data within 0.4 nm of the float. The results, obtained using this approach, are presented in Figure 5.14 versus time. Only data points within 0.4 nm radius of the float were used.

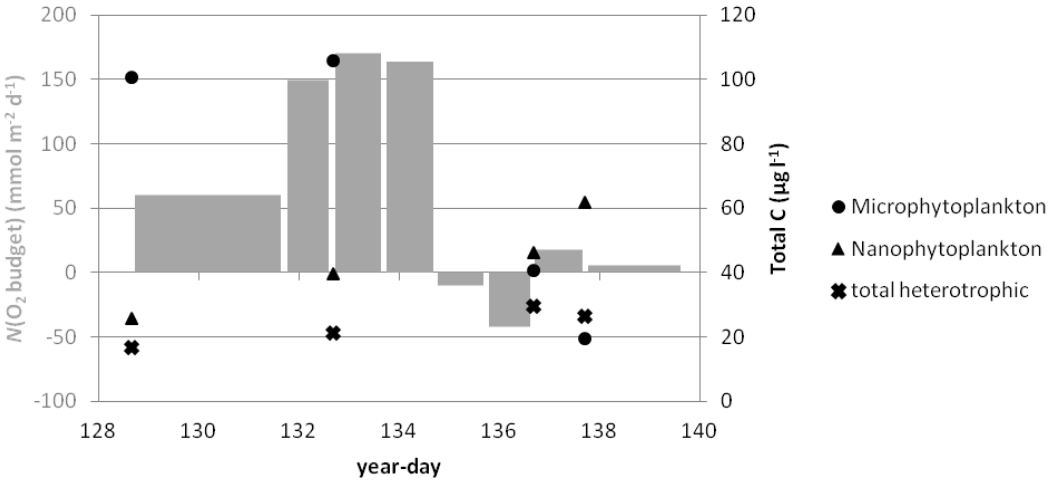

Figure 5.14: Net community production based on O_2 budget for the mixed layer, *N*(O_2 budget), over time. The width of the columns represents the time for which they were integrated. In grey circles, triangles and crosses are the total carbon biomass of microphytoplankton, nanophytoplankton and total heterotrophic organisms (nanoflaggelates and bacteria), respectively .

N(O_2 budget) shows a change over time, with prevailing net autotrophy (positive *N*) between year-days 128.7 and 134.7 with values starting at 60 mmol m^{-2} d^{-1} and reaching 170 mmol m^{-2} d^{-1}. For about 2 days from day 134.7 net heterotrophy dominates, presenting values of -10 and -42 mmol m^{-2} d^{-1}. After that period, the *N*(O_2 budget) increased to positive values (net autotrophy) of 18 and 5 mmol m^{-2} d^{-1}. The net autotrophy prevails for the rest of the sampling period.

Alkire *et al.* (2012) found a similar pattern, with high values for *N* of from year-days 127-134 and a sudden decrease occurring between year-day 134 and 135, which matches our overall trend.

(6) Here are compared the estimates from this study to those of Alkire *et al.* (2012), using only Alkire *et al.*'s *N*(O_2 budget) time span, which extends from year-day 127 to 135 . Alkire *et al.*'s *N*(O_2 budget) for the Main Bloom (year-days 127 to 134) is 115±51 mmol m^{-2} d^{-1}, which corresponds to this study budget calculations from day 128.7 to 134.7, during which *N* was 111±56 mmol m^{-2} d^{-1} (ranging 60 to 170 mmol m^{-2} d^{-1}). The "Termination" stage defined by Alkire *et al.* (year-day 134-135) is characterized by a high heterotrophic event with a *N*(O_2 budget) of -186±83 mmol m^{-2} d^{-1}. Although this study did not find such a low *N*(O_2 budget), it did find a corresponding net heterotrophic event between year-days 134.7-136.7 with an

initial value for *N* of -10 mmol m^{-2} d^{-1} that decreased to -42 mmol m^{-2} d^{-1} on the second day. After this period of net heterotrophy (after year-day 136.7), a new period started characterised by a low net autotrophy that was nearly in metabolic balance with values of 18 and 5 mmol m^{-2} d^{-1}. However, Alkire *et al.* (2012) do not present data for this period as they encounter a different water mass from a cold core eddy, but because this eddy does not appear in surface waters (which are the focus of this study) this period is included (Figure 5.13).

(7) Associated with the changes in *N*(O_2 budget) were the changes in the plankton communities. Measurements of chlorophyll-a concentration -*c*(chlo-a)- (Figure 5.15) and species abundance (Figure 5.14) from the USW followed a very similar pattern to the *N*(O_2 budget) with the highest values between year-days 131.7 until 133.7. The minimum at year-day 136.7 matched the period of net heterotrophy. Afterwards as the *N*(O_2 budget) increases, the *c*(chlo-a) also increases slightly.

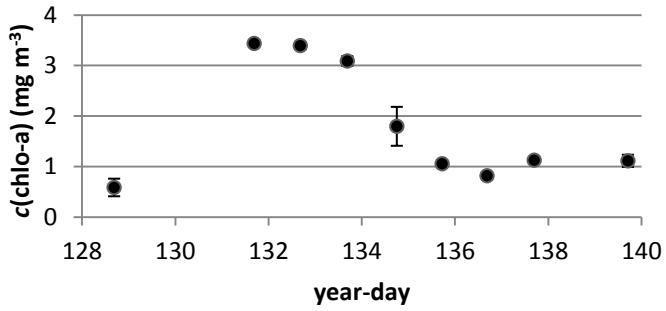

Figure 5.15: USW chlorophyll *a* concentration, *c*(chlo-a), at the locations within 0.4 nm of the float. Bars represent the standard deviation of data for each timing.

Species abundance samples were collected at selected stations by Mike Sieracki and Nicole Poulton (Bigelow Laboratory for Ocean Science) and analyzed with a Becton Dickinson FACScan flow cytometer (Sieracki and Poulton, 2011)). The samples were used for estimating the biomass of microphytoplankton (sum of autotrophic groups: diatom, dinoflagellates, ciliates and other chlorophyll containing particles), nanophytoplankton (including photosynthetic picoeukaryotes, *Synechococcus* and cryptophytes) and the heterotrophic (bacteria and nanoflagellates) organisms within the mixed layer. Four of these stations with plankton abundance data matched the location of the float surfacing (Figure 5.14). The net

autotrophic event between year-days 128.7 and 134.7 coincided with a high carbon (C) abundance of microphytoplankton. The C biomass of these groups of over 100 µg l^{-1} on year-day 132.7 sharply declined during and after the heterotrophic period to 40 and 19 µg l^{-1}. The opposite happened to the carbon biomass of nanophytoplankton, which started at 26 µg l^{-1} and steadily increased to 62 µg l^{-1} at the last station on day 137.7. The biomass of the heterotrophic community started at 17 µg l^{-1} at the first station on year day 128.7 and increased to 29-27 µg l^{-1} at the last two stations. The change in species composition is of special relevance, as has been described earlier (Sieracki *et al.*, 1993) and for this bloom (Briggs *et al.*, 2011; Martin *et al.*, 2011), because the shift from diatoms to smaller phytoplankton (due to the depletion of Si), is generally associated with a high export event to depth. Such export events dominate the annually integrated carbon export, but part of the exported carbon is respired and returned to the atmosphere when the mixed layer deepens in winter. (Körtzinger *et al.*, 2008; Quay *et al.*, 2012).

(8) Estimates of *G* either using the ${}^{i}\delta_{SMOW}$ as reported by Kaiser and Abe (2012) or Barkan and Luz (2011) were much larger than values calculated from the measurements of Quay *et al.* (2012) which gave a G_{KA} of 171±80 mmol m^{-2} d^{-1} or G_{LB} of 124±57 mmol m^{-2} d^{-1}. Values when using Kaiser and Abe were 3.2 times higher than those of Quay *et al.* (2012) and when using the Barkan and Luz the values were 2.5 times higher. Quay *et al.* (2012) reported *f* values of 0.40, but when calculated the *f* ratio from their values I obtained 0.40-0.54, which is considerably larger than the *f* ratio for this present study data of 0.29-0.39.

5.5. Conclusions

(1) The North Atlantic in Bloom presents very high variability which shows in the θ_0, salinity, *c*(chlo-a) and *c*(O_2) with sharp changes over distances of 0.4 nm. This high variability was due to crossing different water masses as shown by the data. It is probable that the different water masses are at different stages of the spring bloom

(2) When not considering the spatial variability it was calculated a first order *N* that ranges 48.5-56 mmol m^{-2} d^{-1} from continuous and discrete measurements, respectively. The *N* of 56 mmol m^{-2} d^{-1} as measured by the discrete samples analyzed at UEA compared very well with the *N* value calculated with the data from Quay *et al.* (2012) of 55±16.8 mmol m^{-2} d^{-1}, for the same wind speed product and z_{mix}.

(3) The selection of the wind speed product is highly relevant for the calculation of *N*. A different wind speed product might explain why the data reported by Quay *et al.* (2012) of 87 mmol m^{-2} d^{-1} differ so strongly from the value of 55±16.8 mmol m^{-2} d^{-1},that I calculate when using his O_2/Ar data.

(4) Net community production in the water mass with the bloom, as identified by the float, is as high as 67.3 mmol m^{-2} d^{-1}. This is considerably higher than the regional estimate of 48.5-56 mmol m^{-2} d^{-1} from continuous and discrete measurements. This highlights the relevance of submesoscale studies of bloom evolution.

(5) Seven replicate samples were analyzed independently as a laboratory intercomparison for their $\Delta(O_2/Ar)$, $^{17}\delta$ and $^{18}\delta$ in Paul Quay's laboratory and in Jan Kaiser's laboratory at UEA. The $\Delta(O_2/Ar)$ ratios were similar, but values for $^{17}\delta$ and $^{18}\delta$ differed considerably between the two laboratories.

(6) When looking at the evolution of O_2 within one water mass, as identified by a Lagrangian float, it was observed a similar development as Alkire *et al.* (2012). High values of net community production, as high as 170 mmol m^{-2} d^{-1}, were followed by a short period of net heterotrophy, before returning to net autotrophy but with lower values than before and not as high as previously when dominated by microphytoplankton (mainly diatoms). This is especially relevant because diatoms are important triggers of ocean carbon export to deeper layers when stressed by silica depletion.

Chapter 6. Conclusions and future work

6.1. Conclusions

The aim of this research was to estimate marine biological production in two distinct areas of the Atlantic Ocean: In the subpolar north Atlantic spring bloom and in the oligotrophic gyre of the South Atlantic. Mixed-layer net community production (*N)* and gross oxygen production (*G*) were estimated by continuous measurements of O_2/Ar and discrete analyses of O_2 isotopologues, respectively.

For the purpose of measuring *G* an automated extraction line was built for the analysis of the isotopic composition of O_2 dissolved in sea water. This was a joint undertaking between another PhD student (Johanna Gloël). This facility is the first of its kinds in Europe and is currently being used for samples from other regions such as the Southern Ocean.

Measurements of *N* and *G* in these two areas of the Atlantic Ocean are of relevance for the biological marine carbon cycle. The North Atlantic is thought to account for 23 % of the total anthropogenic carbon (C) uptake by the oceans (Sabine *et al.*, 2004), due to the high biological activity (in particular during spring blooms) together with enhanced physical gas transfer due to cooling of surface waters. In contrast, it is being debated whether the South Atlantic gyre is net autotrophic (i.e. a net carbon sink) or net heterotrophic (i.e. a net carbon source) (Duarte *et al.*, 2013; Ducklow and Doney, 2013; Williams *et al.*, 2013). The metabolic state of oligotrophic gyres is of relevance for the global marine carbon cycle because of their sheer size.

The results from a cruise in the South Atlantic gyre in austral autumn of 2009 showed consistent net autotrophy for the gyre with net community O_2 production of (10±3) mmol m^{-2} d^{-1} which contrasts with previous measurements by means of bottle incubations that found lower net production and often net heterotrophy (Gist *et al.*, 2009; González *et al.*, 2002; Serret *et al.*, 2006). Net community production measurements using O_2/Ar ratios in different gyres showed agreement with our estimates (Juranek *et al.*, 2012; Luz and Barkan, 2009; Quay *et al.*, 2010). It is true that the techniques used here only considered the production in the mixed layer compared to in vitro estimates that integrate over the whole mixed layer. This applies to both *N* and *G*. So, actually, what might be perceived as a bias (i.e. the flux of O_2 and ^{17}O excess from the upper thermocline into the mixed layer in the gyres) actually just offsets the error made by considering only the mixed layer rather than the entire productive region. Therefore *in situ* measurements using continuous O_2/Ar data confirm that the South Atlantic was net autotrophic at the time of sampling.

The source of nutrients to the gyre is discussed in relation to measurements of N_2 fixation rates and $\delta(^{15}N$, PON) from Mark More. It seems that there are two distinct regions within the gyre. West of 10° W, N_2 fixation dominates and NO_3^- based production is dominant east of 10° W. This is relevant to determine what sustains the observed net autotrophy.

Measurements of *G* in the gyre show high rates of (177±98) mmol m^{-2} d^{-1} when using the isotope delta of mean seawater relative to atmospheric oxygen ($*\delta_{VSMOW}$) of Kaiser and Abe (2012). With the corresponding isotope delta of Luz and Barkan (2011) (122±63) mmol m^{-2} d^{-1} was obtained. Both of these estimates are higher (by at least a factor of two) compared to previous studies in this area made by ^{14}C or O_2 light and dark bottle incubations (Gist *et al.*, 2009; Marañón *et al.*, 2003; Serret *et al.*, 2006). There could be several reasons for this including problems related to bottle incubation methods, which would underestimate gross oxygen production measured with the O_2 light and dark incubation method and primary production derived from ^{14}C measurements. Problems that could lead to overestimation of *G* are the uncertainty in the gas transfer coefficient, entrainment of O_2 from below the mixed layer and processes that might mask the *G* like the Mehler reaction which produces an anomaly in the isotopic composition of the O_2 pool, but does not fix carbon. It was hypothesized that high values of F_v/F_m found in the gyre were indicative of the Mehler reaction playing an important role in this region of the Atlantic. Its contribution to gross O_2 production may be higher than the 15 % that are usually assumed (Bender *et al.*, 1999). The Mehler reaction induced by light and nutrient stress (Grossman *et al.*, 2010) may therefore have led to higher values of *G* compared to other studies.

The measurements of *G* agree well with other studies using O_2 isotopologues in the North Pacific and North Atlantic gyres (Juranek and Quay, 2010; Juranek *et al.*, 2012; Quay *et al.*, 2010).

The second case study was performed during a cruise south of Iceland that studied the North Atlantic Bloom. The surface water showed very high spatial variability in temperature, salinity and oxygen concentrations. This variability is attributed to different water masses, which are interpreted to be in different stages of the bloom. If this variability is ignored, then *N* was estimated to be of 48.5 and 56 mmol m^{-2} d^{-1} from continuous O_2 measurements and discrete O_2/Ar ratio measurements, respectively.

During the cruise, a water parcel was tracked by a Lagrangian float, which was followed over a period of 11 days. The surrounding water parcel was in close proximity to the

float was considered to be in the bloom phase because of the higher $\Delta(O_2)$ in comparison to surrounding waters and *N* was on average of 67 mmol m^{-2} d^{-1}. Over time an evolution in the O_2 concentration was observed similar to that of Alkire *et al.* (2012) who used O_2 measurements on the float directly. Associated with it were changes in the community structure as well as the concentration of chlorophyll.

During the cruise samples were collected for another group led by Paul Quay who also performed production measurements using discrete analyses of O_2 isotopologues and O_2/Ar ratios. Their published results differ from mine because they used a different wind speed product to calculate the gas transfer coefficient. When using the same wind speed product our measurements agreed well. This highlights the systematic uncertainties of the method due to parameterisation of the air-sea gas exchange rates.

During both cruises a change of O_2 concentrations from in situ values (measured in CTD samples) to the point of sampling inside the ship, after the water had been pumped through the ship's pipes. This was –0.87 µmol kg^{-1} for the North Atlantic cruise, which resulted in a net decrease of 0.3 %, and –0.91 µmol kg^{-1} corresponding to a net decrease of 0.5% for the South Atlantic cruise (see Chapter 4). This is slightly lower than values reported by Juranek et al. (2010), which ranged from 1 µmol kg^{-1} to 4 µmol kg^{-1}, indicating that cleaning of the pipes that took place before the cruises may have had a positive effect.

6.2. Future research

Measurements of $\Delta(O_2/Ar)$ and oxygen isotopes are used more and more widely. These methods have the advantage that they can measure in situ and that their sampling requirements are less laborious than incubation methods. For instance, $\Delta(O_2/Ar)$ ratios can be measured at rates as high as 10 s with precisions up to 0.1% (other authors have done better and achieved <0.05 %) using atmosphere-equilibrated water as a standard; for O_2 isotopologues, samples can be collected and kept for future analysis.

To improve these methods it is important to reduce the uncertainty of the following parameters: For both *N* and *G* estimates, it is relevant to have a **(1)** better knowledge of the gas transfer coefficient as currently as this is one of the major sources of error in *N* and *G*. Also using the appropriate wind speed products can considerably change *N* and *G*.

Then, specifically concerning only to *G*, it is important that more work is done to understand the nature of the gross production rates measured with this technique in relation to "conventional" estimates, e.g. using ^{14}C incubations and to improve the accuracy of the underlying isotopic parameters: **(2)** Independent determinations of $^{*}\delta_{VSMOW}$ could help determine their true value and thus more accurate calculations of *G*. **(3)** Better knowledge of the extent of processes that might mask O_2 production such as the Mehler reaction. **(4)** More measurements of the fractionation of O_2 by photosynthesis for different species as currently there are only 5 species for which this is known. **(5)** More experiments to determine $^{*}\delta_{sat}$.

At the locations of study, it was demonstrated that the measurement of O_2/Ar ratios in the gyres can determine *N* but more measurements need to be done in order to determine annual rates and interannual changes. Also, continuous measurements of O_2/Ar ratios are a powerful tool for dynamical regions like the North Atlantic Bloom.

It is true that the techniques used here only considered the production in the surface mixed layer compared to in vitro estimates that can integrate over the whole euphotic zone. This applies to both *N* and *G*. So, actually, what might be perceived as a bias (i.e. the flux of O_2 and ^{17}O excess from the upper thermocline into the mixed layer in the gyres) actually just offsets the error made by considering only the mixed layer rather than the entire productive region.

References

Alkire, M.B., D'Asaro, E., Lee, C., Jane Perry, M., Gray, A., Cetinić, I., Briggs, N., Rehm, E., Kallin, E., Kaiser, J., González-Posada, A., 2012. Estimates of net community production and export using high-resolution, Lagrangian measurements of O_2, NO_3^-, and POC through the evolution of a spring diatom bloom in the North Atlantic. Deep Sea Research Part I: Oceanographic Research Papers 64 (0), 157-174.

Angert, A., Rachmilevitch, S., Barkan, E., Luz, B., 2003. Effects of photorespiration, the cytochrome pathway, and the alternative pathway on the triple isotopic composition of O_2. Global Biogeochemical Cycles 17 (1), 1030, doi:1010.1029/2002GB001933.

Arrigo, K.R., Matrai, P.A., van Dijken, G.L., 2011. Primary productivity in the Arctic Ocean: Impacts of complex optical properties and subsurface chlorophyll maxima on large-scale estimates. Journal of Geophysical Research 116 (C11), C11022.

Atlas, R., Hoffman;, R.N., Ardizzone;, J., Leidner;, S.M., Jusem, J.C., 2009. Development of a new cross-calibrated, multi-platform (CCMP) ocean surface wind product. AMS 13th Conference on Integrated Observing and Assimilation Systems for Atmosphere, Oceans, and Land Surface (IOAS-AOLS).

Barkan, E., Luz, B., 2003. High-precision measurements of $^{17}O/^{16}O$ and $^{18}O/^{16}O$ of O_2 and O_2/Ar ratio in air. Rapid Communications in Mass Spectrometry 17, 2809-2814.

Barkan, E., Luz, B., 2005. High precision measurements of $^{17}O/^{16}O$ and $^{18}O/^{16}O$ ratios in H_2O. Rapid Communications in Mass Spectrometry 19, 3737-3742.

Barkan, E., Luz, B., 2011. The relationships among the three stable isotopes of oxygen in air, seawater and marine photosynthesis. Rapid Communications in Mass Spectrometry 25 (16), 2367-2369.

Behrenfeld, M., Falkowski, P., 1997. Photosynthetic rates derived from satellite-based chlorophyll concentration. Limnology and Oceanography 42, 1-20.

Behrenfeld, M.J., 2010. Abandoning Sverdrup's Critical Depth Hypothesis on phytoplankton blooms. Ecology 91 (4), 977-989.

Behrenfeld, M.J., Marañón, E., Siegel, D.A., Hooker, S.B., 2002. Photoacclimation and nutrient-based model of light-saturated photosynthesis for quantifying oceanic primary production. Marine Ecology Progress Series 228, 103-117.

Bender, M., 1999. Carbon cycle studies based on the distribution of O_2 in air. Tellus. Series B, Chemical and physical meteorology 51. (2), 165-169.

Bender, M., 2000. Oceanography: Tracer from the Sky. Sience. Perspectives 288 (5473), 1977-1978.

Bender, M., Ducklow, H., Kiddon, J., Marra, J., Martin, J., 1992. The carbon balance during the 1989 spring bloom in the North Atlantic Ocean, 47° N, 20° W. Deep Sea Research Part A. Oceanographic Research Papers 39 (10), 1707-1725.

Bender, M., Orchardo, J., Dickson, M.-L., Barber, R., Lindley, S., 1999. In vitro O_2 fluxes compared with ^{14}C production and other rate terms during the JGOFS Equatorial Pacific experiment. Deep Sea Research Part I: Oceanographic Research Papers 46 (4), 637-654.

Bender, M.L., Karen Grande, Kenneth Johnson, John Marra, Peter J. LeB. Williams, John Sieburth, Michael Pilson, Chris Langdon, Hitchcock, G., Joseph Orchardo, Carleton Blunt, Percy Donaghay, Heinemann, K., 1987. A comparison of four methods for determining planktonic community production. Limnology and Oceanography 32 (5), 1085-1098.

Benson, B., Krause, D., Peterson, M., 1979. The solubility and isotopic fractionation of gases in dilute aqueous solution. I. Oxygen. Journal of Solution Chemistry 8 (9), 655-690.

Briggs, N., Perry, M.J., Cetinić, I., Lee, C., D'Asaro, E., Gray, A.M., Rehm, E., 2011. High-resolution observations of aggregate flux during a sub-polar North Atlantic spring bloom. Deep Sea Research Part I: Oceanographic Research Papers 58 (10), 1031-1039.

Buesseler, K.O., Bacon, M.P., Kirk Cochran, J., Livingston, H.D., 1992. Carbon and nitrogen export during the JGOFS North Atlantic Bloom experiment estimated from ^{234}Th:^{238}U disequilibria. Deep Sea Research Part A. Oceanographic Research Papers 39 (7-8), 1115-1137.

Bury, S.J., Boyd, P.W., Preston, T., Savidge, G., Owens, N.J.P., 2001. Size-fractionated primary production and nitrogen uptake during a North Atlantic phytoplankton bloom: implications for carbon export estimates. Deep Sea Research Part I: Oceanographic Research Papers 48 (3), 689-720.

Calvo-Díaz, A., Díaz-Pérez, L., Suárez, L.Á., Morán, X.A.G., Teira, E., Marañón, E., 2011. Bottle enclosure causes a decrease in the autotrophic to heterotrophic biomass ratio of picoplankton in oligotrophic marine waters. Applied and Environmental Microbiology 77 (16), 5739-5746.

Cassar, N., Barnett, B.A., Bender, M.L., Kaiser, J., Hamme, R.C., Tilbrook|, B., 2009. Continuous High-Frequency Dissolved O_2/Ar Measurements by Equilibrator Inlet Mass Spectrometry. Analytical chemistry 81.

Cassar, N., DiFiore, P.J., Barnett, B.A., Bender, M.L., Bowie, A.R., Tilbrook, B., Petrou, K., Westwood, K.J., Wright, S.W., Lefevre, D., 2011. The influence of iron and light on net community production in the Subantarctic and Polar Frontal Zones. Biogeosciences 8 (2), 227-237.

Castro-Morales, K., 2010. Marine productivity estimates from dissolved gas measurements in the Southern Ocean, University of East Antlia, Norwich.

Chipman, D.W., Marra, J., Takahashi, T., 1993. Primary production at 47°N and 20°W in the North Atlantic Ocean: a comparison between the ^{14}C incubation method and the mixed layer carbon budget. Deep Sea Research Part II: Topical Studies in Oceanography 40 (1-2), 151-169.

Craig, H., Hayward, T., 1987. Oxygen Supersaturation in the Ocean: Biological Versus Physical Contributions. Science 235 (4785), 199-202.

Culberson, C., 1991. Dissolved oxygen. WOCE Operations Manual.

Denman, K.L., Brasseur, G., Chidthaisong, A., Ciais, P., Cox, P.M., Dickinson, R.E., Hauglustaine, D., Heinze, C., Holland, E., D. Jacob, Lohmann, U., Ramachandran, S., Dias, P.L.d.S., Wofsy, S.C., Zhang, X., 2007. Couplings Between Changes in the Climate System and Biogeochemistry. In: Solomon, S., D. Qin, M. Manning, Z. Chen, M. Marquis, K.B. Averyt, M.Tignor, Miller, H.L. (Eds.), Climate Change 2007: The Physical Science Basis. Contribution of Working Group I to the Fourth Assessment Report of the Intergovernmental Panel on Climate Change. Intergovernmental Panel on Climate Change, Cambridge University Press,Cambridge, United Kingdom and New York, NY, USA, pp. 499-587.

Dickson, A.G., 1995. Determination of dissolved oxygen in sea water by Winkler titration. WOCE Operations Manual Part 3.1.3 Operations & Methods, WHP Office Report WHPO 91-1.

Dickson, A.G., Goyet, C., 1994. Protocols for the joint global ocean flux study (JGOFS) core measurements.

Duarte, C.M., Regaudie-de-Gioux, A., Arrieta, J.M., Delgado-Huertas, A., Agustí, S., 2013. The Oligotrophic Ocean Is Heterotrophic. Annual Review of Marine Science 5, 551-569.

Ducklow, H.W., Doney, S.C., 2013. What Is the Metabolic State of the Oligotrophic Ocean? A Debate. Annual Review of Marine Science 5, 525-533.

ECMWF, 2009. European Centre for Medium-Range Weather Forecasts ERA-Interim Re-Analysis data. http://badc.nerc.ac.uk/view/badc.nerc.ac.uk__ATOM__dataent_12458543158227759.

Eisenstadt, D., Barkan, E., Luz, B., Kaplan, A., 2010. Enrichment of oxygen heavy isotopes during photosynthesis in phytoplankton. Photosynthesis Research 103 (2), 97-103.

Emerson, S., 1987. Seasonal oxygen cycles and biological new production in surface waters of the subarctic Pacific ocean. Journal of Geophysical Research 92 (C6).

Eppley, R.W., Peterson, B.J., 1979. Particulate organic matter flux and planktonic new production in the deep ocean. Nature 282 (5740), 677-680.

Falkowski, P.G., Raven, J.A., 1997. Aquatic photosynthesis. Blackwell Science Malden, MA.

Fernández, E., Marañón, E., Morán, X.A.G., Serret, P., 2003. Potential causes for the unequal contribution of picophytoplankton to total biomass and productivity in oligotrophic waters. Marine Ecology Progress Series 254, 101-109.

Gaarder, T., Gran, H.H., 1927. Investigations of the production of plankton in the Oslo Fjord. Conseil permanent international pour l'exploration de la mer.

Garcia, H.E., Gordon, L.I., 1992. Oxygen Solubility in Seawater: Better Fitting Equations. Limnology and Oceanography 37 (6).

Gieskes, W.W.C., Kraay, G.W., Baars, M.A., 1979. Current ^{14}C methods for measuring primary production: Gross underestimates in oceanic waters. Netherlands Journal of Sea Research 13 (1), 58-78.

Gist, N., Serret, P., Woodward, E.M.S., Chamberlain, K., Robinson, C., 2009. Seasonal and spatial variability in plankton production and respiration in the Subtropical Gyres of the

Atlantic Ocean. Deep Sea Research Part II: Topical Studies in Oceanography 56 (15), 931-940.

Glueckauf, E., 1951. The composition of atmospheric air. In: Malone, T.F. (Ed.), Compendium of Meteorology, Boston, MA.

Gonfiantini, R., 1977. Consultants' meeting on stable isotope standards and intercalibration in hydrology and in geochemistry IAEA, Vienna, 8-10 September 1976.

Gonfiantini, R., 1978. Standards for stable isotope measurements in natural compounds. Nature 271 (5645), 534-536.

González, N., Anadón, R., Marañón, E., 2002. Large-scale variability of planktonic net community metabolism in the Atlantic Ocean: importance of temporal changes in oligotrophic subtropical waters. Marine Ecology Progress Series 233, 21-30.

Grossman, A.R., Mackey, K.R.M., Bailey, S., 2010. A perspective on photosynthesis in the oligotrophic oceans: hypotheses concerning alternate routes of electron flow. Journal of Phycology 46 (4), 629-634.

Gueguen, C., Tortell, P. D., 2008. High-resolution measurement of Southern Ocean CO_2 and O_2/Ar by membrane inlet mass spectrometry. Marine Chemistry 108 (3-4), 184-194.

Guy, R.D., Fogel, M.L., Berry, J.A., 1993. Photosynthetic fractionation of the stable isotopes of oxygen and carbon. Plant Physiology 101 (1), 37-47.

Hamme, R.C., Emerson, S.R., 2004. The solubility of neon, nitrogen and argon in distilled water and seawater. Deep Sea Research Part I: Oceanographic Research Papers 51 (11), 1517-1528.

Harris, G.P., 1986. Phytoplankton ecology: structure, function, and fluctuation. Chapman and Hall.

Helman, Y., Barkan, E., Eisenstadt, D., Luz, B., Kaplan, A., 2005. Fractionation of the Three Stable Oxygen Isotopes by Oxygen-Producing and Oxygen-Consuming Reactions in Photosynthetic Organisms. Plant Physiology 138 (4), 2292-2298.

Hendricks, M.B., Bender, M.L., Barnett, B.A., 2004. Net and gross O_2 production in the Southern Ocean from measurements of biological O_2 saturation and its triple isotope composition. Deep-Sea Research Part I-Oceanographic Research Papers 51 (11), 1541-1561.

Huang, K., Ducklow, H., Vernet, M., Cassar, N., Bender, M.L., 2012. Export production and its regulating factors in the West Antarctica Peninsula region of the Southern Ocean. Global Biogeochemical Cycles 26 (2), GB2005.

Joint, I., Pomroy, A., Savidge, G., Boyd, P., 1993. Size-fractionated primary productivity in the northeast Atlantic in May-July 1989. Deep Sea Research Part II: Topical Studies in Oceanography 40 (1-2), 423-440.

Juranek, L., Quay, P., 2005. In vitro and in situ gross primary and net community production in the North Pacific Subtropical Gyre using labeled and natural abundance isotopes of dissolved O_2. Global Biogeochemical Cycles 19 (3), GB3009.

Juranek, L.W., Hamme, R.C., Kaiser, J., Wanninkhof, R., Quay, P.D., 2010. Evidence of O_2 consumption in underway seawater lines: Implications for air-sea O_2 and CO_2 fluxes. Geophysical research letters 37 (1), L01601.

Juranek, L.W., Quay, P.D., 2010. Basin-wide photosynthetic production rates in the subtropical and tropical Pacific Ocean determined from dissolved oxygen isotope ratio measurements. Global Biogeochemical Cycles 24 (2), GB2006.

Juranek, L.W., Quay, P.D., Feely, R.A., Lockwood, D., Karl, D.M., Church, M.J., 2012. Biological production in the NE Pacific and its influence on air-sea CO_2 flux: Evidence from dissolved oxygen isotopes and O_2/Ar. Journal of Geophysical Research 117 (C5), C05022.

Kaiser, J., 2008. Reformulated ^{17}O correction of mass spectrometric stable isotope measurements in carbon dioxide and a critical appraisal of historic 'absolute' carbon and oxygen isotope ratios. Geochimica et Cosmochimica Acta 72 (5), 1312-1334.

Kaiser, J., 2011a. Corrigendum to "Technical note: Consistent calculation of aquatic gross production from oxygen triple isotope measurements" published in Biogeosciences, 8, 1793-1811, 2011. Biogeosciences 8 (9), 2561-2565.

Kaiser, J., 2011b. Technical note: Consistent calculation of aquatic gross production from oxygen triple isotope measurements. Biogeosciences 8 (7), 1793-1811.

Kaiser, J., Abe, O., 2012. Reply to Nicholson's comment on "Consistent calculation of aquatic gross production from oxygen triple isotope measurements" by Kaiser (2011). Biogeosciences 9 (8), 2921-2933.

Kaiser, J., M. K. Reuer, B. Barnett, and M. L. Bender 2005. Marine productivity estimates from continuous O_2/Ar ratio measurements by membrane inlet mass spectrometry,. Geophysical research letters 32 (19), L19605, .

Kaiser, J., Röckmann, T., 2008. Correction of mass spectrometric isotope ratio measurements for isobaric isotopologues of O_2, CO, CO_2, N_2O and SO_2. Rapid Communications in Mass Spectrometry 22 (24), 3997-4008.

Kalnay, E., Kanamitsu, M., Kistler, R., Collins, W., Deaven, D., Gandin, L., Iredell, M., Saha, S., White, G., Woollen, J., Zhu, Y., Leetmaa, A., Reynolds, R., Chelliah, M., Ebisuzaki, W., Higgins, W., Janowiak, J., Mo, K.C., Ropelewski, C., Wang, J., Jenne, R., Joseph, D., 1996. The NCEP/NCAR 40-Year Reanalysis Project. Bulletin of the American Meteorological Society 77 (3), 437-471.

Kana, T.M., 1990. Light-dependent oxygen cycling measured by an oxygen-18 isotope dilution technique. Marine Ecology Progress Series 64, 293-300.

Kana, T.M., 1992. Relationship between photosynthetic oxygen cycling and carbon assimilation in *Synechococcus* wh7803 (cyanophyta). Journal of Phycology 28 (3), 304-308.

Kana, T.M., 2007. MIMS Denitrification NSF-RCN Training http://www.hpl.umces.edu/~kana/index_files/Onlinetraining.htm.

Kana, T.M., Darkangelo, C., Hunt, M.D., Oldham, J.B., Bennett, G.E., Cornwell, J.C., 1994. Membrane Inlet Mass-Spectrometer for rapid high-precission determination of N_2,O_2 and Ar in environmental water samples. Analytical chemistry 66 (23), 4166-4170.

Karl, D., Michaels, A., Bergman, B., Capone, D., Carpenter, E., Letelier, R., Lipschultz, F., Paerl, H., Sigman, D., Stal, L., 2002. Dinitrogen fixation in the world's oceans. Biogeochemistry 57 (1), 47-98.

King et al., B.A., 2010. RSS James Cook Cruise JC032, 07Mar-21Apr 2009. Hydrographic sections across the Brazil Current and at 24° N in the Altantic. In: King, B.A., Hamersley, D.R.C. (Eds.). National Oceanography Centre, Southampton Cruise Report, 48

University of Southampton, p. 173.

Knox, M., Quay, P.D., Wilbur, D., 1992. Kinetic Isotopic Fractionation During Air-Water Gas Transfer of O_2, N_2, CH_4, and H_2. Journal of Geophysical Research 97 (C12), 20335-20343.

Kolber, Z.S., Prášil, O., Falkowski, P.G., 1998. Measurements of variable chlorophyll fluorescence using fast repetition rate techniques: defining methodology and experimental protocols. Biochimica et Biophysica Acta (BBA)-Bioenergetics 1367 (1), 88-106.

Körtzinger, A., Send, U., Lampitt, R.S., Hartman, S., Wallace, D.W.R., Karstensen, J., Villagarcia, M.G., Llinás, O., DeGrandpre, M.D., 2008. The seasonal pCO_2 cycle at 49ºN/16.5ºW in the northeastern Atlantic Ocean and what it tells us about biological productivity. Journal of Geophysical Research 113 (C4), 1-15.

Lämmerzahl, P.R., Thomas; Brenninkmeijer, Carl A. M.; Krankowsky, Dieter; Mauersberger, Konrad, 2002. Oxygen isotope composition of stratospheric carbon dioxide. Geophysical research letters 29 (12), 1582.

Ledwell, J.R., Watson, A.J., Law, C.S., 1998. Mixing of a tracer in the pycnocline. Journal of Geophysical Research 103 (C10), 21499-21529.

Liss, P., Merlivat, L., 1986. Air-sea gas exchange rates: Introduction and synthesis. In: Buat-Ménard, P. (Ed.), The Role of Air-Sea Exchange in Geochemical Cycling.

Longhurst, A.R., 2007. Ecological geography of the sea Academic Press.

Luz, B., Barkan, E., 2000. Assessment of oceanic productivity with the triple-isotope composition of dissolved oxygen. Science 288 (5473), 2028-2031.

Luz, B., Barkan, E., 2005. The isotopic ratios $^{17}O/^{16}O$ and $^{18}O/^{16}O$ in molecular oxygen and their significance in biogeochemistry. Geochimica et Cosmochimica Acta 69 (5), 1099.

Luz, B., Barkan, E., 2009. Net and gross oxygen production from O_2/Ar, $^{17}O/^{16}O$ and $^{18}O/^{16}O$ ratios. Aquatic Microbial Ecology (56), 133-145.

Luz, B., Barkan, E., 2011. Proper estimation of marine gross O_2 production with $^{17}O/^{16}O$ and $^{18}O/^{16}O$ ratios of dissolved O_2. Geophysical research letters 38 (19), L19606.

Luz, B., E. Barkan, Y. Sagi, and Y. Z. Yacobi, 2002. Evaluation of community respiratory mechanisms with oxygen isotopes: A case study in Lake Kinneret. Limnology and Oceanography (47), 33-42.

Mahadevan, A., D'Asaro, E., Lee, C., Perry, M.J., 2012. Eddy-Driven Stratification Initiates North Atlantic Spring Phytoplankton Blooms. Science 337 (6090), 54-58.

Marañón, E., Behrenfeld, M.J., González, N., Mouriño, B., Zubkov, M.V., 2003. High variability of primary production in oligotrophic waters of the Atlantic Ocean: uncoupling from phytoplankton biomass and size structure. Marine Ecology Progress Series 257, 1-11.

Marañón, E., Holligan, P.M., Varela, M., Mouriño, B., Bale, A.J., 2000. Basin-scale variability of phytoplankton biomass, production and growth in the Atlantic Ocean. Deep Sea Research Part I: Oceanographic Research Papers 47 (5), 825-857.

Marra, J., 2002. Approaches to the Measurement of Plankton Production. Phytoplankton Productivity. Blackwell Science Ltd, pp. 78-108.

Martin, J.H., Fitzwater, S.E., Michael Gordon, R., Hunter, C.N., Tanner, S.J., 1993. Iron, primary production and carbon-nitrogen flux studies during the JGOFS North Atlantic bloom experiment. Deep Sea Research Part II: Topical Studies in Oceanography 40 (1-2), 115-134.

Martin, P., Lampitt, R.S., Jane Perry, M., Sanders, R., Lee, C., D'Asaro, E., 2011. Export and mesopelagic particle flux during a North Atlantic spring diatom bloom. Deep Sea Research Part I: Oceanographic Research Papers 58 (4), 338-349.

Moum, J., Osborn, T., 1986. Mixing in the main thermocline. Journal of Physical Oceanography 16, 1250-1259.

Neess, J.C., Dugdale, R.C., Dugdale, V.A., Goering, J.J., 1962. Nitrogen Metabolism in Lakes. I. Measurement of Nitrogen Fixation with N^{15}. Limnology and Oceanography 7 (2), 163-169.

Nemcek, N., Ianson, D., Tortell, P.D., 2008. A high-resolution survey of DMS, CO_2, and O_2/Ar distributions in productive coastal waters. Global Biogeochemical Cycles 22 (2).

Nicholson, D.P., Stanley, R.H.R., Barkan, E., Karl, D.M., Luz, B., Quay, P.D., Doney, S.C., 2012. Evaluating triple oxygen isotope estimates of gross primary production at the Hawaii Ocean Time-series and Bermuda Atlantic Time-series Study sites. Journal of Geophysical Research 117 (C5), C05012.

Nightingale, P.D., Malin, G., Law, C.S., Watson, A.J., Liss, P., Liddicoat, M.I., Boutin, J., Upstill-Goddard, R.C., 2000. In situ evaluation of air-sea gas exchange parameterizations using novel conservative and volatile tracers. Global Biogeochemical Cycles 14 (1), 373-387.

Peterson, E.W., Hennessey, J.P., 1978. On the Use of Power Laws for Estimates of Wind Power Potential. Journal of Applied Meteorology 17 (3), 390-394.

Prokopenko, M.G., Pauluis, O.M., Granger, J., Yeung, L.Y., 2011. Exact evaluation of gross photosynthetic production from the oxygen triple-isotope composition of O_2: Implications for the net-to-gross primary production ratios. Geophysical research letters 38 (14), L14603.

Quay, P., Stutsman, J., Steinhoff, T., 2012. Primary production and carbon export rates across the subpolar N. Atlantic Ocean basin based on triple oxygen isotope and dissolved O_2 and Ar gas measurements. Global Biogeochemical Cycles 26 (2), GB2003.

Quay, P.D., Peacock, C., Björkman, K., Karl, D.M., 2010. Measuring primary production rates in the ocean: Enigmatic results between incubation and non-incubation methods at Station ALOHA. Global Biogeochemical Cycles 24 (3), GB3014.

Reuer, M.K., Barnett, B.A., Bender, M.L., Falkowski, P.G., Hendricks, M.B., 2007. New estimates of Southern Ocean biological production rates from O_2/Ar ratios and the triple isotope composition of O_2. Deep Sea Research Part I: Oceanographic Research Papers 54 (6), 951-974.

Robertson, J.E., Watson, A.J., Langdon, C., Ling, R.D., Wood, J.W., 1993. Diurnal variation in surface pCO_2 and O_2 at 60° N, 20° W in the North Atlantic. Deep Sea Research Part II: Topical Studies in Oceanography 40 (1-2), 409-422.

Sabine, C.L., Feely, R.A., Gruber, N., Key, R.M., Lee, K., Bullister, J.L., Wanninkhof, R., Wong, C.S., Wallace, D.W.R., Tilbrook, B., Millero, F.J., Peng, T.-H., Kozyr, A., Ono, T., Rios, A.F., 2004. The Oceanic Sink for Anthropogenic CO_2. Science 305 (5682), 367-371.

Sambrotto, R.N., Savidge, G., Robinson, C., Boyd, P., Takahashi, T., Karl, D.M., Langdon, C., Chipman, D., Marra, J., Codispoti, L., 1993. Elevated consumption of carbon relative to nitrogen in the surface ocean. Nature 363 (6426), 248-250.

Sarma, V., Abe, O., Saino, T., 2003. Chromatographic separation of nitrogen, argon, and oxygen in dissolved air for determination of triple oxygen isotopes by dual-inlet mass spectrometry. Analytical chemistry 75 (18), 4913-4917.

Sarma, V.V.S.S., Abe, O., Hinuma, A., Saino, T., 2006. Short-term variation of triple oxygen isotopes and gross oxygen production in the Sagami Bay, central Japan. Limnology and Ocenaography: Methods 51 (3).

Serret, P., C. Robinson, E. Fernández, E. Teira, G. Tilstone, and V. Pérez, 2009. Predicting plankton net community production in the Atlantic Ocean Deep Sea Research Part II: Topical Studies in Oceanography 56 (15).

Serret, P., Fernández, E., Robinson, C., 2002. Biogeographic differences in the net ecosystem metabolism of the open ocean. Ecology 83 (11), 3225-3234.

Serret, P., Fernández, E., Robinson, C., Woodward, E.M.S., Pérez, V., 2006. Local production does not control the balance between plankton photosynthesis and respiration in the open Atlantic Ocean. Deep Sea Research Part II: Topical Studies in Oceanography 53 (14-16), 1611-1628.

Serret, P., Robinson, C., Fernández, E., Teira, E., Tilstone, G., 2001. Latitudinal variation of the balance between plankton photosynthesis and respiration in the eastern Atlantic Ocean. Limnology and Oceanography 46 (7), 1642-1652.

Sieracki, M., Poulton, N., 2011. The 2008 North Atlantic Bloom Experiment Abundance and Biomass Determination of heterotrophic and autotrophic bacteria, phototrophic and heterotrophic nanoplankton, & microplankton -including instrument calibration.

Sieracki, M.E., Verity, P.G., Stoecker, D.K., 1993. Plankton community response to sequential silicate and nitrate depletion during the 1989 North Atlantic spring bloom. Deep Sea Research Part II: Topical Studies in Oceanography 40 (1-2), 213-225.

Spitzer, W.S., Jenkins, W.J., 1989. Rates of vertical mixing, gas exchange and new production: Estimates from seasonal gas cycles in the upper ocean near Bermuda. Journal of Marine Research 47, 169-196.

Stanley, R.H.R., Kirkpatrick, J.B., Cassar, N., Barnett, B.A., Bender, M.L., 2010. Net community production and gross primary production rates in the western equatorial Pacific. Global Biogeochemical Cycles 24 (4), GB4001.

Steeman_Nielsen, E., 1952. The use of radiactive carbon (C^{14}) for measuring organic production in the sea. Journal Pour la Conseil International d'Exploration de la Mer 18 (2), 117-140.

Suggett, D., Kraay, G., Holligan, P., Davey, M., Aiken, J., Geider, R., 2001. Assessment of photosynthesis in a spring cyanobacterial bloom by use of a fast repetition rate fluorometer. Limnology and Oceanography, 802-810.

Suggett, D., Moore, C., Hickman, A., Geider, R., 2009. Interpretation of fast repetition rate (FRR) fluorescence: signatures of phytoplankton community structure versus physiological state. Marine Ecology Progress Series 376, 1-19.

Sverdrup, H.U., 1953. On conditions for the vernal blooming of phytoplankton. Journal du Conseil International pour l'Exploration de la Mer 18 (287-295).

Sweeney, C., Gloor, E., Jacobson, A.R., Key, R.M., McKinley, G., Sarmiento, J.L., Wanninkhof, R., 2007. Constraining global air-sea gas exchange for CO_2 with recent bomb ^{14}C measurements. Global Biogeochemical Cycles 21 (2), GB2015.

Takahashi, T., Olafsson, J., Goddard, J.G., Chipman, D.W., Sutherland, S.C., 1993. Seasonal variation of CO_2 and nutrients in the high-latitude surface oceans: A comparative study. Global Biogeochemical Cycles 7 (4), Pages: 843-878.

Takahashi, T., Sutherland, S.C., Wanninkhof, R., Sweeney, C., Feely, R.A., Chipman, D.W., Hales, B., Friederich, G., Chavez, F., Sabine, C., Watson, A., Bakker, D.C.E., Schuster, U., Metzl, N., Yoshikawa-Inoue, H., Ishii, M., Midorikawa, T., Nojiri, Y., Körtzinger, A., Steinhoff, T., Hoppema, M., Olafsson, J., Arnarson, T.S., Tilbrook, B., Johannessen, T., Olsen, A., Bellerby, R., Wong, C.S., Delille, B., Bates, N.R., de Baar, H.J.W., 2009. Climatological mean and decadal change in surface ocean pCO2, and net sea-air CO_2 flux over the global oceans. Deep Sea Research Part II: Topical Studies in Oceanography 56, 554-577.

Tanhua, T., 2010. Matlab Toolbox to Perform Secondary Quality Control (2^{nd} QC) on Hydrographic Data. ORNL CDIAC-158. Carbon Dioxide Information Analysis Center, Oak Ridge National Laboratory, U.S. Department of Energy, Oak Ridge, Tennessee 158.

Taylor, J.R., Ferrari, R., 2011. Shutdown of turbulent convection as a new criterion for the onset of spring phytoplankton blooms. Limnology and Oceanography 56 (6), 2293-2307.

Tcherkez, G., Farquhar, G.D., 2007. On the $^{16}O/^{18}O$ isotope effect associated with photosynthetic O_2 production. Functional Plant Biology 34 (11), 1049-1052.

Tengberg, A., Jostein Hovdenes, Henrik Johan Andersson, Olivier Brocandel, Robert Diaz, David Hebert, Tony Arnerich, Christian Huber, Arne Körtzinger, Alexis Khripounoff, Francisco Rey, Christer Rönning, Jens Schimanski, Stefan Sommer, Stangelmayer, A., 2006. Evaluation of a lifetime-based optode to measure oxygen in aquatic systems. Limnology and Oceanography: Methods 4, 7-17.

Thiemens, M.H., Jackson, T., Zipf, E.C., Erdman, P.W., van Egmond, C., 1995. Carbon Dioxide and Oxygen Isotope Anomalies in the Mesosphere and Stratosphere. Science 270 (5238), 969-972.

Tortell, P.D., 2005a. Dissolved gas measurements in oceanic waters made by membrane inlet mass spectrometry. Limnology and Oceanography: Methods 3, 24-37.

Tortell, P.D., 2005b. Small scale heterogeneity of dissolved gas concentrations in marine continetal shelf waters. Geochemistry Geophysics Geosystems 6, Q11M04.

Uchida, H.K., T.;A Kaneko, I.; Fukasawa, M., 2008. In Situ Calibration of Optode-Based Oxygen Sensors. Journal of Atmospheric and Oceanic Technology 25 (12), 2271-2281.

Volk, T., Hoffert, M.I., 1985. Ocean carbon pumps: Analysis of relative strengths and efficiencies in ocean-driven atmospheric CO_2 changes. In: Sundquist, E.T., Broecker, W.S. (Eds.), The Carbon Cycle and Atmospheric CO_2: Natural Variations Archean to Present, Geophys. Monograph Series. AGU Geophysical Monograph Board, Washington, DC:AGU, pp. 99-110.

Waniek, J.J., 2003. The role of physical forcing in initiation of spring blooms in the northeast Atlantic. Journal of Marine Systems 39 (1-2), 57-82.

Wanninkhof, R., 1992. Relationship Between Wind Speed and Gas Exchange Over the Ocean. Journal of Geophysical Research 97 (C5), 7373-7382.

Westberry, T.K., Dall'Olmo, G., Boss, E., Behrenfeld, M.J., Moutin, T., 2010. Coherence of particulate beam attenuation and backscattering coefficients in diverse open ocean environments. Optics Express 18 (15), 15419-15425.

Wieser, M.E.a.B.M., 2007. Atomic weights of the elements 2007 (IUPAC Technical Report). Pure and Applied Chemistry 81 (11).

Williams, P.J.B., Lefevre, D., 1996. Algal ^{14}C and total carbon metabolisms. 1. Models to account for the physiological processes of respiration and recycling. Journal of Plankton Research 18 (10), 1941-1959.

Williams, P.J.L.B., Quay, P.D., Westberry, T.K., Behrenfeld, M.J., 2013. The Oligotrophic Ocean Is Autotrophic. Annual Review of Marine Science 5, 535-549.

Yung, Y.L., DeMore, W.B., Pinto, J.P., 1991. Isotopic exchange between carbon dioxide and ozone via O (^1D) in the stratosphere. Geophysical research letters 18 (1), 13-16.

Glossary

γ_R	Ratio of $^{17}O/^{16}O$ isotopic fractionation to $^{18}O/^{16}O$ isotopic fractionation during respiration, calculated as $^{17}\varepsilon_r / ^{18}\varepsilon_r$
ϑ_o	Sea surface temperature
δ	Relative isotope ratio difference
$^{17}\delta_P$, $^{18}\delta_P$	Relative isotope ratio difference of biologically produced O_2
$^{17}\delta_{sat}$, $^{18}\delta_{sat}$	Relative isotope ratio difference of dissolved O_2 in equilibrium with the atmosphere
$^{17}\delta_{VSMOW}$, $^{18}\delta_{VSMOW}$	Relative isotope ratio difference of VSMOW compared to atmospheric O_2
$^{17}\delta_W$, $^{18}\delta_W$	Relative isotope ratio difference of water compared to atmospheric O_2
$\delta(N_2/O_2)$	Relative N_2/O_2 gas ratio difference between two samples
$\delta(O_2/Ar)$	Relative O_2/Ar gas ratio difference between two samples
$\Delta(O_2/Ar)$	Biological oxygen saturation anomaly
$\Delta(Ar)$	Ar saturation anomaly
$\Delta(O_2)$	O_2 saturation anomaly
$^{17}\Delta$	^{17}O excess, defined as equation 1.7
$^{17}\Delta_{sat}$	$^{17}\Delta$ of O_2 in equilibrium with the atmosphere and calculated from $^{17}\delta_{sat}$ and $^{18}\delta_{sat}$
$^{17}\Delta_P$	$^{17}\Delta$ of biologically produced O_2 calculated from $^{17}\delta_p$ and $^{18}\delta_p$
$^{17}\varepsilon_E$, $^{18}\varepsilon_E$	Isotopic fractionation during evasion of O_2 from water to atmosphere
$^{17}\varepsilon_I$, $^{18}\varepsilon_I$	Isotopic fractionation during invasion of O_2 from atmosphere into water
$^{17}\varepsilon_p$, $^{18}\varepsilon_p$	Isotopic fractionation during photosynthesis
$^{17}\varepsilon_R$, $^{18}\varepsilon_R$	Isotopic fractionation during respiration
c(chlo-a)	Chlorophyll a concentration
$c(O_2)$, c(Ar)	Concentration of dissolved O_2 and Ar in water
$c_{sat}(O_2)$, c_{sat}(Ar)	Saturation concentration of O_2 and Ar in water
f	Ratio of net community oxygen production to gross oxygen production (N/ G)

F_{bio}	Biological O_2 air-sea flux
FRRF	Fast repetition rate fluorometer
G	Gross oxygen production, determined with triple oxygen isotope method
g	Ratio of gross production G to gas exchange
IRMS	Isotope ratio mass spectrometer
k	Gas exchange coefficient
k_w	Weighted gas exchange coefficient, adapted after Reuer *et al.* (2007)
K_v	Vertical diffusivity coefficient
m/z	Mass to charge ratio
MIMS	Membrane inlet mass spectrometer
N	Net community production, defined as equation 1.3
ppm	1 part per million
PS II	Photosystem II
S_0	Sea surface salinity
USW	Underway sea water supply
VSMOW	Vienna Standard Mean Ocean Water
z_{lim}	Nutrient limitation index
z_{mix}	Mixed layer depth
z_{NO3-}	Nitracline